UTS UNIVERSITY OF TECHNOLOGY SYDNEY

Smouldering Fuel Processing, Emission Flammability, and Carbon Footprint

by Yuying Chen

Thesis submitted in fulfilment of the requirements for the degree of

Doctor of Philosophy

under the supervision of Dr Nic Surawski
Dr Xinyan Huang
Prof John Zhou

University of Technology Sydney
Faculty of Engineering and Information Technology

August 2023

Certificate of Original Authorship

I, Yuying Chen, declare that this thesis is submitted in fulfilment of the requirements for the award of Doctor of Philosophy, in the School of Civil and Environmental Engineering/Faculty of Engineering and Information Technology at the University of Technology Sydney.

This thesis is wholly my own work unless otherwise referenced or acknowledged. In addition, I certify that all information sources and literature used are indicated in the thesis.

I certify that the work in this thesis has not previously been submitted for a degree nor has it been submitted as part of the requirements for a degree at any other academic institution except as fully acknowledged within the text. This thesis is the result of a Collaborative Doctoral Research Degree program with the Hong Kong Polytechnic University.

This research is supported by the Australian Government Research Training Program.

Signature: Production Note:
Signature removed prior to publication.

Date: 31/8/2023

Acknowledgements

First and foremost, I would like to express my deepest appreciation and gratitude to my chief supervisor at UTS, Dr Nic Surawski, for his invaluable mentorship, support, and encouragement throughout my PhD journey. I am truly grateful for your willingness to share your insights and expertise with me, and I have learned so much from your vast knowledge and experience.

I would like to express my sincere gratitude to my chief supervisor at PolyU, Dr Xinyan Huang. Thank you for your unwavering support, guidance, and dedication to my academic and personal growth during my PhD. Your optimism towards life and passion for research have always inspired me and enabled me to overcome any difficulties and challenges in my life.

I would like to genuinely thank my co-supervisors, Dr Ben Shao-Yuan Leu at PolyU and Prof John Zhou at UTS, who kindly offered their expertise and guidance during this journey. I appreciate your invaluable suggestions and comments, that are essential to the improvement of this thesis.

For this thesis, I would like to thank all my co-authors, Dr Zhirong Liang (Chapters 2 and 3, assistance in experiments), Dr Shaorun Lin (Chapters 2, 3, 4, and 5, assistance in experiments and data analysis), and Mr Yunzhu Qin (Chapter 5, assistance in experiments).

I wish to thank my academic peers and friends in PolyU Fire Lab: Shaorun Lin, Peiyi Sun (Sally), Lingchu Su (Sue), Zilong Wang, Tianhang Zhang, Caiyi Xiong, Yanhui Liu, Xiaoning Zhang, Zhuojun Nan, Yunzhu Qin, Yizhou Li, Yichao Zhang, Yanfu Zeng, Ho Yin Wong, Jin Qiu, Cheng Chen, Tianwei Chu, Xiuqi Xi, Zhirong Liang, Han Yuan, Xiqiang Wu, Tsz Him Chow (Alvis), Siyan Wang, Gulzhan Aldan, Atif Ali Khan, Anwar Orabi, and Domada Veera Venkata Ramakanth. It has been a wonderful and unforgettable experience to study and work with you.

I would also thank my colleagues and friends in UTS and Sydney: Zhengheng Xu, Jianyuan Zhen, Xutong Zhang, Lan Wu, Xiaoqing Liu, Xingdong Shi, Jiaqi Zhang, Marcos Canales, Zhichao Yu, Dan Hu (Nikki), Zhengxiao Du, and Miaoying Sun. Your kind help and support made my study and life fabulous in Sydney.

I want to acknowledge the financial support from the Hong Kong Polytechnic University and University of Technology Sydney.

I would like to express my gratitude to my beloved family. Thank you, mom and dad, for your love, understanding, and unwavering belief in me. Thank you, Yulin Chen, my lovely sister, for being a constant source of joy, inspiration, and motivation. Thank you, Liye Fu, for your company, support, and encouragement all the time.

Finally, I would like to dedicate this thesis to my late grandfather, who gives me unconditional love and support. I hope to continue to make you proud.

Yuying Chen

Sydney, Australia

August 2023

Research Publications

Publications included in this thesis

1. **Y. Chen**, Z. Liang, S. Lin, X. Huang*. Limits of Sustaining a Flame above Smouldering Woody Biomass. *Combustion Science and Technology*, **2022**, 1-19. (Chapter 4)
2. **Y. Chen**, S. Lin, Z. Liang*, N. C. Surawski, and X. Huang*. Smouldering Organic Waste Removal Technology with Smoke Emissions Cleaned by Self-Sustained Flame. *Journal of Cleaner Production*, **2022**, 362: 132363. (Chapter 5)
3. **Y. Chen**, S. Lin, Z. Liang, and X. Huang*. Clean Smouldering Biowaste Process: Effect of Burning Direction on Smoke Purification by Self-sustained Flame. *Fuel Processing Technology*, **2022**, 237: 107453. (Chapter 6)
4. **Y. Chen**, S. Lin, Y. Qin, N. C. Surawski* and X. Huang*. Carbon Distribution and Multi-criteria Decision Analysis of Flexible Biowaste Smouldering Processing Technologies. *Waste Management*, **2023**,167: 183-193. (Chapter 7)

Other publications during candidature

5. **Y. Chen**, Z. Wang*, S. Lin, Y. Qin, and X. Huang*. A review on biomass thermal-oxidative decomposition data and machine learning prediction of thermal analysis. *Cleaner Materials*, **2023**,100206.
6. M. Raza#, **Y. Chen#**, J. Trapp, H. Sun, X. Huang*, and W. Ren*. Smouldering peat fire detection by time-resolved measurements of transient CO_2 and CH_4 emissions using a novel dual-gas optical sensor. *Fuel*, **2023**, 334: 126750. (#indicates co-first author)
7. Y. Qin, **Y. Chen**, S. Lin, and X. Huang. Limiting oxygen concentration and supply rate of smouldering propagation. *Combustion and Flame*, **2022**, 245: 112380.

Table of Contents

List of Tables

List of Figures

Nomenclature

Symbols

A	Area (m^2)
C	Fuel-related constant value
c	Specific heat capacity (J/kg·K)
D	Diameter (m)
F	Fuel
FL	Flaming combustion
f	Flame
G/g	Gas
HC	Hydrocarbon
h	Convection coefficient ($W/(m^2\text{-}K)$)
$\dot{m}''$	Mass flux ($g/m^2 \cdot s$)
$\dot{q}''$	Heat flow (kW/m^2)
S	Spread rate (m/s)
SM	Smouldering
T	Temperature (°C or K)
t	Transient time (s)
U	Flow velocity (m/s)
$\dot{V}$	Volume flow rate (m^3/min)
X	Volume fraction (%)
Y	Mass fraction (%)

Greek symbols

α	Thermal conductivity (W/m·K)
ΔH	Heat of reaction (MJ/kg)
Δt	Time duration (s)
κ	Thermal diffusivity (m^2/s)
v	Stochiometric coefficient (-)/
ρ	Density (kg/m^3)
σ	Sample standard deviation
Φ	Net outranking flow in PROMETHEE-GAIA

Acronyms

EF	Emission factor (g/kg)
SE	Standard error

Subscripts

a/∞	Ambient
c	Cooling
crt	Critical
ex	Extinction
for	Forward smouldering
G/g	Gas
i	Gas species *i*
ig	Ignition
j	Gas species *j*
L	Liquid by-products
opp	Opposed smouldering
ox	Oxygen
pre	Preheat zone
py	Pyrolysis
S	Solid by-products
sm	Smouldering
T	Tar
W	Condensed water
w	Wall

Abstract

Smouldering is an emerging method for biowaste removal, which has demonstrated many attractive advantages. However, as smouldering is an in-completed combustion, it tends to release many toxic emissions, like CO, CH_4, and volatile organic compounds (VOCs), limiting its further promotion and application. Therefore, this thesis proposes and thoroughly investigates a novel combustion method for biowaste removal that uses a self-sustained flame co-existing with smouldering to clean the toxic smouldering emissions.

Firstly, it is verified through experiments that the smouldering emission of biomass can be piloted to sustain a flame and the flame can co-exist with smouldering combustion. The critical smouldering flux of wood waste for maintaining a stable flame remains constant at 10-12 $g/m^2 \cdot s$. To reach such a smouldering flux, the minimum opposed airflow velocity required is 6 mm/s. Then, the effects of fuel property and smouldering direction (forward or opposed) on the critical conditions are investigated. It is found that an equivalent critical mass flux of flammable gases required for igniting the smouldering emissions is 0.5 $g/m^2 \cdot s$, regardless of the fuel type. Additionally, it is easier for the flame to remove more emissions from opposed smouldering which is recommended for the proposed biowaste removal process. The efficiency of the pollution mitigation of the applied flame is demonstrated by significantly lower CO and VOCs emissions (with $\Delta CO/\Delta CO_2<0.05$ and $\Delta VOCs/\Delta CO_2<0.0005$) after purification. Finally, four smouldering-based biowaste processing strategies: (a) full smouldering, (b) partial smouldering, (c) full smouldering with a flame, and (d) partial smouldering with a flame, are proposed and evaluated. The results show that full smouldering achieves the highest removal efficiency but generates significant greenhouse and toxic gases, while partial smouldering effectively generates stable biochar (with $0.2<H:C<0.5$, $0.2<O:C<0.3$, and $R_{50}=0.6$), sequestering over 30 % carbon. And, a smaller airflow rate is recommended for the partial smouldering strategy to fix more carbon. It is also proved that the equivalent GHG from the four proposed processing strategies are all smaller than that from the conventional landfilling treatment. This work enriches strategies for the clean treatment of smouldering emissions and promotes an energy-efficient and environmentally friendly method for biowaste removal.

Keywords: biowaste; smouldering; flaming; carbon; biochar; bio-oil; emission; flammability; multi-criteria analysis

CHAPTER 1

Introduction

1.1 Research background

Waste is a common problem in modern society. Especially, with the development of the economy and the acceleration of urbanization, more and more waste is produced every day. Municipal solid waste (MSW) is a waste type consisting of solid waste discarded from households as well as commercial and industrial sources. According to the report from United States Environmental Protection Agency (EPA), 292 million tons of MSW were generated in America in 2018 (EPA, 2020). And in Hong Kong, the daily disposal of MSW increases significantly in recent years, which has reached over 10 thousand tons per day in 2018 (Environmental Protection Department of Hong Kong, 2019). Biowaste (also called waste biomass) is a major component of MSW, typically including food waste, woody/garden waste, paper waste, sewage sludge, agriculture waste, etc.

Waste management and utilization strategies are significant concerns in many countries. At present, biochemical conversion (landfilling, composting, anaerobic digestion, and fermentation) and thermochemical conversion (pyrolysis, liquefaction, gasification, combustion) technologies are the most common methods of biowaste disposal across the world. In the biochemical conversion process, the biowastes are broken down into smaller molecules by bacteria or enzymes. However, as this process is usually conducted under ambient temperature, it is much slower than a thermochemical conversion. Thermochemical conversion technology typically includes pyrolysis, gasification, liquefaction, and combustion. The difference between different thermochemical conversion technologies lies in the composition of the reactive gases, operating temperature, and pressure. Pyrolysis takes place in the total absence of oxygen where large hydrocarbon molecules are broken down into smaller ones. Depending on the heating rate and reactor ambient, the major product could be gas, liquid, or solid. Gasification requires a medium for reaction, which can include air, oxygen, subcritical steam, or a mixture of these. After gasification, the organic waste could be converted into synthetic gases. Liquefaction is a by-process of pyrolysis and gasification, and it often requires a higher temperature (300-350 °C) and pressure (12-20 MPa) for a longer reaction time. Combustion is a complex oxidation process, which has been considered the fastest, most cost-effective way to remove solid waste. It is most effective in the volume reduction of waste and the destruction, capture, and concentration of hazardous substances. Moreover, it can produce substantial heat for potential electricity generation

and industrial heating, i.e., energy recovery. However, the current thermochemical conversion method demonstrates many deficiencies. Firstly, the energy consumption and cost are very high as complex pre-treatments (such as grinding and drying) and external energy (like co-firing with coal and supply of fuel gas) are required. Secondly, the high-temperature reactions inside reactors pose safety hazards, which may cause an explosion, thus limiting the scale and location of the waste treatment device. Thirdly, many pollutants will be generated from the conventional high-temperature incineration process. Most seriously, the toxic dioxins produced can cause cancer in human beings. In summary, nowadays, effective and environmentally friendly treatment facilities to cope with the large quantities of biowaste are still absent, posing a globally big challenge to mankind.

Smouldering is an emerging method for organic waste removal. Smouldering is the slow, low-temperature, flameless burning of porous fuels and the most persistent type of combustion phenomenon. Common smouldering combustion can be found in burning cigarette, charcoal, and incense, as shown in Figure 1.1. Smouldering is fundamentally different from flaming in terms of reaction chemistry and transport processes (Ohlemiller, 1985; Palmer, 1957; Rein, 2014). The initiation of smouldering requires a relatively small amount of energy (Lin et al., 2019a), and it may be sustained in an oxygen concentration as low as 12% and a moisture content higher than 100% (Huang et al., 2016; Huang and Rein, 2016a). In general, the maximum smouldering temperature ranges from 500 to 800 ℃, depending on the fuel types and operation conditions (Rein, 2016), which is much lower than the flaming temperature (>1100 ℃) (Law, 2010).

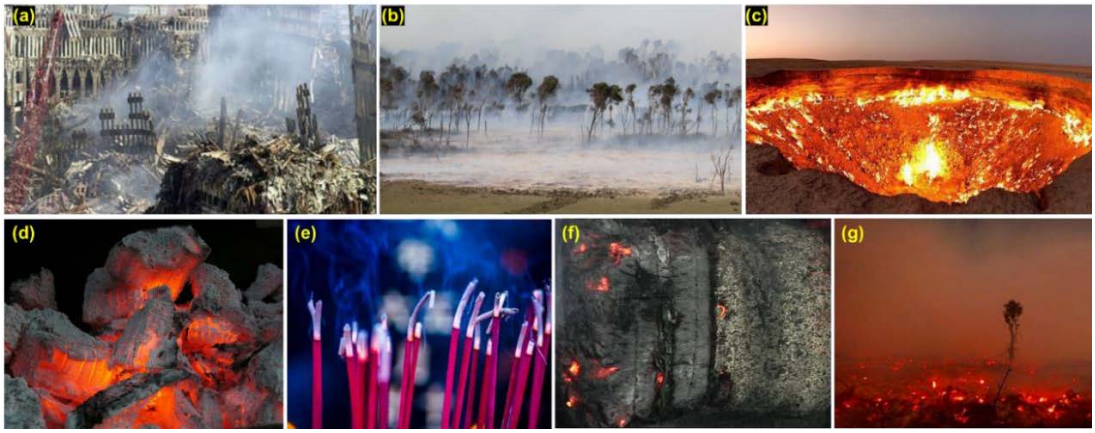

Figure 1.1. Typical example of smouldering combustion in different fuels, (a) debris of WTC, (b) peat fire, (c) underground coal fire, (d) charcoal, (e) incenses, (f) cotton, and (g) wildland firebrands.

Recently, novel technologies based on smouldering have been developed to successfully remove bioliquid (Kinsman et al., 2017; Zanoni et al., 2018), organic soils (Hadden et al., 2013; Huang and Rein, 2016b; Rein et al., 2017), facet (Fabris et al., 2017), wastewater biosolids and sludge (Tarek L. Rashwan et al., 2016), and oil shale (M.F. Martins et al., 2010). Such a smouldering-based process requires a minimum amount of pre-treatment and can handle different kinds of feedstocks with high moisture content. Moreover, the smouldering removal technology can be self-sustained without external heating. Besides, as an intensive pyrolysis is involved in the smouldering front, smouldering also shows strong potential as a green waste-to-energy technology, which has been applied to convert biowaste (like forestry waste, faces, and used types) into bio-oil (Vantelon et al., 2005; L Yermán et al., 2017a) and biochar (Rein, 2009a; Wyn et al., 2020b). Biochar is a solid product with a high carbon content, which has potential usage in a wide field and is suitable for carbon sequestration. Converting waste to biochar could avoid the complete return of greenhouse gases (GHG) to the atmosphere, compared to natural decay or burning processes [82,83]. Unlike the conventional pyrolysis technology, pyrolysis involved in the smouldering can be sustained by the heat generated from the weak oxidation of original fuel, requiring no external energy input. Therefore, the high operative cost associated with the input of thermal energy and inert purge gas of conventional pyrolysis can be avoided.

However, the pure smouldering organic waste treatment technology also has limitations. As an incomplete combustion process, smouldering produces a larger portion of greenhouse gases (CO_2, CH_4), PAHs, and PMs (Hu et al., 2018; Rein et al., 2009), posing severe threats to humans and the environment. Considering most smouldering emissions are still flammable because they still contain a large number of hydrocarbon pyrolysis gases and CO (H. Wang et al., 2021), this work aims to apply a flame on the smouldering emissions to convert them into H_2O and CO_2 (Rein, 2016). Sustaining a flame above the smouldering process can not only generate extra heat, but also remove a large portion of flammable and toxic smouldering emissions, thus, promoting more efficient and cleaner smouldering applications. However, the co-existence of flaming and smouldering on biomass has not been well explored so far, posing a significant knowledge gap.

1.2 Objectives and scope of the research

Therefore, this work aims to propose a novel combustion method for biowaste disposal which combines the advantages of smouldering and flaming. Specifically, the biowaste will be firstly burned through smouldering, meanwhile, the toxic emissions from smouldering will be cleaned by a flame. The co-existence mode of smouldering and flaming will be investigated in the round. The results are expected to help promote more environmentally friendly and energy efficient smouldering applications. Specifically, it is accomplished by addressing the following objectives:

1. Quantify the combustion efficiency and emission characteristics of both smouldering and flaming processes of various common wood, organic soil (simulated sludge), and coffee ground (food waste) biowastes.
2. Reveal the limiting conditions (critical oxygen supply rate and smouldering burning rate) of sustaining a flame on the smouldering emissions (i.e., co-existence of smouldering and flaming).
3. Explore the effects of biowaste properties (bulk density, particle size, and proximate analysis) and smouldering propagation direction (forward and opposed smouldering) on the critical conditions for the co-existence of smouldering and flaming.
4. Determine the purification effect of the flame on the toxic smouldering emissions by quantifying the emissions (CO_2, CO, CH_4, and VOC_s) before and after the flame is applied.
5. Explore the effectiveness of using smouldering to generate biochar for carbon sequestration. The biochar yield, fixed carbon fraction, and biochar stability under various air supply rates are quantified. The carbon footprints of full-smouldering and partial-smouldering processes are compared.

1.3 Research significance

Firstly, this study provides a clean and energy efficient biowaste removal method with the advantages of (1) a minimum pre-treatment requirement, (2) great flexibility in feedstocks and scale, (3) the minimum environmental impact, and (4) generate fixed carbon to reduce carbon emission. This proposed method is desired to be an important compensation to the existing solid waste disposal facilities. Secondly, this study solves the key problem existing in smouldering applications, that is, the smouldering emissions

contain large amounts of polluted and toxic species. The results are expected to help promote more environmentally friendly and energy-efficient smouldering applications. Finally, the knowledge gap of the co-existence of flaming and smouldering combustion on biomass is addressed, contributing to the development of combustion theory.

1.4 Organization of the thesis

This thesis is a compilation of four publications achieved during the Ph.D. study. Overall, this thesis is presented in a manuscript style: **Chapter 1** introduces the research background and significance. **Chapter 2** introduces the literature review. **Chapter 3** introduces the methodology of this thesis. The following chapters (**Chapters 4-7**) take the form of independent papers, which have been published in a journal. **Chapter 8** summarizes the conclusions and suggests some ideas for future research.

Firstly, **Chapter 4** investigates whether the emissions from smouldering woody biowaste can sustain a robust flame and quantifies the critical conditions (smouldering burning flux and oxygen supply rate) for the co-existence of smouldering and flame. Peer reviewed paper associated with **Chapter 4**: Y. Chen, Z. Liang, S. Lin, and X. Huang. *Limits of Sustaining a Flame above Smouldering Woody Biomass.* **Combustion Science and Technology**, 2022: 1-19.

Then, **Chapter 5** further applied the proposed combustion method to other types of biowastes (coffee waste and simulated sludge) and investigated the purification effects of the flame on the toxic smouldering emissions. Peer reviewed paper associated with **Chapter 5**: Y. Chen, S. Lin, Z. Liang, N. C. Surawski, and X. Huang (2022). *Smouldering Organic Waste Removal Technology with Smoke Emissions Cleaned by Self-Sustained Flame.* **Journal of Cleaner Production**, 2022, 362: 132363.

After that, **Chapter 6** discussed the effects of the smouldering direction on the co-existence of the smouldering and flaming by comparing their critical smouldering burning fluxes and minimum airflow velocities. Peer reviewed paper associated with **Chapter 6**: Y. Chen, S. Lin, Z. Liang, and X. Huang (2022). *Clean smouldering biowaste process: Effect of burning direction on smoke purification by self-sustained flame.* **Fuel Processing Technology**, 2022, 237: 107453.

Chapter 7 developed a flexible smouldering biowaste processing technology with four processing strategies. The gaseous, liquid, and solid products of each strategy are quantified. A multi-criteria analysis in terms of environmental impact, carbon

sequestration, waste removal efficiency, and by-product value is performed. Peer reviewed paper associated with **Chapter 7**: Y. Chen, S. Lin, Y. Qin, N. C. Surawski and X. Huang (2022). *Carbon Distribution and Multi-criteria Decision Analysis of Flexible Biowaste Smouldering Processing Technologies.* **Waste Management**, 2023,167: 183-193.

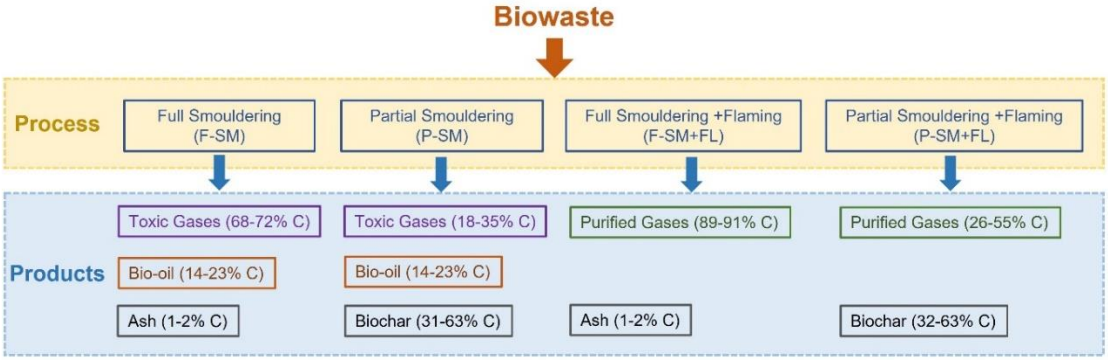

Figure 1.2. Graphic abstract of Chapter 7 – Flexible smouldering processes with four processing strategies.

Finally, **Chapter 8** summarizes the major contributions of this thesis and presents possible future works.

CHAPTER 2

Literature Review

2.1 Fundamental smouldering process

Smouldering is a heterogeneous process sustained when oxygen directly attacks the hot fuel surface, which is the dominant burning phenomenon of reactive porous media like woods (Anca-Couce et al., 2012; S. Wang et al., 2021), coals (Melody and Johnston, 2015), and organic soils (Huang and Rein, 2016a; Lin et al., 2020). Generally, the combustion of the porous media can be approximated as two lumped chemical pathways, namely, pyrolysis and oxidation (Lin et al., 2019b; Rein, 2013). As shown in Eq. (2.1), pyrolysis will result in pyrolysis gas and char. Subsequently, the oxidation of char leads to smouldering combustion (Eq. (2.2)), while the gas-phase oxidation leads to flaming combustion (Eq. (2.3)) (Rein, 2009b). Before pyrolysis, solid fuel needs to undergo the preheating and drying process (Rein, 2014). Above 200 ℃, the pyrolysis occurs, and continuing to increase the fuel temperature above 250 ℃. Then, the char oxidation process starts to release a net heat and becomes self-sustained if the oxygen supply is sufficient.

$$\text{Fuel (solid)}+\text{Heat}\rightarrow\text{Pyrolyzate (gas)}+\text{ Char (solid)} \quad \text{(Pyrolysis)} \quad (2.1)$$

$$\text{Char (solid)}+O_2\text{(gas)}\rightarrow\text{Heat}+CO_2+H_2O+\text{other gases}+\text{Ash (solid)} \quad \text{(Smouldering)} \quad (2.2)$$

$$\text{Pyrolysis (gas)}+O_2\text{(gas)}\rightarrow\text{Heat}+CO_2+H_2O+\text{other gases} \quad \text{(Flaming)} \quad (2.3)$$

Smouldering propagates through a porous material like a wave, or a front (named as smouldering front). The propagation of the smouldering front is facilitated by exothermic oxidation reactions. When the heat produced by these reactions overcomes heat losses, the smouldering can propagate continuously and can be defined as self-sustained smouldering (Wyn et al., 2020a).

According to the smouldering propagation direction relative to the direction of the oxygen, smouldering can be categorized as *Forward* and *Opposed* smouldering. As illustrated in Figure 2.1, forward propagation occurs when the oxygen supply is moving in the same direction as the smouldering front, while opposed propagation (also called reverse smouldering) occurs when the oxygen supply is moving opposite to the smouldering front (Combustion, 2016). Generally, the smouldering front consists of three sub-fronts: the preheating and drying, the pyrolysis, and the char oxidation sub-fronts (Combustion, 2016). In forward smouldering, the oxygen first flows through the char where it is consumed (by char oxidation) and then the hot reacted gases of combustion flow through the pyrolysis sub-front and the virgin fuel in sequence. This convective

transport results in enhanced drying and preheating processes. By contrast, in opposed smouldering, the oxygen flows through the virgin fuel in the first place, and then through the preheating and drying and pyrolysis sub-fronts before reaching the char oxidation sub-front. This means that heat is transferred by convection in the opposite direction to the virgin fuel, resulting in a weaker smouldering process (Combustion, 2016). Consequently, forward smouldering is faster than opposed smouldering under the same fuel and oxygen supply. Therefore, forward smouldering is the most widely used and efficient mode of smouldering for the removal of organic wastes (Yermán et al., 2016a; Zanoni et al., 2019a).

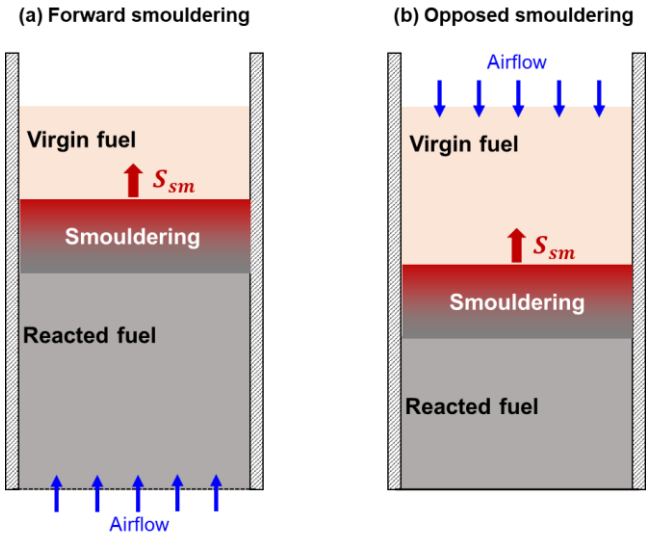

Figure 2.1. The schematic diagram of (a) forward and (b) opposed smouldering.

2.2 Parameters affecting smouldering

Generally, smouldering is controlled by two key parameters: oxygen transport and heat transfer, like most other combustion and fire processes. Meanwhile, many parameters may affect the oxygen transport and heat transfer processes. This section reviews how different parameters affect smouldering process. These parameters are categorized into the environmental conditions, such as oxygen concentration, airflow rate, external heat flux, and fuel physicochemical properties, such as moisture, particle size, and density.

2.2.1 Oxidizer flow

Oxidizer flow has a great influence on the smouldering process, as it directly affects the amount of oxygen that can be transported to the smouldering oxidation front (Torero

et al., 2020). Airflow can be divided into internal airflow inside the porous fuel and the external wind. The former is relatively small (< 5 cm/s) and mainly affects the smouldering process which spreads inside the porous fuel, while the latter forms a boundary layer flow on the fuel surface and mainly affects the surface smouldering spread over the interface between fuel and ambient. An increase in oxygen flow rate can improve oxygen availability and facilitate oxidation reactions. This is beneficial as it provides the necessary heat to sustain the smouldering reaction. It is demonstrated that the relationship between internal airflow and smouldering velocity is mostly linear (Torero et al., 2020; Wyn et al., 2020a). However, an extremely large airflow may cool the smouldering zone, reducing the temperature and the spread rate or even blowing off the combustion (Wang et al., 2018). Moreover, increasing the external wind speed can reduce the thickness of boundary layer, and thereby increase the diffusion of oxygen into the porous media. For a large-porosity fuel, such as PU foam, a pile of charcoals, and forest litter layer, the internal Darcian flow inside the porous fuel also increases due to the increases of flow pressure (Xie et al., 2020). Therefore, the influence of external wind on smouldering is indirect.

Oxygen concentration is one of the most important parameters for almost all combustion processes (Law, 2010; Ohlemiller, 1985), and it is often written in the form of volume fraction (X_{O_2}) in the fire research. The increase in oxygen concentration will cause the temperature and spread rate of smouldering to rise increased (Malow M, 2018; Putzeys et al., 2007, 2008; Putzeys Olivier, Carlos Fernandez-Pello, 2006; Ronda et al., 2017; Schmidt et al., 2003; Wang et al., 2016; Wu et al., 2017; Yang et al., 2016). This is because the rate of char oxidation ($\dot{\omega}'''$) and the heat release rate (HRR or $\dot{Q}'''$) will increase with the oxygen concentration, which can be expressed by Arrhenius law as

$$\dot{\omega}''' = Ae^{\frac{E}{RT}} y_F^n y_{O_2}^{n_{O_2}} \tag{2.4}$$

$$\dot{Q}''' = \dot{\omega}''' \Delta H_{sm} \tag{2.5}$$

where A is the pre-exponential factor, E is the activation energy for the char oxidation, R is the universal gas constant, T is the temperature, y_F is the concentration of fuel, n is the reaction order of fuel, y_{O_2} is the concentration of oxygen, n_{O_2} is the reaction order of oxygen, ΔH_{sm} is the heat of smouldering.

As reported, for the wood chips, if the oxygen concentration increases from 3.6% to 21%, the smouldering temperature increases from 337 to 521 ℃, that is, a temperature

rise of 10 ℃ for every 1% increase of oxygen concentration (Malow M, 2018). However, above the atmospheric oxygen level (21%), the influence of oxygen concentration on smouldering flattens. For example, when the oxygen concentration increases from 23% to 35%, the smouldering temperature of peat only increases by 8 ℃ (Yang et al., 2019). Thus, the rate of char oxidation may change from oxygen-controlled to fuel-controlled, as the fuel properties (e.g. pore structures and intra-particle diffusion) also affect the oxygen supply. Note that smouldering combustion can be maintained when the oxygen concentration is as low as 3% (Schmidt et al., 2003).

In addition, increasing the oxygen concentration can trigger the smouldering-to-flaming (StF) transition (Putzeys et al., 2008). For PU foam, as the oxygen concentration increases from 21% to 23% under the same external heat flux of 7.23 kW/m^2, the smouldering-to-flaming transition occurs (Putzeys et al., 2008). This is because the flammability limit can be extended by the increased oxygen concentration, and the gaseous mixture inside the pores becomes easier to reach the lower flammability limits. Also, the increased smouldering temperature by the rich oxygen becomes hot enough to pilot the flammable mixture.

2.2.2 External heat flux

The external heat flux, especially external radiation, is almost common in any fire scenario, and it is also an important factor affecting the smouldering process. In contrast, the flame temperature is insensitive to the external radiation, because the radiation absorption of the flame sheet is negligible. In general, it has been experimentally observed that smouldering is not observed over 40 kW/m^2, under which condition piloted ignition is considered to occur (Bilbao et al., 2001).

The increased heat flux can directly raise the temperature of the solid-phase fuels via both the convection by the direct contact of the hot smoke or flame and the radiation by remote fire or hot walls, thus, increasing the rate of smouldering and heat release (Eqs. (2.4-2.5)). On the other hand, the increased heat flux can increase the smouldering reaction rate, further raising the heat generation and the solid-phase temperature. For wood, an increase of heat flux from 25 to 37 kW/m^2 increases the smouldering temperature from 472 to 529 ℃, with a temperature rise of around 5 ℃ for every 1 kW/m^2 increase of external radiation (Bilbao et al., 2001).

2.2.3 Bulk density

The fuel physicochemical properties affect the smouldering process in a more complicated manner (He et al., 2014; Saastamoinen et al., 2000; Yang et al., 2005). The bulk density of a porous material reflects its porosity and permeability. The relationship between density and porosity ($\emptyset$) can be expressed as:

$$\emptyset = 1 - \frac{Bulk\ density}{Particle\ density} \tag{2.6}$$

Furthermore, the permeability (k) is assumed to be vary with the porosity, which can be estimated according to Kozeny-Carman (KC) model, as

$$k = C_{KC} \frac{\emptyset^3}{(1-\emptyset)^2} \tag{2.7}$$

where C_{KC} is an empirical parameter which is related to the geometry, tortuosity and specific internal surface area of the material.

Permeability has been observed to affect the intensity of smouldering, since it controls the flow of the oxygen across the particles (Ohlemiller, 1990; Wang et al., 2019). According to Eqs. (2.6)&(2.7), the permeability will decrease with the density, resulting in poor oxygen supply, thus decreasing the HRR. However, decreasing porosity can reduce the heat loss at the same time. Such a competition mechanism eventually leads to an increase in smouldering temperature. For many low-density fuel beds (< 150 kg/m^3), such as PU foam, cotton, peat, and pine needles, they are easy to be compressed (also called highly compressible fuels) (Huang and Rein, 2019). As a result, their smouldering temperature and smouldering propagation rate increase significantly with their density.

However, for many fuel beds with large particles, such as coal dust, wood chip, and fibreboard, they are not easy to be compressed. Some other porous fuels are rigid, such as natural wood, coal layer, and shale, so they are almost incompressible. For these high-density and weakly compressible fuels, the smouldering process is not sensitive to the fuel density. Therefore, it can be concluded that the effect of bulk density on the smouldering process depends on the nature and state of the fuel beds and particles.

2.2.4 Particle size

The particle size of the fuel bed has a complex influence on smouldering, as it changes both the surface-to-volume ratio of the fuel particle and the solid porosity of the fuel bed (Wyn et al., 2020a). On the one hand, as the particle size is reduced, the surface-to-volume ratio of the fuel particle will increase; therefore, the available surface for heterogeneous oxidation increases reaction, so the HRR per unit volume will increase.

On the other hand, lowering the particle size may increase the fuel bulk density and reduce the air permeability, leading to larger thermal inertia and poor oxygen supply. For example, as the peat particle size increases from less than 1 mm to that greater than 4 mm, the smouldering temperature keeps almost constant at about 600 ℃ (Chen et al., 2014). Similarly, Ronda et al.(Ronda et al., 2017) showed that an increase of approximately 4 mm in particle size of pine bark decreases the peak smouldering temperature by only about 30 ℃. Moreover, Ryu *et al*. showed that the ignition front speed and burning rate will decrease with the particle size (Ryu et al., 2006; Yang et al., 2005). Ronda and He also showed smaller particle sizes determined a lower ignition temperature of pine bark (He and Behrendt, 2011; Ronda et al., 2017). In short, the overall influence of particle size on smouldering process still needs more future research.

2.2.5 Moisture content

As the moisture contents (MC) of most biowaste, like food waste, yard waste, and sludge, are usually very high (> 100% dry basis), it is of vital importance to learn about the effects of MC on the smouldering process. Actually, the effect of moisture content on smouldering combustion has been reported in many studies, especially in biomass (HE F, TANG Q X, 2012; He et al., 2014; Huang and Rein, 2017; Prat-Guitart et al., 2016a; Xiang ZHE, Weitao ZHAO, 2016). It has been observed that the moisture content of fuel could significantly lower the smouldering propagation rate, but has little effect on the maximum smouldering temperature within a certain range (Porteiro et al., 2010; Prat-Guitart et al., 2016b; Prat et al., 2015; Saastamoinen et al., 2000).

Moisture mainly affects the water evaporation process before the thermochemical processes, so it is a heat sink and may decrease the smouldering temperature (Wyn et al., 2020a). For example, as the MC of corn stalk ranges from 0% to 21%, the peak smouldering temperature keeps constant at about 710 ℃ (He et al., 2014). For peat, as the MC increases from 0% to 100%, the variation of smouldering temperature is less than 50 ℃ (Huang et al., 2016; Huang and Rein, 2017; Prat-Guitart et al., 2016a). Although the heat of evaporation (2.26 MJ/kg) is much higher than the heat of pyrolysis (about 1 MJ/kg), it is still much smaller than the heat of smouldering (10-20 MJ/kg). Also, there is a layer of dry fuel of several centimeters between the front of drying and the front of char oxidation, so that the cooling of oxidation front by the wet fuel is limited. Nevertheless, near the extinction limit of smouldering combustion, the smouldering

temperature will decrease sharply with a small increase of MC. In addition, there exists an upper moisture limit for self-sustaining smouldering, which has been reported by the previous literature (Prat-Guitart et al., n.d.; Watts and Kobziar, 2012).

2.2.6 Chemical components

Chemical properties, such as the composition of the fuel, can also influence the behaviour and products of smouldering. Specifically, the chemical property of biomass is usually characterized by the proximate analysis and the ultimate analysis (elemental analysis). The proximate analysis provides information on the mass fraction of moisture, volatile matter, fixed carbon, and ash. Material with high volatile matter was found to release high amounts of combustible gases (Wyn et al., 2020a). Ash has little effect on the combustion characteristics; however, metal impurities in the ash can catalyse the reactions, which has been explored by some authors (Belviso, 2018; Rizkiana et al., 2014). For example, Porteiro et al. pointed out that the ash content of the biomass has a major effect on the ignition front velocity (Porteiro et al., 2010).

Regarding the elemental composition for most biomasses, such as corn stalk (He et al., 2014), pine bark (Ronda et al., 2017), peat (Huang and Rein, 2019; Yang et al., 2016), and wood chips (Daouk et al., 2017), the C/H mass ratio is in the range of 6 to 10. In this range, the peak smouldering temperature shows an increasing trend as the C/H ratio increases. For example, as the C/H ratio increases from 6 to 10, the peak smouldering temperature increases from about 350 to 700 ℃. The C/H ratio of coal and char (or charcoal) is very large (over 15), the smouldering temperature can reach 710 ℃ when the C/H ratio is 17 (He et al., 2014; Wu et al., 2017). Therefore, it can be seen that for a similar type of fuel, the C/H mass ratio has a relatively monotonic effect on the smouldering temperature. However, if the types of fuel are very different (such as polymer and coal), the C/H mass ratio no longer reflects their smouldering temperature, while their other physicochemical properties become more important.

2.3 Smouldering emissions

As smouldering is in-completed combustion, far more complex and numerous emissions are emitted compared with flaming combustion. The plenty of toxic and polluting species inside of the smouldering emissions pose severe threats to humans and the environment.

The smouldering-originated toxic smoke is mainly comprised of CO_2, CO, CH_4, HCN, volatile organic compounds (VOCs), and particulate matter (PM) (Hu et al., 2018). Among the gas pollutants, CO_2 and CH_4 are the most significant greenhouse gases (GHG), while CO and VOCs are the major precursors for forming O_3 and secondary organic aerosol (SOA) via photochemical processes in the atmosphere (Urbanski et al., 2008). It is reported the smouldering peat fires that occurred in Indonesia in 1997 are responsible for 30 % of greenhouse gas (GHG) emissions that year (Page et al., 2002). Moreover, in smouldering combustion, the ratio of CO/CO_2 is much higher than that in conventional flaming combustion (Turetsky et al., 2015).

For the PM emissions from smouldering combustion, it can significantly vary in terms of size-resolved distributions (PM_1 to PM_{10}) and particulate concentrations depending on the test conditions (Iinuma et al., 2007; Tissari et al., 2008). The fine PM emissions from smouldering are a key factor leading to the haze event, which will cause respiratory diseases in humans and affect normal traffic. For example, during the El Nino event in 1997, an unprecedented severe smouldering fire occurred in Indonesia, which caused a large-scale transnational haze disaster affecting 100 million people in Southeast Asian countries (Page et al., 2002). This haze reduced visibility and further caused Garuda Indonesia Flight 152 to crash into mountains, killing all 234 people on board (Hu et al., 2018).

However, most smouldering emissions are still flammable because they still contain a large number of hydrocarbon pyrolysis gases and CO (H. Wang et al., 2021). In contrast, a flame can convert most smouldering emission gases into H_2O and CO_2 (Rein, 2016). Therefore, if applying a self-sustained flame above the smouldering process, we can not only generate extra heat, but also remove a large portion of flammable and toxic smouldering emissions, thus, promoting more efficient and cleaner smouldering applications. In addition, the smouldering emissions can be further handled to produce high-value products. For example, by condensing the smouldering emissions, bio-oil could be obtained (Vantelon et al., 2005; L Yermán et al., 2017a), which will be further discussed in the next section.

2.4 Waste treatment by smouldering

2.4.1 Waste removal by smouldering

Smouldering is an emerging technology for organic waste removal and valorization.

In recent decades, it has been successfully demonstrated to remove many kinds of organic waste such as bioliquid (Kinsman et al., 2017; Zanoni et al., 2019b), faeces (Fabris et al., 2017; L Yermán et al., 2017b), wastewater sludge (Feng et al., 2021; Rashwan et al., 2021), food waste (Song et al., 2022), and oil shale (Marcio F Martins et al., 2010). Yerman *et al.* (Tarek L Rashwan et al., 2016; Yermán et al., 2015) showed that self-sustained smouldering could be achieved in faeces with a moisture content up to 70% (wet mass basis) (L Yermán et al., 2017b; Yermán et al., 2015). And the pathogens inside the faeces can be effectively eliminated under the smouldering temperature (Yermán et al., 2015). Rahwan *et al.* reported that a robust smouldering in sludge could be sustained, the lower heating value of which was only 1.6 MJ/kg (Tarek L. Rashwan et al., 2016). Additionally, many efforts have been taken to improve the efficiency of smouldering-based waste removal technology, such as enhancing the oxygen supply (Pironi et al., 2009; Vantelon et al., 2005; L Yermán et al., 2017a; Yermán et al., 2016a) or increasing the porosity by adding sands (Switzer et al., 2014; L Yermán et al., 2017b). Smouldering is also used for co-waste management, which combines wastes that cannot smoulder alone with those that can smoulder, like sewage sludge mixed with wood chips and oil blended with agricultural waste (Rashwan et al., 2023). Moreover, not only laboratory-scale experiments, but also large-scale tests of organic waste smouldering have been developed (Rashwan et al., 2021).

Through the current research and successful applications, many attractive advantages and prospects of smouldering in organic waste removal have been demonstrated: (i) smouldering is able to treat the waste with high moisture content, thus, minimizing the pre-treatment processes; (ii) smouldering does not require an extra supply of fuel or energy (after ignition) to sustain its combustion process; (iii) smouldering can be self-sustained even in material with low calorific contents, like coal tar mixed with sand at about 1 MJ/kg (Pironi et al., 2011); (iv) smouldering technology is flexible in waste type and scale; (v) smouldering reactor has a lower temperature (500-800 ℃) than traditional incineration reactor, which improves the safety of the waste treatment process; and (vi) the efficiency of the smouldering process can be easily controlled by adjusting the airflow rate and oxygen concentration.

2.4.2 Waste-to-energy by smouldering

In addition, smouldering shows strong potential as a green waste-to-energy

technology, which has been applied to convert biowaste into high-value products (Torero et al., 2020; Wyn et al., 2020a). This is because intensive pyrolysis (Eq. (2.1)) occurs inside the smouldering front, which can convert biomass feedstock into biochar (solid), bio-oil (liquid), and bio-gas (Babu, 2008; Demirbas and Arin, 2002; Wang et al., 2010). Biochar is a solid product from biomass pyrolysis, which has a high carbon content. Biochar has potential usage in a wide field and is suitable for carbon sequestration due to its resistance to chemical and biological decomposition. Converting waste to biochar avoids the complete return of greenhouse gases (GHG) to the atmosphere, compared to natural decay or burning processes (Lee et al., 2020; Woolf et al., 2010). More importantly, different from the conventional pyrolysis process, pyrolysis involved in the smouldering can be sustained by the heat generated from the weak oxidation of the original fuel (Eq. (2.2)), requiring no external energy input. Up to now, researchers have successfully produced liquid bio-oil from the smouldering of faeces and used tyres (Vantelon et al., 2005; L Yermán et al., 2017a). Besides, the production of biochar through forestry waste smouldering has also been investigated (Rein, 2009a; Wyn et al., 2020b). For example, prior research (Wyn et al., 2020b) has shown that under the internal airflow velocities of 8 mm/s and 2 mm/, the yields of charcoal from forward smouldering are 40 % and 53 %, respectively, and the biochar under the airflow velocity of 8 mm/s has H:C and O:C ratio ranging from 0.01 to 0.23, and 0.35 to 0.71, respectively.

2.5 Concluding remarks

Smouldering is an emerging technology for organic waste removal and valorization, demonstrating attractive advantages. Previous research has proved that a self-sustained smouldering process can be successfully applied to remove various organic wastes with high moisture contents and low heating values. Smouldering also shows strong potential as a green waste-to-energy technology, which has been applied to convert waste into high-value products, like bio-oil and biochar. However, incomplete smouldering combustion generates a large amount of polluting and toxic emissions, which limits its further promotion and application.

CHAPTER 3

Methodology

Chapter 3 introduces the experimental material and methods used in **Chapters 4-7**.

3.1 Materials

3.1.1 Biowaste samples

Wood waste, coffee waste and organic soil were selected as representative biowaste and food waste as well as simulated sludge, as shown in Figure 3.1. The wood waste is provided by a local supplier (ECO-Greentech Ltd.). Initially, all the fuel samples were oven-dried at 90 ºC for 48 h, and their moisture contents were measured to be <8% when reaching a new equilibrium with ambient moisture. The density of coffee waste is measured to be 420 kg/m^3, which is much larger than that of wood waste (200 kg/m^3) and organic soil (145 kg/m^3), while the particle size of it is the smallest, which is less than 1 mm (20-40 mm for wood waste and ~2 mm for organic soil).

Figure 3.1. Photos of the biowaste samples used in experiments.

3.1.2 Charaterisation of samples

All biowaste samples are analyzed by three methods, namely, thermal analysis, elemental analysis, and proximate analysis. Before each analysis, the samples were pulverized into powders and dried at 90 °C for 48 h.

The thermal analysis for all samples was conducted with a PerkinElmer STA 6000 Simultaneous Thermal Analyzer in both air and N_2 atmospheres with a flow rate of 20 mL/min. Experiments were repeated twice for each case, and good repeatability is shown. Figure 3.2 shows the mass fraction, mass loss rate, and heat flow curves of (a) wood chips (wood waste), (b) organic soil, and (c) coffee waste. From the mass-fraction (TG) curves, it can be observed that the pyrolysis could consume nearly 70% of the fuel. The heat of smouldering (ΔH_{sm}) can be calculated by integrating the heat flow curve, which are 23.6 MJ/kg, 25.7 MJ/kg, and 33.4 MJ/kg for wood waste, organic soil, and coffee waste, respectively. Regardless of the oxygen concentration, the mass loss rate rapidly increases

at about 250 °C, which can be defined as the pyrolysis temperature.

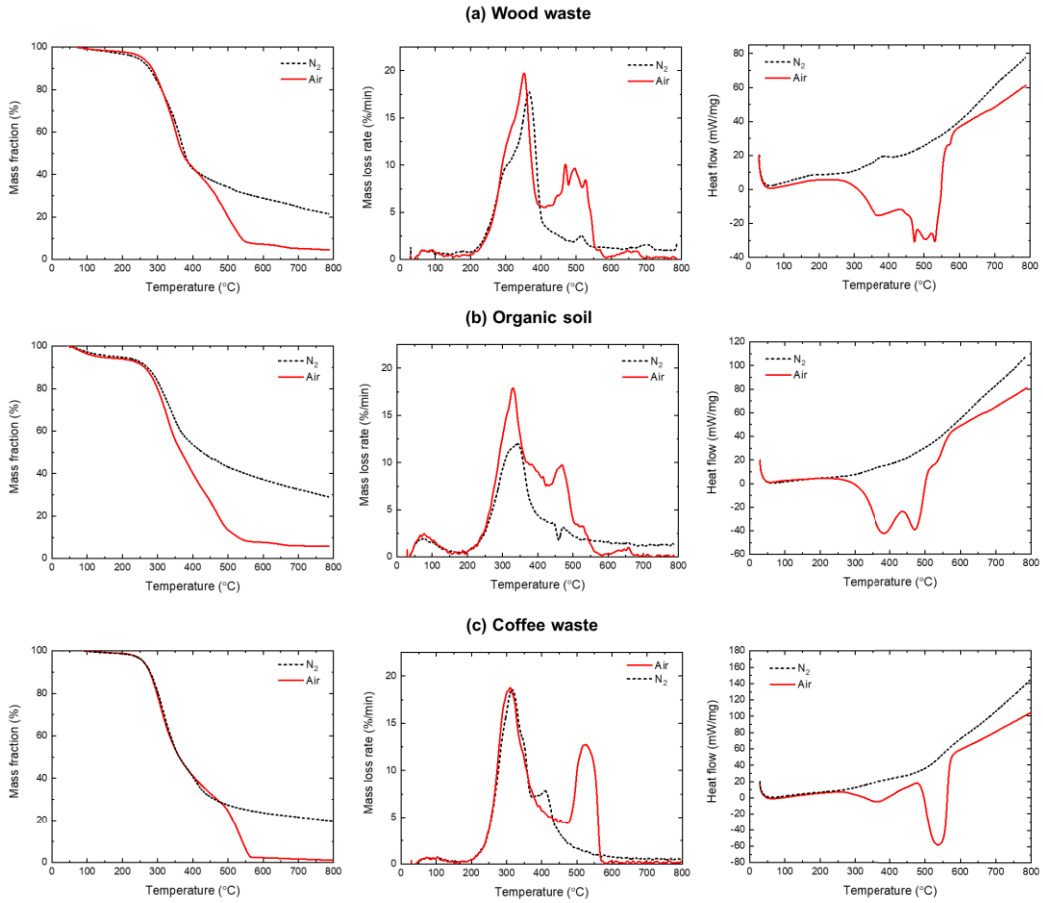

Figure 3.2. TGA-DSC results of (a) wood waste, (b) organic soil, and (c) organic waste at a heating rate of 30 K/min

The elemental and proximate analysis results are summarized in Table 3.1. It can be found that the volatile fraction of these three wastes only shows a slight difference, with the largest volatile fraction being observed for coffee waste (80.1%) and the smallest fraction for organic soil (70.8%). In terms of elemental analysis, the coffee waste has the highest C content of 53.21%, while the wood waste has the highest O content of 59.47%. In addition, coffee waste has both the highest C/O ratio (1.45) and H/O ratio (0.21).

Table 3.1. Properties of the tested materials

Properties	Wood waste	Organic soil	Coffee waste
Bulk density (kg/m^3)	200±10	145±10	420±10
Particle size (mm)	20-40	~2	< 1
Volatile fraction (%)	78.4	70.8	80.1
Fixed carbon (%)	17.0	23.5	18.8
Ash (%)	4.6	5.7	1.1

C (%)	36.30	46.09	53.21
H (%)	3.73	5.75	7.72
O (%)	59.47	47.46	36.71
N (%)	0.44	0.47	2.01
S (%)	0.06	0.23	0.35
C/O	0.61	0.97	1.45
H/O	0.06	0.12	0.21

3.2 Experimental setup

3.2.1 Smouldering burner

Two types of smouldering burner are used in this work, a metal-made bigger burner and a glass-made smaller burner. Depending on the objectives of each study, different burners will be selected. Besides, there are small differences in the dimensions of the burners used in different chapters, which is because new implementations and modifications are made during the research process to optimize the burners. However, it should be emphasized that all the data comparisons shown in this thesis are fair comparisons which is generated from the same experimental setup.

As shown in Figure. 3.2, the metal top-open smouldering reactor had a depth of 20 cm, an internal diameter of 14 cm, and a thickness of 3 mm. A 1-cm ceramic insulation layer was attached to the surface of the reactor to reduce the heat losses. At the bottom of the burner, there was a 5-cm deep air mixer to straighten and homogenize the upward airflow. The burning area of the reactor and the air mixer were separated by a steel mesh and a 4-cm gravel layer. To monitor the smouldering temperature, an array of eight K-type thermocouples (1-mm bead diameter) was inserted from the sidewall into the biomass sample, and their beads were aligned along the reactor axis from 0 cm (bottom) to 14 cm (1 cm below the top surface) with an interval of 2 cm.

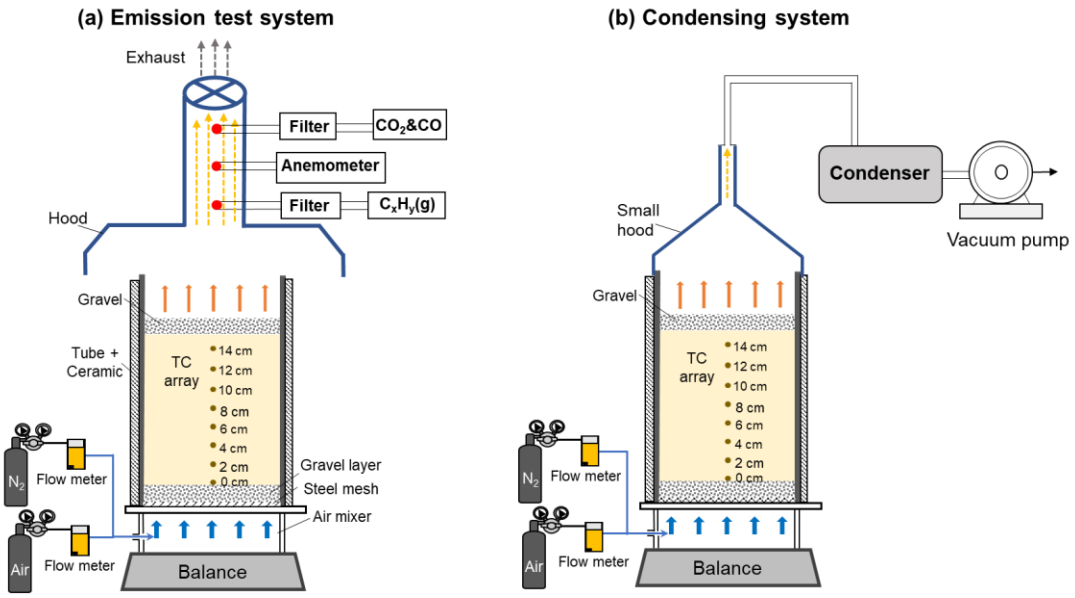

Figure 3.3. Self-designed experimental setup

To better observe the location and intensity of the glowing smouldering front, a quartz glass-made smouldering is also used (*Chapter 5*). The design of the glass burner is similar with that of the metal one with differences in size. It had a depth of 20 cm and an internal diameter of 10 cm. A 1 cm ceramic insulation layer was attached to the surface of the reactor to reduce the heat losses. To straighten and homogenize the air supply from the bottom, a steel mesh was placed 3 cm above the bottom of the reactor, and a 2-cm gravel layer was poured onto the top surface of the steel mesh. To monitor the temperature and trace the position of the smouldering front, an array of five K-type thermocouples (1.5 mm bead diameter) was inserted into the fuel along the axis from 0 cm (bottom) to 12 cm (top) with an interval of 3 cm.

For both burners, a forced oxidizer flow was supplied from the bottom of the reactor, and the flow rate was controlled by the flow meter. The oxygen concentration of the input oxidizer was modified by adding N_2 to the air stream. A coil heater buried in fuel bed was used to initiate the smouldering combustion, and a lighter or a spark (as a pilot source) was installed at 2 cm above the outlet of the reactor to ignite the smouldering emissions. The burner was located at an electrical balance during the whole smouldering process to record the real-time mass.

3.2.2 Emission test system

To quantify the emissions from biowaste smouldering, a gas collection and measurement system was built, as shown in Figure 3.3a. The emissions were entirely

collected using a fume extraction hood located above the reactor. In the extraction hood, three measuring points were designed in the centreline of the hood duct. The flow rate in the test point was measured by an anemometer (Testo 405i), which was almost constant during the tests. Three different kinds of gas species were measured in this study: carbon dioxide (CO_2), carbon monoxide (CO), and hydrocarbons ($C_xH_y(g)$). Detailed information for the measurement of each species will be introduced in *Chapter 5&7*.

3.2.3 Condensing system

As a pyrolysis-dominant process, significant liquid (called bio-oil) including the condensable organic compounds (tar) and water will be generated from the smouldering combustion under controlled airflow (Neves et al., 2011). Thus, a condensation system was built to quantify the liquid product from smouldering, as shown in Figure 3.3b. The emission from smouldering was collected via a hood entirely covering the top outlet of the burner. Then, the vapour was passed through a long pipe and finally condensed in the ice-cooled trappers. The mass of the bio-oil produced was obtained by weighing the trappers.

3.3 Experimental procedure

The smouldering combustion was initiated by the coil heater with the ignition protocol at 100 W, which was strong enough to generate a robust smouldering for the dry biomass. After forced ignition, a layer of fine and clean gravel with a constant heifht was placed on the fuel surface, as shown in Figure 3.3. This fine gravel layer prevented (1) the flying ash, (2) flame from flashing back to the smouldering reactor, and (3) the internal smouldering-to-flaming transition under a large high airflow rate, and it also provided an insulation layer to prevent the flame from directly heating the solid fuel.

Meanwhile, the forced oxidizer flow was then fed from the bottom with a prescribed flow velocity and oxygen concentration. Afterward, a lighter or a spark near the outlet was applied to ignite the emissions released from the smouldering biomass. If the flame was successfully piloted and self-sustained, the oxidizer flow velocity and oxygen concentration were gradually adjusted to find the limiting conditions.

Additionally, the experiments were also conducted without a pilot source to quantify the characteristics of gas-phase smouldering emissions and the condensed liquid by-products. The experiments were stopped when all thermocouple measurements were

below 200 ℃. For each case, at least three repeating tests were carried out to ensure the repeatability of the experiments. During the tests, the ambient temperature (T_a) was 23 ± 2 ℃, and the relative humidity was 50 ± 10%, and the pressure was 1 atm.

For this thesis, different biowastes, ignition positions, and smouldering time will be tested. More detailed information is illustrated in specific chapters.

CHAPTER 4

Limits of Sustaining a Flame above Smouldering Woody Biomass

4.1 Introduction

Smouldering is slow, low-temperature, and flameless burning of porous fuels and one of the most persistent types of combustion phenomena (Ohlemiller, 1985; Rein, 2014). Smouldering is a heterogeneous process sustained when oxygen directly attacks the hot fuel surface, which is the dominant burning phenomenon of reactive porous media like woods (Anca-Couce et al., 2012; Richter et al., 2021), coals (Melody and Johnston, 2015), and organic soils (Huang and Rein, 2016a; Lin et al., 2020). Generally, the combustion of the porous media can be approximated as two lumped chemical pathways, namely, pyrolysis and oxidation (Lin et al., 2019a; Rein, 2013). Pyrolysis will result in pyrolysis gas and char, which are both susceptible to subsequent oxidative reactions (Rein, 2014). The oxidation of char leads to smouldering combustion, while the gas-phase oxidation leads to flaming combustion (Rein, 2009b).

Although there are some similarities between flaming and smouldering combustion (Lin and Huang, 2021), smouldering is fundamentally different from flaming in terms of reaction chemistry and transport processes (Ohlemiller, 1985; Palmer, 1957; Rein, 2014). The initiation of smouldering requires a relatively small amount of energy (Lin et al., 2019a), and it may be sustained at an oxygen concentration as low as 12% and a moisture content higher than 100% (Huang et al., 2016; Huang and Rein, 2016a). In general, the maximum smouldering temperature ranges from 500 to 800 ℃, depending on the fuel types and operation conditions (Rein, 2016), which is much lower than the flame temperature (>1100 ℃) (Law, 2010). However, with a rich oxygen supply, the maximum smouldering temperature may exceed 1000 °C (Gao et al., 2021; Huang and Gao, 2021), causing the smouldering-to-flaming (StF) transition (Santoso et al., 2019) or the co-existence of smouldering and flaming (Huang and Gao, 2021; Lin et al., 2021b).

Combustion is considered to be an effective way to remove municipal solid wastes (MSW). Incineration, the traditional waste combustion method, has been widely used around the world. Over the last few decades, the incineration of waste has been investigated mainly from four aspects: (1) combustion characteristics under various conditions (Barnes, 2015; Donghoon and Sangmin, 2000; Tarelho et al., 2011), (2) cofiring with primary fuel (e.g. coal and natural gas) (Dmitrienko et al., 2018; Tillman, 2000), (3) incineration emissions (Hasselriis and Licata, 1996; Vainikka et al., 2012; Werther, 2007), and (4) incineration residues (Abbas et al., 2003; Łach et al., 2016).

Recently, smouldering, as a different combustion process from incineration, has been proposed for organic waste removal technology and has been successfully applied in the removal of bioliquids (Kinsman et al., 2017; Zanoni et al., 2019b), feces (Fabris et al., 2017; L Yermán et al., 2017b), sludges (Tarek L Rashwan et al., 2016), and oil shales (Marcio F Martins et al., 2010). Compared with incineration, the temperature inside the smouldering reactor is much lower (500-800 ℃), which improves the safety of the waste removal process. Moreover, such a smouldering-based technology minimizes the complex pre-treatment processes and is suitable for different kinds of organic wastes with high moisture contents (Tarek L Rashwan et al., 2016; Yermán et al., 2015). In recent years, many efforts have also been taken to improve the efficiency of smouldering-based waste removal technology (Pironi et al., 2009; Vantelon et al., 2005; L Yermán et al., 2017a; Yermán et al., 2016a). As oxygen concentration and oxidizer flow velocity are two critical parameters that directly affect the amount of oxygen transported to the smouldering front, they are crucial to the propagation and efficiency of smouldering combustion (Huang and Rein, 2016a; Lin and Huang, 2021; Ohlemiller, 1985; Rein, 2016; L Yermán et al., 2017b; Yermán et al., 2016a). Generally, a higher oxygen flow rate and concentration can make a more robust smouldering propagation (Lin and Huang, 2021; Pironi et al., 2009; Yang et al., 2019).

On the other hand, as an incomplete combustion process, smouldering generates many pollutions, posing severe threats to humans and the environment (Hu et al., 2018). The primary smouldering emissions include greenhouse gases (CO_2, CH_4), toxic compounds (e.g., CO, volatile organic carbon (VOC), NH_3), and particulate matters (PMs) (Michel et al., 2005; Van Der Werf et al., 2006; Wiedinmyer et al., 2006). Specifically, smouldering combustion has higher emission factors (EFs) of incomplete combustion products, such as CO and CH_4 than flaming combustion (Turetsky et al., 2015). And PM derived from smouldering combustion varies greatly from PM_1 to PM_{10} (Iinuma et al., 2007; Tissari et al., 2008). However, most smouldering emissions are still flammable because they still contain a large number hydrocarbon pyrolysis gases and CO (H. Wang et al., 2021). In contrast, a flame can convert most smouldering emission gases into H_2O and CO_2 (Rein, 2016). By sustaining a flame above the smouldering process not only can generate extra heat, but also remove a large portion of flammable and toxic smouldering emissions, thus, promoting more efficient and cleaner smouldering applications. However, the co-existence of flaming and smouldering on biomass has not been well explored so

far, posing a knowledge gap.

The purpose of this study is to explore whether the emissions from smouldering biomass can sustain a robust flame. Considering the oxygen supply is a key parameter of smouldering combustion, the critical airflow velocities (4-24 mm/s) and oxygen concentrations (14-21%) for the co-existence of smouldering and flaming are quantified experimentally and analyzed theoretically. The results are expected to help promote more environmentally friendly and energy-efficient smouldering applications.

4.2 Experimental method

4.2.1 Setup and fuel preparation

Wood chips, as representative biomass fuel, were chosen in this experiment (Figure 4.1). The particle size of the wood chips ranges from 2 mm to 20 mm, with an average of 12 mm, provided by a local supplier (ECO-Greentech Ltd.). The dry bulk density, solid density, and porosity were measured to be 200 ± 10 kg/m^3, 600 ± 20 kg/m^3, and 0.67, respectively. Before the test, the raw wood chips were thoroughly dried in an oven at 90 ℃ for 48 h and then stored in a sealed box to avoid the re-absorption of the ambient moisture (about 5% on the mass basis).

The schematic diagram of the experimental setup is also shown in Figure 4.1, and it mainly consisted of a tubular smouldering reactor, an ignition system, an oxidizer supply system, and two video cameras. The top-open smouldering reactor was made of 3-mm thick stainless steel, and it had a depth of 27 cm and an internal diameter of 13 cm. A 1-cm ceramic insulation layer was attached to the surface of the reactor to reduce the heat losses. Initially, a 5-cm sand layer was poured into the bottom of the reactor. Afterward, a test sample with a controlled mass of 405 ± 5 g was placed above the sand layer with a constant height of 15 cm. To monitor the smouldering temperature, an array of eight K-type thermocouples (1-mm bead diameter) was inserted from the sidewall into the biomass sample, and their beads were aligned along the reactor axis from 0 cm (bottom) to 14 cm (1 cm below the top surface) with an interval of 2 cm. To better observe the location and intensity of the glowing smouldering front, the glass tubular reactor was also used during the tests and was monitored by a side-view camera.

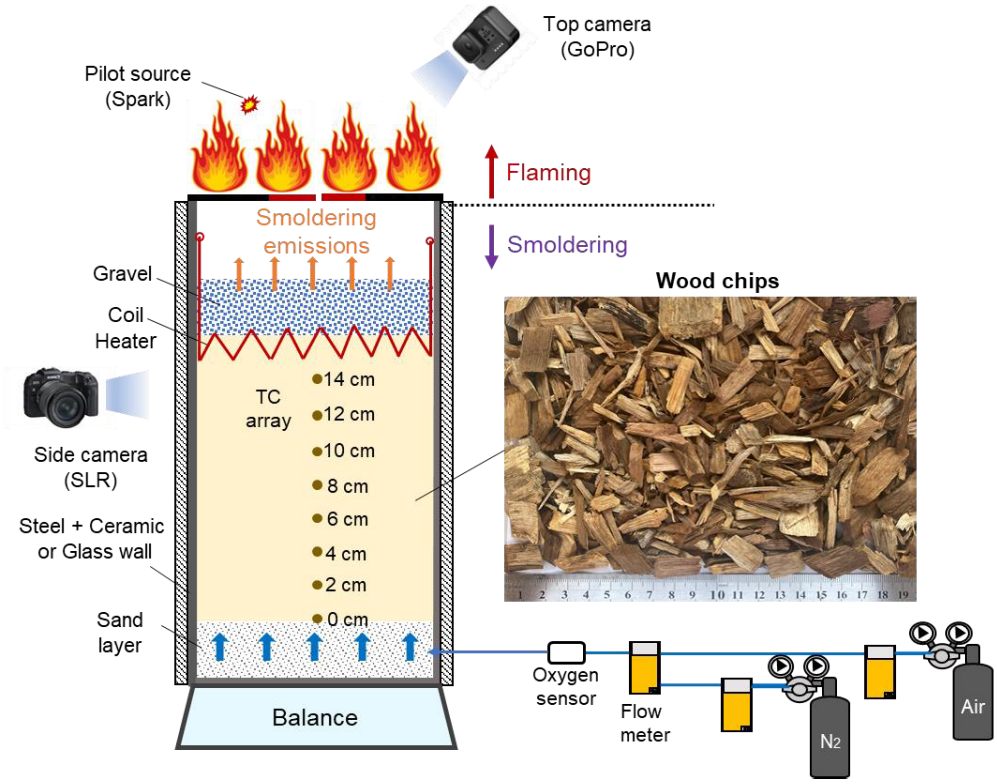

Figure 4.1. Schematic diagram of the experimental setup and the photo of wood chips samples.

A coil heater buried 1 cm below the surface of wood chips was used to initiate the smouldering combustion, and a lighter or a spark (as a pilot source) was installed at 2 cm above the outlet of the reactor. A forced oxidizer flow was supplied from the bottom of the reactor, and the flow rate was controlled by the flow meter. The oxygen concentration of the input oxidizer was modified by adding N_2 to the air stream. The experiments were performed at various oxygen concentrations (volume fraction, X_{O_2}) ranging from 14% to 21% and different internal flow velocities (u_g) from 4 mm/s to 24 mm/s. Note that the flow velocity was an overall value for the porosity of 1, and for the current wood-chip bed with a porosity of 0.67, the average velocity through the pores was 4.5 mm/s to 36 mm/s. The oxidizer flow was homogenized by the 5-cm sand layer below the wood chips. A top-view GoPro camera was used to record the experiment.

4.2.2 Experimental procedure

The smouldering combustion was initiated by the coil heater with the ignition protocol at 100 W for 15 min, which was strong enough to generate a robust smouldering for the dry biomass. After ignition, a layer of fine and clean gravel with a height of 7 cm was placed on the fuel surface, as shown in Figure 4.1. This fine gravel layer prevented

(1) the flying ash, (2) flame from flashing back to the smouldering reactor, and (3) the internal smouldering-to-flaming transition under a large high airflow rate, and it also provided an insulation layer to prevent the flame from directly heating the solid fuel.

Afterwards, the forced oxidizer flow was then fed from the bottom with a prescribed flow velocity and oxygen concentration. Afterward, a lighter or a spark near the outlet was applied to ignite the emissions released from the smouldering biomass. If the flame was successfully piloted and self-sustained, the oxidizer flow velocity and oxygen concentration were gradually adjusted to find the limiting conditions. The experiments were stopped when all thermocouple measurements were below 200 ℃. For each case, at least three repeating tests were carried out to ensure the repeatability of the experiments. During the tests, the ambient temperature (T_a) was 23 ± 2 ℃, and the relative humidity was 50 ± 10%, and the pressure was 1 atm.

Table 4.1. Average values of peak temperature of 1st stage ($T_{max,1}$) and 2nd stage ($T_{max,2}$), duration of 1st stage (Δt_1) and 2nd stage (Δt_2), and maximum mass flux of wood smouldering ($\dot{m}''_{max}$) under different airflow velocities (u_{air}) with uncertainties. ($\dot{m}''_g$ and $\dot{m}''_{O_2}$ are the mass flux of oxidizer flow and oxygen, respectively.)

u_{air} (mm/s)	$\dot{m}''_g$ (g/m^2·s)	$\dot{m}''_{O_2}$ (g/m^2·s)	$T_{max,1}$ (℃)	Δt_1 (min)	$T_{max,2}$ (℃)	Δt_2 (min)	$\dot{m}''_{max}$ (g/m^2·s)
4	4.8	1.1	465±33	54±3	650±20	386±10	5.3±0.5
5	6.0	1.4	473±45	44±4	700±22	320±9	8.0±0.6
7	8.4	1.9	493±23	37±4	788±36	217±10	10.3±0.4
9	10.8	2.5	514±43	31±2	927±29	178±8	15.0±0.6
12	14.4	3.3	619±48	26±3	1140±29	113±7	16.8±0.5
18	21.6	4.9	678±30	18±2	1180±32	76±8	21.4±0.4
24	28.8	6.6	738±35	15±2	1294±26	71±5	22.7±0.7

Table 4.2. Average values of peak temperature of 1st stage ($T_{max,1}$) and 2nd stage ($T_{max,2}$), and duration of 1st stage (Δt_1) and 2nd stage (Δt_2) under different oxygen concentrations (X_{O_2}) when u_g=12 mm/s with uncertainties. ($\dot{m}''_g$ and $\dot{m}''_{O_2}$ are the mass flux of oxidizer flow and oxygen, respectively.)

X_{O_2} (%)	$\dot{m}''_g$ (g/m^2·s)	$\dot{m}''_{O_2}$ (g/m^2·s)	$T_{max,1}$ (℃)	Δt_1 (min)	$T_{max,2}$ (℃)	Δt_2 (min)

14	13.5	2.2	581±44	50±4	836±24	184±7
15	13.6	2.3	588+48	46±3	841±30	157±5
16	13.6	2.5	597±31	40±4	930±26	149±6
18	13.7	2.8	610±47	31±5	1015±20	140±10
21	14.4	3.3	619±48	26±3	1140±29	113±7

4.3 Results and discussion

4.3.1 Co-existence of smouldering and flaming

To show the smouldering process clearly, photos of smouldering in the glass tubular reactor are presented. Figure 4.2 (a) shows an example of fire phenomena at a relatively low internal airflow velocity of 4 mm/s, where the smouldering combustion was observed, but no flame was successfully piloted. Once the electrical heating was applied, a reaction front was observed near the top surface, which was hot enough to emit visible light (glowing incandescence) (Huang and Gao, 2021). After ignition, there were two smouldering propagation stages, namely 1st-stage downward propagation and the 2nd-stage upward propagation, which were the same as past findings (Huang and Rein, 2019, 2017; Lin and Huang, 2021; H. Wang et al., 2021).

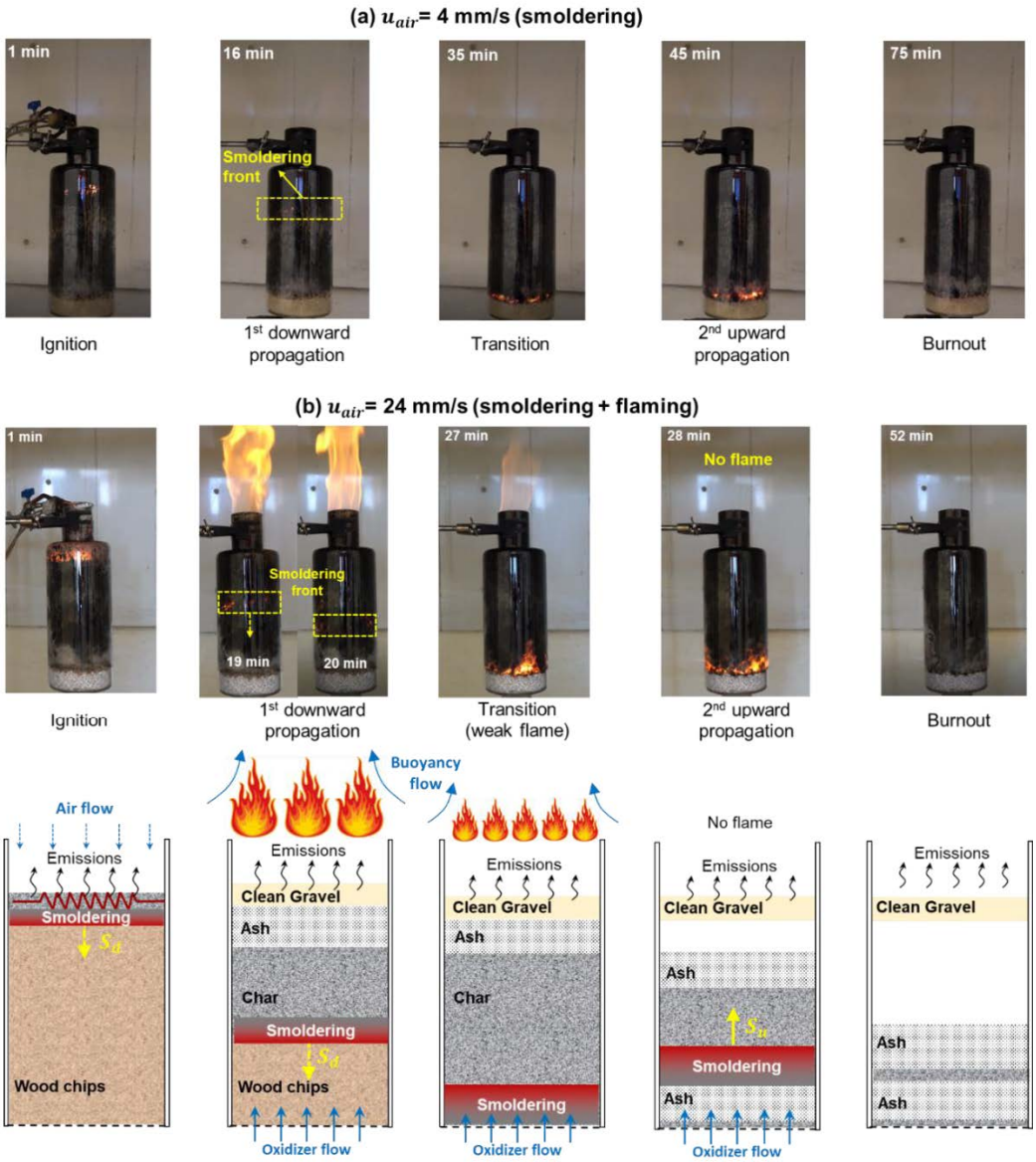

Figure 4.2. Snapshots of combustion phenomena of wood chips under airflow velocity of (a) 4 mm/s and (b) 24 mm/s with schematic diagrams.

In the 1st-stage downward propagation, the smouldering front moved as opposed to the internal airflow, and its structure included a drying sub-front, a fuel-pyrolysis sub-front, and a char oxidation sub-front. The endothermic pyrolysis of wood generated the gaseous pyrolyzates and solid char as

$$\text{Wood} \xrightarrow[\text{smouldering}]{\text{heat}} \nu_{py}\text{Pyrolyzates} + \left(1-\nu_{py}\right)\text{Char} \quad \text{(Wood pyrolysis)} \quad (4.1)$$

Thus, the white smoke was always observed, which was in the form of condensed tiny droplets of the pyrolysis gases and water vapor (Lin and Huang, 2021). The pyrolysis front was driven by the exothermic char oxidation.

$$\text{Char} + O_2 \rightarrow \text{Ash} + CO_2 + H_2O\ (g) + \text{other gases} + \text{Heat} \quad \text{(Char oxidation)} \quad (4.2)$$

Note that not all char were oxidized or burnt because only a limited oxygen supply was provided from the bottom. This heterogeneous char oxidation produced a mixture of hydrocarbons, CO_2, and CO (Lin et al., 2021b; Rein et al., 2009). Nevertheless, the smouldering emission gases (from both wood-pyrolysis and char-oxidation) cannot be piloted to sustain a flame, because under such a low airflow supply, the pyrolysis process inside the smouldering front was too weak to release sufficient fuel gases.

As the smouldering front approached the fuel-bed bottom, it transitioned to the 2nd-stage upward propagation mode to burn out all the remaining char. Then, the internal airflow was in the same direction as the smouldering propagation (i.e., the forward smouldering). For forward smouldering, it is essentially a fuel-regression process, where the smouldering front moved due to the burnout of fuel (Huang and Gao, 2021; Huang and Rein, 2019; Lin and Huang, 2021). The fuel for the 2nd stage propagation was primary char, so the char oxidation dominated, where more black smoke was observed. Eventually, wood chips were almost burned out and turned into white ash accompanied by a small amount of char. During the whole process, no flame could be piloted.

Figure 4.2(b) displays the burning process (photos and schematic diagram) at a higher airflow velocity of 24 mm/s (see Video. S2.2). Compared to the low-flow case in Figure 2.2(a), a similar two-stage smouldering propagation was observed, while the glowing smouldering front was brighter. More importantly, a flame could be piloted and sustained outside the reactor, co-existing with the downward smouldering propagation. Therefore, we conclude that flame can co-exist with the intense smouldering biomass inside the reactor and burn out almost all smouldering emissions. The oxygen supply to the external flame mainly comes from the buoyant flow from the ambient rather than the internal flow, because the oxygen of internal flow has been mostly consumed inside the smouldering front via char oxidation (H. Wang et al., 2021).

In the 1st-stage, the wood pyrolysis released large quantities of pyrolyzates (e.g., CO, H_2, CH_4, C_2H_4, and C_2H_6) (Eq. 4.1) (Dufour et al., 2008), which were highly flammable (Quintiere, 2006a). The mass flux of these flammable pyrolysis gases was controlled by the strength of the smouldering (char-oxidation) front which could be intensified by oxygen supply. Once the abundant pyrolysis emissions were released, a flame could be piloted as

$$\text{Smouldering emissions} + O_2 \rightarrow CO_2 + H_2O\ (g) \quad \text{(Flaming)} \quad (4.3)$$

The flame was initially intense with a bright orange color (see Figure 4.2(b)) that consumed almost all smouldering emissions during the 1st stage and effectively mitigated the pollutants. Afterward, as the smouldering front gradually approached the fuel-bed bottom, the flame became weaker and shorter, and it eventually extinguished from the 2nd stage to the final burnout due to the end of pyrolysis.

4.3.2 Smouldering temperature

Figure 4.3 shows the time evolution of the smouldering temperature at the airflow velocities of (a) 4 mm/s and (b) 24 mm/s of the same tests in Figure 4.2(a-b). The trends of the temperature profiles at different airflow velocities are similar, which are characterized by two characteristic peak values. The (peak) smouldering temperature of the 1st stage ($T_{max,1}$) is usually lower than that of the 2nd stage ($T_{max,2}$), consistent with the findings from previous studies (Huang and Rein, 2017; Lin and Huang, 2021; Wang et al., 2017). It is because the (1) biomass pyrolysis is endothermic, and (2) additional heat is required to maintain a fast propagation front in the 1st stage (Huang and Rein, 2019, 2017). Afterward, as the pyrolysis front reaches the bottom, only char oxidation exists, and the reaction front stays on the bottom, so a higher temperature is observed.

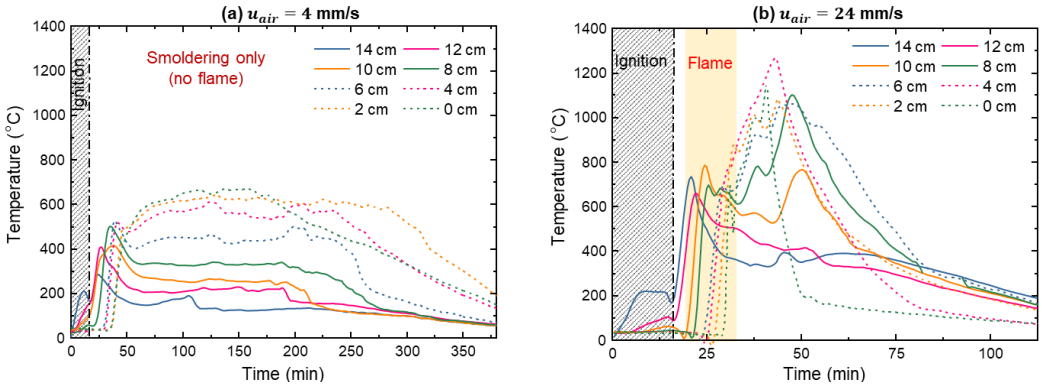

Figure 4.3. Smouldering temperature profiles at the airflow velocity of (a) 4 mm/s and (b) 24 mm/s, where the orange-color shaded area indicates the co-existence of flaming and smouldering.

Figure 4.4 further summarizes the average values of the peak temperature of two stages ($T_{max,1}$ and $T_{max,2}$) under varying oxygen supply. As expected, both peak temperatures increase with the flow velocity and oxygen concentration, because of stronger char oxidation. For example, as the airflow velocity increases from 4 to 24 mm/s in Figure 4.4(a) and Table 4.1, the 1st-stage peak ($T_{max,1}$) increases from 465 to 738 °C, and the 2nd-stage peak ($T_{max,2}$) increases from 650 to 1294 °C. However, as the flow

velocity continuously increases, their sensitivity to flow decreases, because the cooling effect of internal airflow becomes important (Lin et al., 2021a).

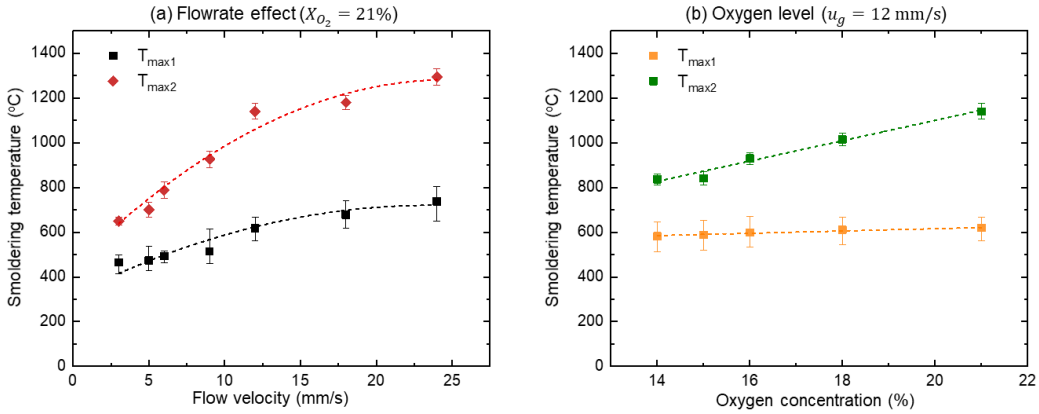

Figure 4.4. Peak smouldering temperatures of two stages vs. (a) flow velocity and (b) oxygen concentration, where the error bars show the experimental uncertainty of repeating tests.

4.3.3 Critical fuel-burning mass flux

The burning mass flux ($\dot{m}''$) is the mass loss rate per unit area of the fuel, which is an important parameter to quantify the combustion limits (Rich et al., 2007). Figure 4.5 shows the time evolution of the remaining mass fraction and the mass flux of the burning of wood under two representative internal airflow rates of (a) 4 mm/s and (b) 18 mm/s. Within a shorter period, nearly 60% of the fuel mass is consumed in the 1st-stage downward smouldering due to the release of all pyrolyzates. This is also supported by TGA results under inert atmosphere (Figure 3.2(a)), where 50-70% wood mass is lost due to pyrolysis depending on the final temperature. Although the 2nd char-oxidation smouldering stage lasts for a much longer period, the mass loss is smaller than 40%, and the burning mass flux remains stable at about 1-2 g/m^2·s until burnout.

At the low airflow velocity of 4 mm/s (Figure 4.5(a)), the maximum mass flux is about 4.3 g/m^2·s in the 1st-stage, and the flame of smouldering emission cannot be piloted. As the internal airflow velocity is increased to 18 mm/s, the maximum mass flux is increased to 22 g/m^2·s. As a result, a flame can be piloted outside when the smouldering burning flux reaches about 10 g/m^2·s, co-existing with smouldering (Figure 4.5(b)). The solid symbol in Figure 4.5(b) represents the moment of flame ignition, and the hollow symbol signifies the moment of flame extinction. The critical mass flux for flame ignition is similar to that of flame extinction at about 11 ± 1 g/m^2·s.

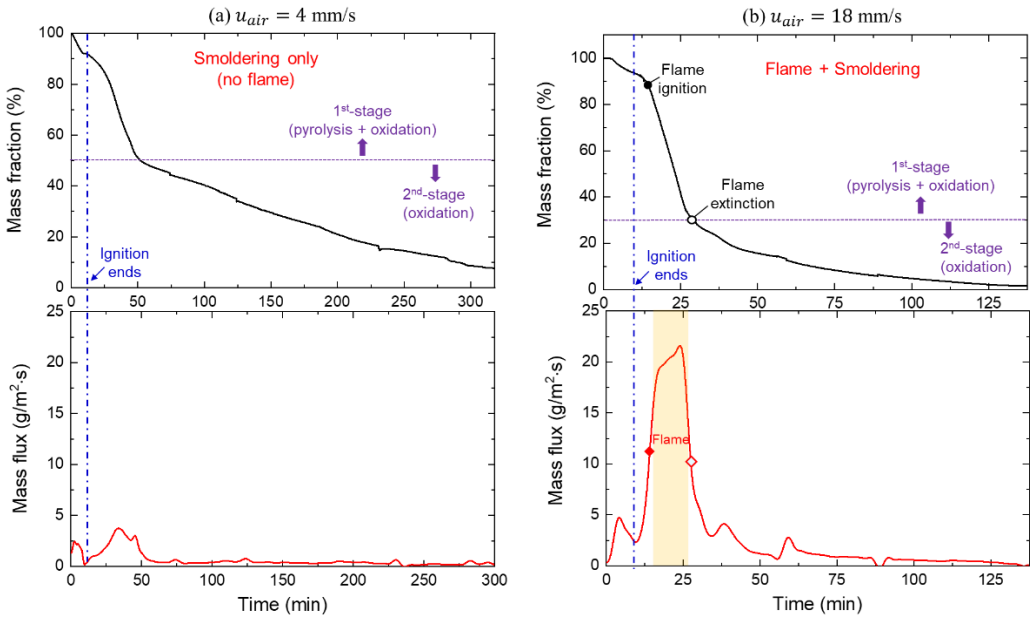

Figure 4.5. Evolution of fuel mass fraction and mass flux under the internal airflow velocity of (a) 4 mm/s and (b) 18 mm/s, where the oxygen concentration is 21%.

Figure 4.6 further summarizes the maximum fuel smouldering mass flux under different airflow velocities, as well as the critical mass flux for the co-existence of flaming and smouldering. As shown in Figure 4.6, the maximum mass flux increases from 5.3 g/m^2·s to 22.7 g/m^2·s, as the airflow velocity increases from 4 mm/s to 24 mm/s. However, the critical mass flux for piloting a flame on the biomass smouldering emissions or the co-existence of flaming and smouldering is almost constant at 11 ± 1 g/m^2·s. Moreover, as the airflow velocity is lower than about 6 mm/s, the maximum mass flux is below such a critical mass flux required for flame ignition. Therefore, we can also define a minimum airflow velocity for the 1st-stage smouldering front to sustain the flame on the smouldering emission, that is, 6 mm/s with 21% oxygen concentration.

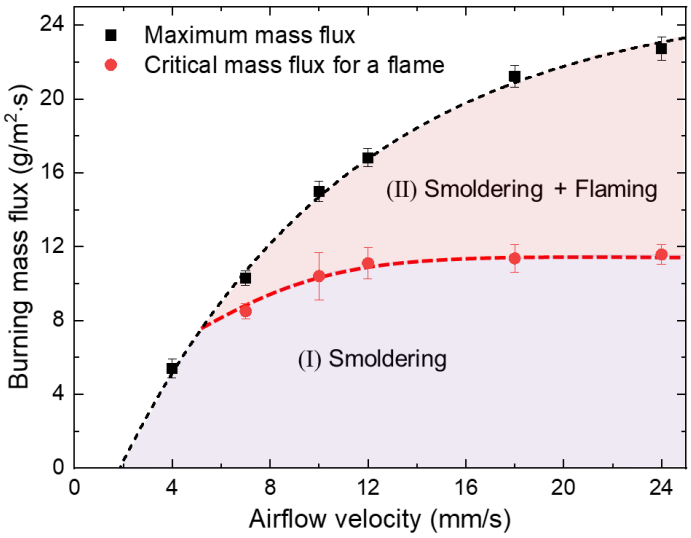

Figure 4.6. The maximum mass flux of smouldering burning and the critical mass flux for the co-existence of flaming and smouldering vs. the airflow velocity. The error bars represent the points for flame ignition (upper boundary) and flame extinction (lower boundary), and the lines are the manual fitting curves.

4.3.4 Critical fuel-burning mass flux

Figure 4.7 shows the durations of two smouldering stages versus airflow velocities from 4 mm/s to 24 mm/s. The duration of co-existed flame is also compared, where the flame must be stable, and the smoke from smouldering is almost consumed by the flame. In general, the durations for all combustion processes decrease, as the airflow velocity increases. The rising oxygen supply and oxidation rate increase the smouldering temperature, thus, accelerating both the heat-transfer and burning processes (Lin et al., 2021b). The 1st-stage downward smouldering lasts for a much shorter period than the 2nd-stage upward propagation. For instance, at the airflow velocity of 7 mm/s, the duration of the 2nd smouldering stage (217 min) is about sixfold of the 1st stage (37 min).

For the duration of flame, it is slightly shorter than that of the 1st smouldering stage, because the flame can only be piloted after reaching the critical smouldering mass flux of 11 ± 1 g/m^2·s. Thus, the flaming duration follows the same trend of 1st-stage smouldering, which decreases with the increase of airflow velocity. Specifically, at the airflow velocity of 7 mm/s, the flame duration is 25 min, which is 12 min less than the duration of 1st-stage smouldering. As the airflow velocity increases to 24 mm/s, the flame duration is the same as the 1st-stage smouldering, because of an intensive smouldering front.

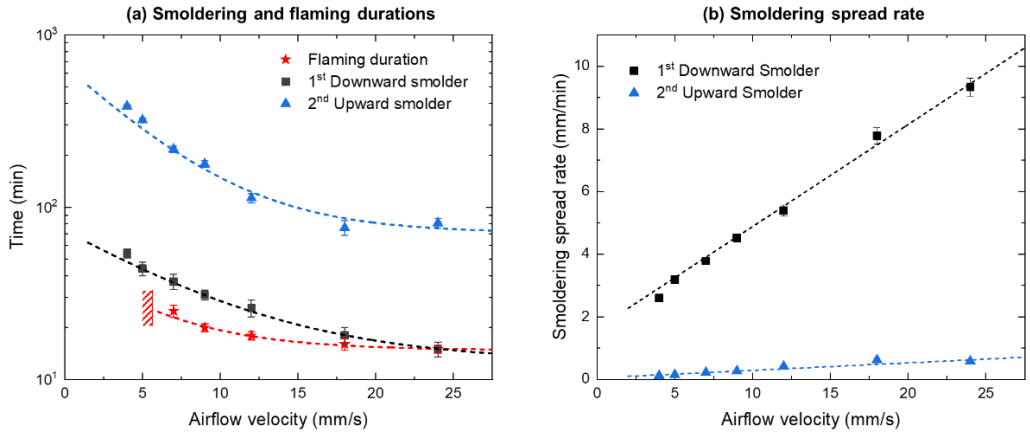

Figure 4.7. Duration of the flame and smouldering propagation at different airflow velocities, where symbols show the experimental data (with standard deviations), and lines are the manual fitting curves.

4.3.5 Effect of oxygen concentration

The effect of the oxygen concentration on the critical (minimum) flow velocity (u_{crt}) for the co-existence of smouldering and flaming is shown in Figure 4.8. The critical oxidizer flow velocity increases significantly as the oxygen concentration decreases. As previously shown in Figure 4.6, the critical flow velocity of air (X_{O_2} =21%) required for maintaining a flame is 6 mm/s. As the oxygen concentration (X_{O_2}) decreases to 18%, 16%, 15%, and 14%, the critical oxidizer velocity increases to 8 mm/s, 11 mm/s, 18 mm/s, and 24 mm/s, respectively. By fitting the experimental data in Figure 4.8, we can find an empirical correlation for the critical flow velocity (u_{crt}) and oxygen concentration (X_{O_2}) for the co-existence of smouldering and flaming as

$$u_{crt} = \frac{0.53}{Y_{O_2} - 11.6\%} \tag{4.4}$$

where the R^2 value is 0.96, showing a good quality of fitting.

The effect of oxygen concentration on the smouldering temperature is also shown in Figure 4.3(b). The peak temperature of the 2nd smouldering stage (T_{max2}) increases significantly with the oxygen concentration, whereas the 1st smouldering stage temperature (T_{max1}) is not so insensitive to the oxygen concentration. This is because the oxygen has a relatively weak effect on the wood pyrolysis in the 1st stage, while the 2nd-stage smouldering temperature is dominated by char oxidation. Moreover, increasing either the oxygen concentration or flow rate can lead to a stronger and taller flame because (1) the pyrolysis process inside the smouldering front becomes stronger (i.e., more

gaseous fuels emitted), and (2) the flame becomes partial premixed with the internal flow (i.e., some oxygen is not fully consumed in the smouldering front).

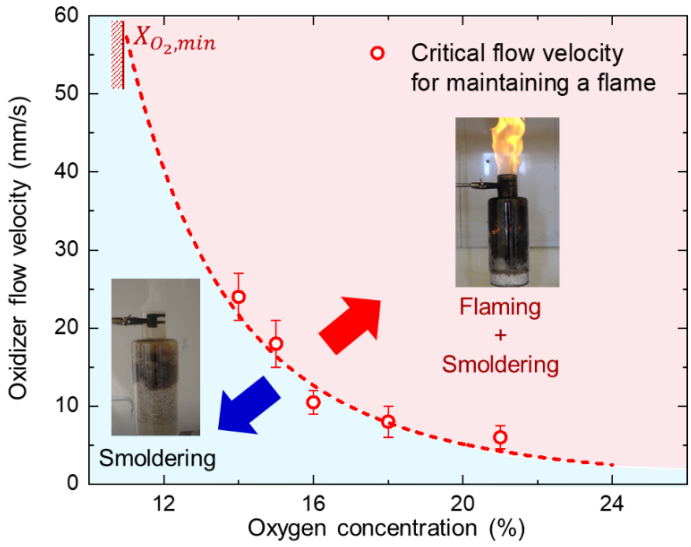

Figure 4.8. Critical oxidizer flow velocity (u_{crt}) for a stable flame under different oxygen concentrations (X_{O_2}) where the error bars represent the upper and lower boundaries of measuring points.

4.4 Theoretical analysis

4.4.1 Limits for flaming

In the conventional flaming process (e.g., a wood flame), the pyrolysis of wood is driven by the flame heat flux and other external heating, and the burning rate can be estimated by the mass transfer number (or B number) (Drysdale, 2011; Rich et al., 2007). In this work, the pyrolysis of wood chips is driven by the exothermic char oxidation inside the smouldering front, making a fundamental difference. To further understand the co-existence of flaming and smouldering combustion on typical biomass fuels, the limiting conditions for both (1) igniting and maintaining a flame and (2) the required smouldering front should be quantified.

To ignite and maintain a flame, a minimum mass flux of fuel gas is required. In the fire research community, such limiting conditions are called the “flash point” (to pilot a flame) and “fire point” (to maintain a piloted flame) (Drysdale, 2011; Rich et al., 2007). The limiting conditions of a robust and stable flame are considered in this research, so it is essentially a “fire point.” A simplified heat transfer analysis is proposed for the premixed fuel gases and flame, as illustrated in Figure 4.9(a).

The flame heat release rate ($\dot{q}''_f$) by burning the premixed pyrolysis gas should at least overcome the heat loss to the environment ($\dot{q}''_\infty$) and burner wall ($\dot{q}''_w$) as

$$\dot{q}''_f = \dot{m}''_{py,crt}\Delta H_f = \dot{q}''_\infty + \dot{q}''_w \quad (4.5)$$

where $\dot{m}''_{py,crt}$ is the minimum mass flux of pyrolysis gases; and ΔH_f is the heat of flaming combustion. Therefore, a minimum amount of pyrolysis gases should be generated to maintain the flame right above the fuel, which is found to range from 2 to 10 g/m^2·s for PMMA (Rich et al., 2007), wood (Emberley et al., 2017), and peat (Lin et al., 2019a). In this research, the smouldering emission ($\dot{m}''_{sm}$) is also found to be a constant, but at a slightly higher value of 11 ± 1 g/m^2·s (see Section 4.3.3 and Figure 4.6). It is because the total smouldering emissions also include the less flammable emission from char oxidation ($\dot{m}''_{sm} = \dot{m}''_{py} + \dot{m}''_{ox} > \dot{m}''_{py}$), although the pyrolysis gases of wood chips inside the smouldering reactor is primary.

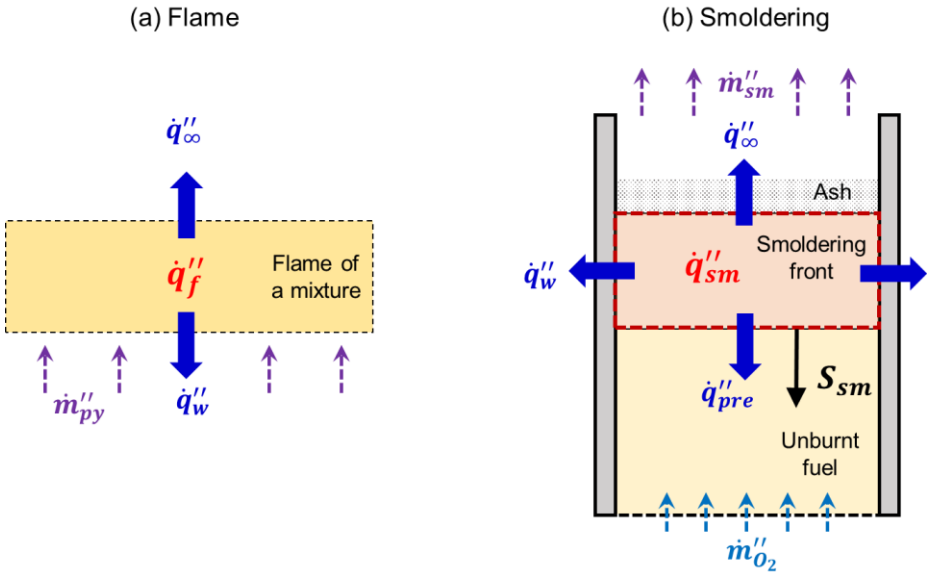

Figure 4.9. The energy balance of (a) flame of a mixture and (b) smouldering front inside the reactor.

4.4.2 Limits for smouldering and oxygen supply

To generate a minimum mass flux of fuel gas for sustaining a flame, the smouldering front and char oxidation should be strong enough to drive a strong pyrolysis process. Therefore, the limiting condition of sustaining a flame becomes the limiting condition of the smouldering front. Then, a simplified heat transfer analysis is also proposed for the smouldering front, as illustrated in Figure 4.9(b).

The smouldering heat release rate ($\dot{q}''_{sm}$) should first overcome the overall cooling

rate ($\dot{q}_c''$) as

$$\dot{q}_{sm}'' \geq \dot{q}_c'' \tag{4.6}$$

In general, the smouldering front is cooled by the environment ($\dot{q}_\infty''$), reactor wall ($\dot{q}_w''$), and the preheat zone ($\dot{q}_{pre}''$). Moreover, it should also ensure strong pyrolysis to generate sufficient gaseous fuel ($\dot{m}_{py,crt}''$), which is controlled by the oxygen supply as

$$\dot{q}_{sm}'' = \dot{m}_F'' \Delta H_{sm} = \frac{\dot{m}_{py,crt}''}{\nu_{py}} \Delta H_{sm} = \dot{m}_{O_2,crt}'' \Delta H_{ox} = \rho_g Y_{O_2} u_{crt} \Delta H_{ox} \tag{4.7a}$$

where ν_{py} is the stoichiometric coefficient of pyrolysis gas in Eq. (4.1); $\dot{m}_{O_2,crt}''$ is the critical mass flux of oxygen; ρ_g, Y_{O_2} and u_{crt} are the density, oxygen mass fraction, and critical velocity of the supplied oxidizer flow, respectively. By reorganizing, we have

$$u_{crt} = \frac{\dot{m}_{py,crt}'' \Delta H_{sm}}{\nu_{py} \rho_g \Delta H_{ox} Y_{O_2}} \propto \frac{1}{Y_{O_2}} \tag{4.8a}$$

Therefore, the critical opposed flow velocity for the co-existence of flaming and smouldering combustion is inversely proportional to the oxygen concentration, which explains the overall trend of experimental data in Figure 4.8.

As seen from Figure 4.9 and Eq. (4.8), by decreasing the oxygen concentration, the required opposed flow velocity will dramatically increase to maintain an independent flame outside the smouldering reactor. However, as the flow velocity continuously increases, its direct cooling effect on the smouldering front can no longer be ignored. Eventually, smouldering will be blown off by a fast and oxygen-lean flow (Huang and Gao, 2021; Lin et al., 2021a). The cooling of oxidizer flow could be considered as a reduction in the heat of oxidation as

$$\frac{\dot{m}_{py,crt}''}{\nu_{py}} \Delta H_{sm} = \dot{m}_{O_2,crt}'' \Delta H_{ox} - \dot{q}_{flow}'' \tag{4.7b}$$

where the cooling effect of internal flow is reflected by the increase of flow enthalpy after passing through the smouldering front as

$$\dot{q}_{flow}'' = \nu_{em} \rho_g u_{crt} c_p (T_{sm} - T_\infty) \tag{4.9}$$

where ν_{em} is the stoichiometric coefficient of emission gases. Thus, there is minimum oxygen concentration ($Y_{O_2,min}$), below which the gas flow through the smouldering front become a net cooling ($\dot{m}_{O_2,crt}'' \Delta H_{ox} - \dot{q}_{flow}'' = 0$). From Eq. (4.7a), we can derive

$$Y_{O_2,min} = \frac{\nu_{em} c_p (T_{sm} - T_\infty)}{\Delta H_{ox}} \tag{4.10}$$

By re-arranging Eq. (4.7b), we have

$$u_{crt} = \frac{\dot{m}''_{py,crt}\Delta H_{sm}}{\rho_g \nu_{py}\Delta H_{ox}\left(Y_{O_2} - Y_{O_2,min}\right)} = \frac{C}{\left(Y_{O_2} - Y_{O_2,min}\right)} \qquad (4.8b)$$

where $C = \dot{m}''_{py,crt}\Delta H_{sm}/\nu_{py}\rho_g\Delta H_{ox}$ is a fuel-related constant. Based on experimental data in Figure 4.8 and Eq. (4.4), we can find that for the current fuel of wood chips, $C = 0.53$ [mm/s] and $Y_{O_2,min} \approx 11.6\%$.

On the other hand, if the forced oxygen supply is removed, there could still be a natural oxygen supply, driven by a minimum buoyancy and diffusion flow (u_{diff}) when the fuel is exposed to the ambient. In that case, there could also be an upper limit of the critical oxygen concentration, above which the co-existence of flaming and smouldering is guaranteed, even if under a very small natural diffusion flow. In the future, more experiments and numerical simulations can be conducted for different fuel types, flow compositions, and environmental conditions to explore the co-existence of flame and smouldering and further verify the limiting conditions.

4.5 Concluding remarks

In this work, we successfully verify that (1) the smouldering emission of biomass can be piloted to sustain a flame and (2) flame can co-exist with smouldering combustion. With the smouldering ignition from the top and the flow from the bottom, the smouldering front first propagates downwards (1st-stage opposed smouldering) to the fuel-bed bottom and then propagates upward (2nd-stage forwards smouldering). The flame could only be piloted and self-sustained in the 1st-stage smouldering because of an intense pyrolysis process within the smouldering front. The critical smouldering burning mass flux for maintaining a stable flame remains constant at 10-12 g/m^2·s.

The co-existence of flaming and smouldering depends on the oxygen supply to the smouldering front, which is verified by theoretical analysis. The minimum opposed flow velocity required to maintain the stable flaming increases from 6 mm/s to 24 mm/s, as the oxygen concentration decreases from 21% to 14%. Moreover, increasing oxygen supply enhances the flame intensity and height, but the flame duration is reduced due to the accelerated burning processes. This work enriches strategies for the clean treatment of smouldering emissions and promotes an energy-efficient and environment-friendly method for biowaste removal.

CHAPTER 5

Smouldering-based Organic Waste Removal with Smoke Emissions Cleaned by a Self-sustained Flame

5.1 Introduction

Smouldering is slow, low-temperature and flameless burning of porous fuels, which is a heterogeneous oxidative process sustained by the heat evolved when oxygen directly attacks a hot fuel surface and is different from flaming combustion in terms of transport processes and time scales (Ohlemiller, 1985; Rein, 2014). Once ignited, smouldering can survive in extreme conditions (e.g. with poor oxygen supply and high fuel moisture) and is the primary burning phenomenon of condensed-phase reactive porous media such as wood (Ohlemiller, 1991; S. Wang et al., 2021), incense (Lin et al., 2021a), peat (Huang and Rein, 2016a), cotton (Xie et al., 2020), and coal (Wu et al., 2015). Smouldering is the leading cause of casualties and injuries in residential fires, industrial fires and natural fires (Quintiere, 2006b), but recent innovative developments (Hernandez-Soriano et al., 2016; Xin et al., 2021) have potentially revealed its wide application prospects.

In recent years, smouldering combustion has become one of the attractive alternatives for organic waste removal (Rashwan et al., 2021; Torero et al., 2020) that has been successfully applied in small- and large-scale tests to remove organic wastes with high moisture content like bioliquid (Kinsman et al., 2017; Zanoni et al., 2019b), feces (Fabris et al., 2017; L. Yermán et al., 2017), wastewater sludge (Feng et al., 2021; Rashwan et al., 2021), and oil shale (Marcio F Martins et al., 2010). For example, Yerman *et al.* (Tarek L. Rashwan et al., 2016; Yermán et al., 2015) showed that self-sustained smouldering could be achieved in feces with moisture contents up to 70%. Rahwan *et al.* (Tarek L. Rashwan et al., 2016) reported that robust smouldering in sludge could be sustained with a lower heating value of 1.6 MJ/kg. Also, many efforts have been also taken to improve the efficiency of smouldering-based waste removal technology, such as enhancing the oxygen supply (Pironi et al., 2009; Vantelon et al., 2005; L Yermán et al., 2017a; Yermán et al., 2016b) and adding sand to create a porous matrix (Switzer et al., 2014; L. Yermán et al., 2017).

On the other hand, toxic emissions from smouldering-based removal technology may pose severe threats to human health and environmental quality, which is a major public concern that limits its further promotion and application. Smoke produced by smouldering is mainly comprised of CO_2, CO, CH_4, HCN, NO_x, volatile organic compounds (VOCs) and particulate matter (PM) (Hu et al., 2018; Ravindra et al., 2019). Among them, CO_2 and CH_4 are the most significant greenhouse gases which accelerate

the global warming. NO_x and VOCs (including a wide range of hydrocarbons, halocarbons and oxygenates) are the major precursors of O_3 and secondary organic aerosol (SOA) after complex photochemical processes (Urbanski et al., 2008). CO exposure can lead to health effects of human being, and even causes death. PMs emitted from smouldering, ranging from PM_1 to PM_{10}, is the key factor for causing haze episodes and can cause respiratory disease and induce cancer of people (Hu et al., 2018). Thus, with the fast-growing demand for clean environment and sustainable development, it is urgent to deepen our understanding and develop new strategies to mitigate the pollution of smouldering-based removal technology.

Considering that smouldering emissions are flammable, owing to the existence of large amounts of unburnt hydrocarbons, our previous work has proposed a novel method to clean the toxic smoke via igniting these smouldering emissions (Chen et al., 2023). As shown in Figure 3.1, a flame that combusts the smouldering emissions can co-exist with the smouldering combustion of wood wastes underneath with an appropriate air supply. However, whether the fuel type affects the critical conditions and the efficiency for a flame to purify the smouldering emissions is still unknown, posing a significant knowledge gap.

Therefore, the main purpose of this study is to explore the impacts of fuel types on the smouldering characteristics and the critical conditions for maintaining a flame to purify the smouldering emissions. The experiments were conducted with three different organic wastes, including coffee waste, wood waste, and organic soil (simulated sludge) at airflow velocities from 3 mm/s to 24 mm/s. During the tests, smouldering emissions were measured with and without purification of flame to quantify the efficiency of pollution mitigation. The results obtained from this study will be helpful for the development of organic waste treatment by using smouldering combustion in an environmentally friendly and energy efficient way.

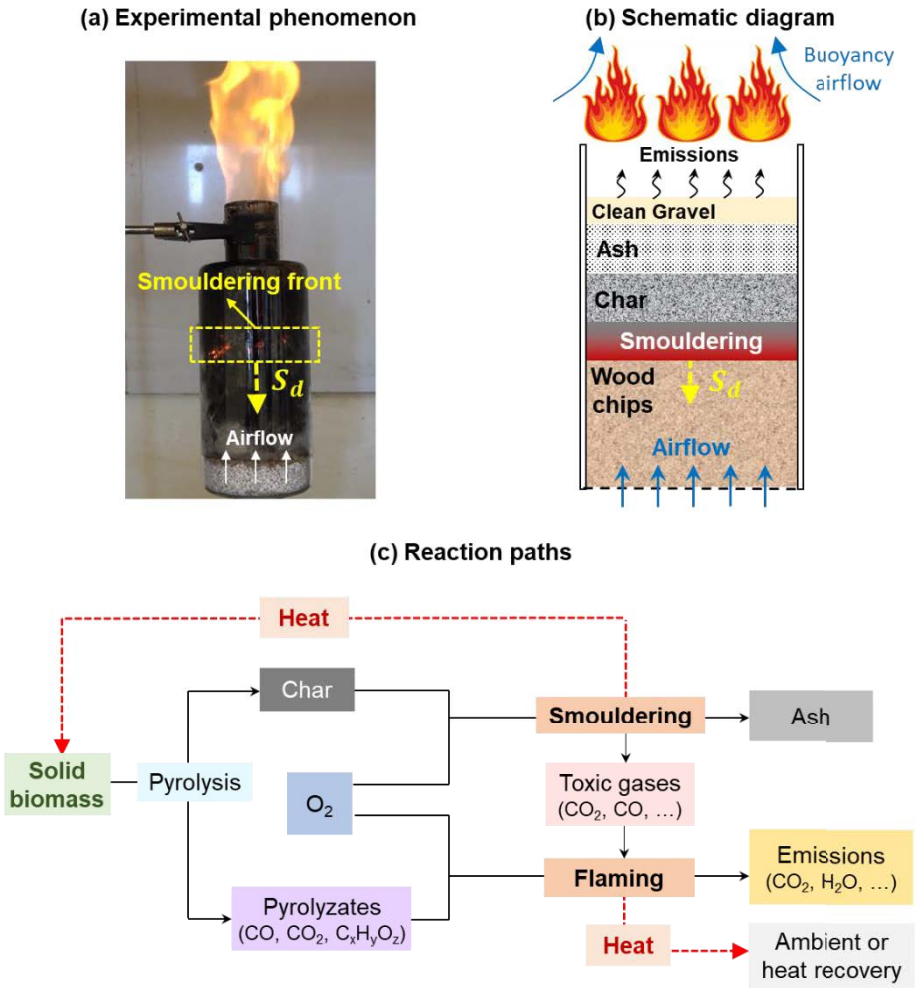

Figure 5.1. Co-existence of smouldering and flaming of the wood waste (Chen et al., 2023): (a) experimental phenomenon, (b) schematic diagram, and (c) reaction paths.

5.2 Methods

5.2.1 Organic waste samples

Wood waste, coffee waste and organic soil were selected as representative biowaste and food waste as well as sludge, as shown in Figure 3.1. Initially, all the fuel samples were oven-dried at 90 ^{o}C for 48 h, and their moisture contents were measured to be <8% when reaching a new equilibrium with ambient moisture. The main properties of the three fuel samples are compared in Table 3.1, with clear differences in terms of density and particle size. In particular, the density of coffee waste is measured to be 420 kg/m^3, which is much larger than that of wood waste (200 kg/m^3) and organic soil (145 kg/m^3), while the particle size of it is the smallest, which is less than 1 mm (20-40 mm for wood waste and ~2 mm for organic soil). On the other hand, the volatile fraction of these three wastes

only shows a slight difference, with the largest volatile fraction being observed for coffee waste (80.1%) and the smallest fraction for organic soil (70.8%). In terms of elemental analysis, coffee waste had both the highest C/O ratio (1.45) and H/O ratio (0.21). The thermal analysis for all the samples was conducted with a PerkinElmer STA 6000 STA and the representative TG-DSC data are shown in Figure 3.2.

5.2.2 Experimental setup

The experimental setup was upgraded from our previous device in Chapter 4 (Chen et al., 2023), which included a cylindrical smouldering reactor, an electrical balance, an ignition system, an air supply system, and an emission test system, as illustrated in Figure 5.2. The open-top reactor was made of 3-mm thick quartz glass, and it had a depth of 20 cm and an internal diameter of 10 cm. A 1 cm ceramic insulation layer was attached to the surface of the reactor to reduce the heat losses. To straighten and homogenize the air supply from the bottom, a steel mesh was placed 3 cm above the bottom of the reactor, and a 2-cm gravel layer was poured onto the top surface of the steel mesh. Afterwards, a test sample was placed on the gravel layer with a constant height of 14 cm. To monitor the temperature and trace the position of the smouldering front, an array of five K-type thermocouples (1.5 mm bead diameter) was inserted into the fuel along the axis from 0 cm (bottom) to 12 cm (top) with an interval of 3 cm.

A coil heater buried 1 cm below the top of the fuel surface was used to initiate the smouldering combustion, and a lighter (as a pilot source) was installed at 2 cm above the outlet of the reactor to ignite the smouldering emissions. A forced airflow was supplied from the bottom end of the reactor, and the airflow rate was controlled by a flow meter. The experiments were performed at various airflow velocities (u) ranging from 3 mm/s to 24 mm/s.

The emissions were entirely collected using a fume extraction hood located above the reactor (Figure 5.2). In the extraction hood, two measuring points were designed in the centreline of the hood duct. The flow rate in the test point was measured by an anemometer (Testo 405i), which was constant at 0.017 ± 0.005 m^3/s during the tests. Three different gas species were measured in this study: carbon dioxide (CO_2), carbon monoxide (CO), and unburnt hydrocarbons (HC). After collecting the PM emissions using a quartz filter, CO and CO_2 were measured concurrently by a TSI 7575 Gas Analyzer, and the unburnt HC was measured by SKY2000 Portable Gas Analyzer.

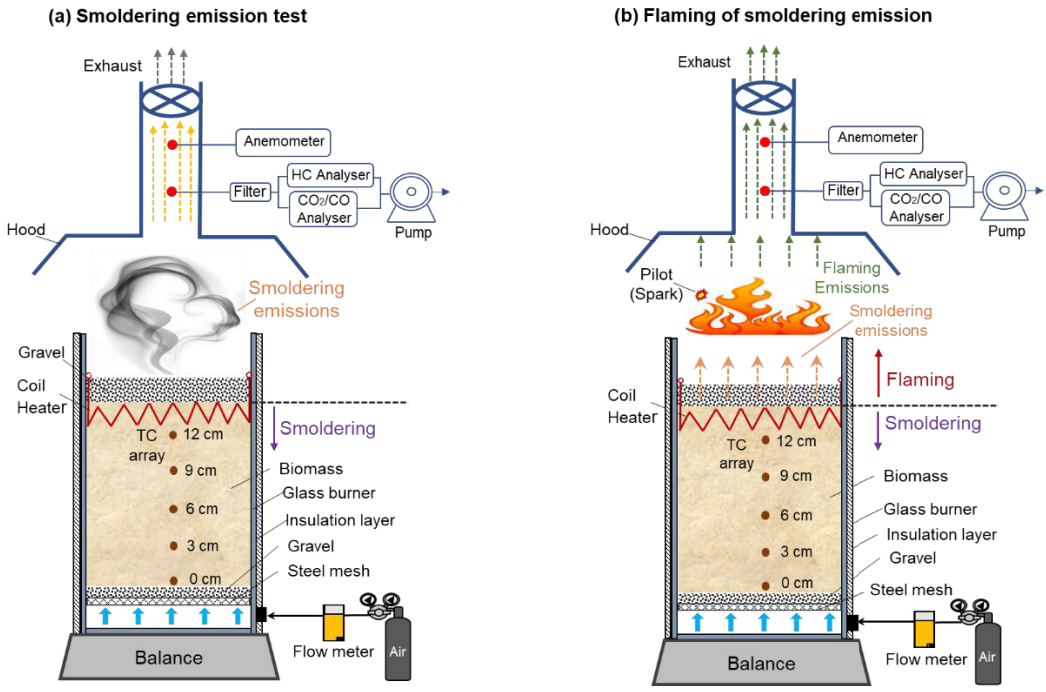

Figure 5.2. Schematics of the experimental setups for (a) smouldering waste removal without smoke emission removal, and (b) smouldering waste removal with smoke emission removed by flame.

5.2.3 Experimental procedure

The ignition protocol involved setting the pilot heating rate to 100 W for 2 min, which was strong enough to initiate robust smouldering combustion of dry biomass. After forced ignition, a layer of fine and clean gravel with a height of 3 cm was placed on the fuel surface (Chen et al., 2023), and the forced airflow was fed from the bottom of the reactor with a prescribed flow velocity. Initially, the experiments were conducted without a pilot source to quantify the characteristics of smouldering emissions, as shown in Figure 5.2a. Afterward, a fresh sample was tested under the same airflow velocity, but a pilot source was applied, aiming to ignite the smouldering emissions, as shown in Figure 5.2b. Meanwhile, the emissions purified by the flame were also quantified and compared with those without flame.

All the experiments were stopped when all thermocouple measurements were below 200 °C. For each case, at least two tests were carried out to ensure the repeatability of the experiments. During tests, the ambient temperature (T_a) was 23 ± 2 °C, relative humidity was 50 ± 10%, and pressure was 1 atm.

5.3 Results and discussion

5.3.1 Phenomena of co-existence of smouldering and flaming

Figure 5.3 shows an example of the combustion phenomenon of the wood waste at a relatively large airflow velocity of 18 mm/s. Similar to our previous findings (Chen et al., 2023), once ignited on the top, the smouldering front first propagated downward (1st stage, opposed). As the smouldering (glowing) front approached the fuel-bed bottom, it transitioned to the upward propagation (2nd stage, forward). More importantly, under such a large airflow velocity, the smouldering emissions from the 1st downward spread stage could be ignited and sustained a stable flame because the pyrolysis process dominated in this stage where a large number of flammable pyrolyzates were emitted. However, the flame can no longer be maintained at the 2nd stage until burnout because the pyrolysis process was almost finished at the first stage.

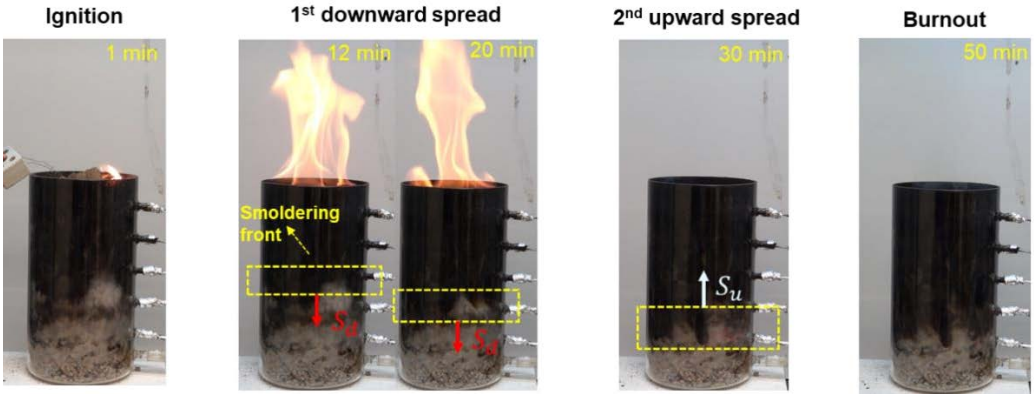

Figure 5.3. Combustion phenomenon of wood waste with a bottom airflow velocity of u = 18 mm/s.

5.3.2 Smouldering temperature and spread rate

Figure 5.4 shows the smouldering temperature evolutions of wood waste, coffee waste, and organic soil at the airflow velocities of 18 mm/s. In general, the temperature profiles of different organic wastes are similar, showing two characteristic peak values. These two peaks correspond to the two smouldering stages as shown in Figure 5.3, that is, 1st downward (opposed) spread, and 2nd upward (forward) spread. The peak temperature of the 1st stage ($T_{max,1}$) is usually lower than that of the 2nd stage ($T_{max,2}$), consistent with the major findings from previous studies (Huang and Rein, 2017; Lin and Huang, 2021). It is because fuel pyrolysis dominates the 1st stage, which is an endothermic process. Then, additional heat is required to maintain fast propagation of the

flame front.

After the pyrolysis front reaches the fuel bottom, only char oxidation exists, which is an exothermic process. Thus, higher temperatures can be observed. As airflow is applied from the bottom, the reaction front stays at the bottom, and the fuel starts to regress with the burnout of the char. Therefore, at the 2nd stage, the temperature near the bottom is highest. Figure 5.5a shows the mean peak temperatures of three organic wastes at two stages at different airflow velocities. Generally, both peak temperatures increase with the airflow velocity because of stronger char oxidation, especially at the 2nd stage. Furthermore, the temperature was also found not to be very sensitive to waste types, where the peak temperatures of organic soil at both stages are slightly lower than those of the other two wastes. This may be because the density of organic soil is much smaller, causing less heat generated per fuel volume.

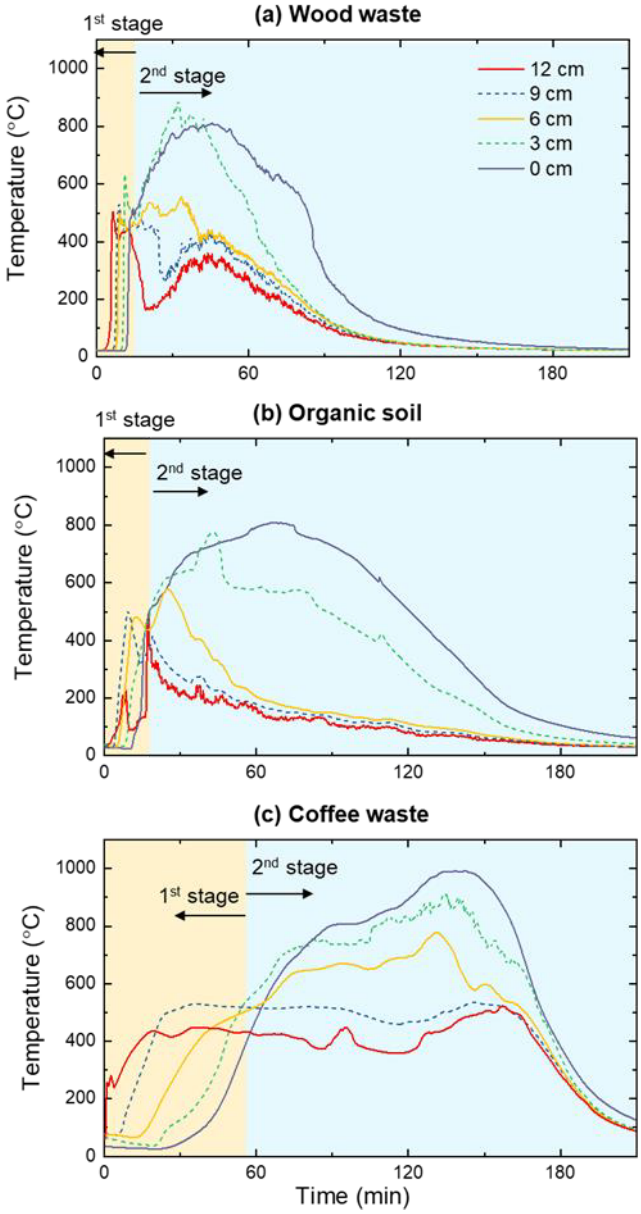

Figure 5.4. Smouldering temperature profiles of (a) wood waste, (b) organic soil, and (c) coffee waste under the bottom airflow velocity of u = 18 mm/s.

Figure 5.5b shows the average spread rate of smouldering front versus airflow velocity. The average spread rate is calculated based on thermocouple readings. Specifically, the duration of 1st stage is determined by tracking the moments when the bottom thermocouple (0 cm) reaches its first peak temperature, while the duration of the 2nd stage is determined as the moments when all thermocouples are lower than 200 °C. As shown in Figure 5.5a, for all the fuels, the smouldering spread rates at both smouldering stages increase with the airflow velocity. As the airflow velocity increases, the oxidation rate increases that accelerates both the heat-transfer and burning processes

that promote the propagation of the smouldering front. More importantly, it was found that the smouldering spread rates of coffee waste are significantly lower than those of other wastes, especially at the 1st stage. This may be because of its smaller thermal diffusivity ($\alpha = k/\rho c$) resulting from a larger fuel density that could delay the rate of heat transfer (Incropera, 2007), thus slowing the propagation of the smouldering front.

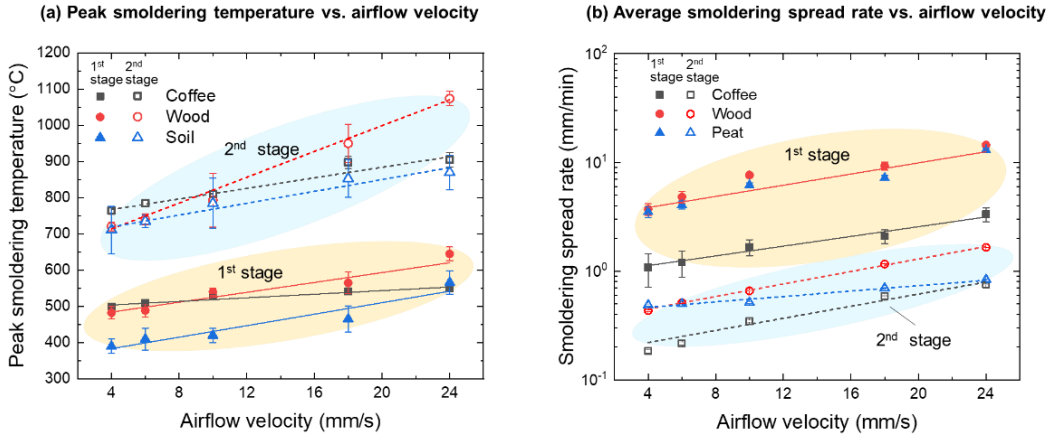

Figure 5.5. (a) Peak smouldering temperatures and (b) average smouldering propagation rates of different organic wastes at two stages for different airflow velocities. Symbols show the experimental data (with standard deviations), lines are the manual fitting curves, yellow shading show the temperature region of the 1st stage, and blue shading show the temperature region of the 2nd stage.

5.3.3 Smouldering burning flux

The smouldering burning flux ($\dot{m}''$) is the mass loss rate per unit area of the fuel, where the area of the fuel is determined by the inner diameter of the burner. These emission gases include both the pyrolysis gases and char-oxidation emissions, as illustrated in Figure 5.1c. Figure 5.6a-c shows the time evolution of the smouldering burning flux and remaining mass fraction of three organic wastes at a representative airflow velocity ($u = 18$ mm/s). The profiles of the burning flux of different organic wastes are similar: during the 1st stage, the burning flux increases rapidly, reaching a peak value. Afterwards, it dramatically decreases and remains stable at about 1-2 g/m^2·s during the 2nd stage until burnout occurs. For all the fuels, about 60%-70% of the mass is consumed at the 1st stage due to the release of pyrolyzates, consistent with the volatile contents reported in Table 3.1. Moreover, it can be found that the total fuel consumption through smouldering can reach over 90%.

Figure 5.6d compares the average burning fluxes of different organic wastes at

different airflow velocities. In general, the average burning flux increases with the airflow velocity. However, it can be observed that the average burning flux of wood waste is slightly larger under a certain airflow velocity, while the burning flux of organic soil is the smallest. For example, at $u = 24$ mm/s, the average burning flux of wood waste is 22 g/m^2·s, which is about 5 g/m^2·s greater than that of organic soil and 2 g/m^2·s larger than that of coffee waste.

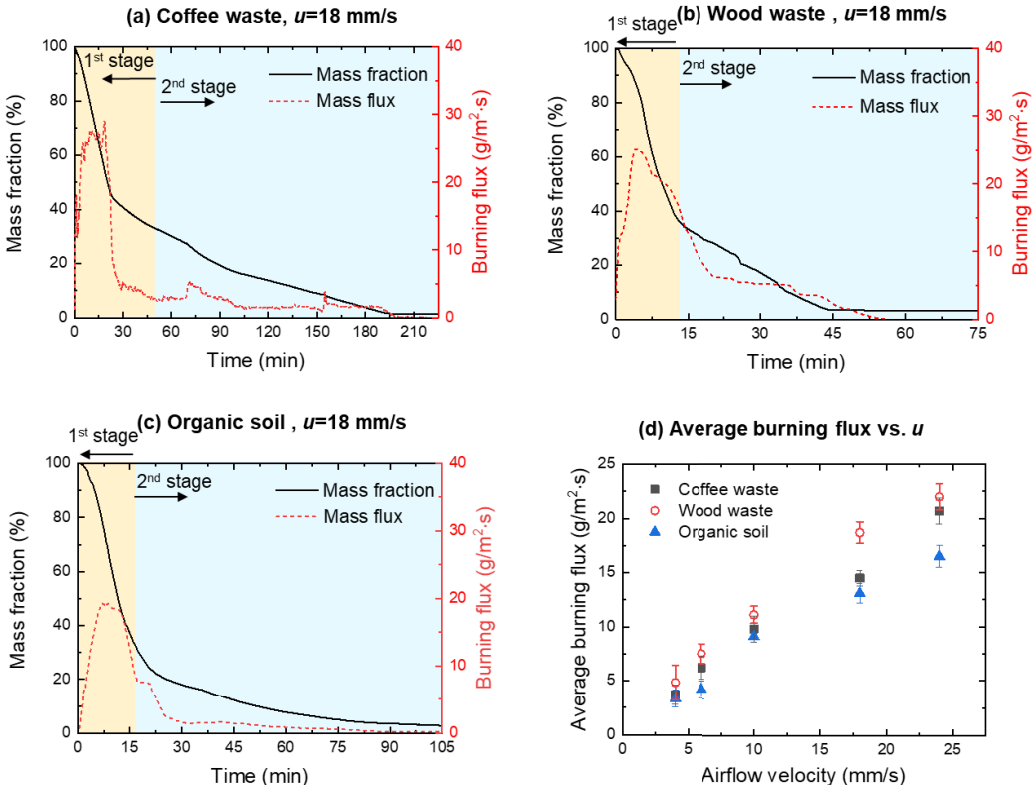

Figure 5.6. Evolution of fuel mass fraction remaining and smouldering burning flux of (a) coffee waste, (b) wood waste, and (c) organic soil at the airflow velocity of 18 mm/s; and (d) the average smouldering burning flux versus the airflow velocity, where the error bars (SE $= \sigma/\sqrt{n}$, where n=2) show uncertainty of repeated tests.

Considering a 1-step global smouldering reaction, the smouldering burning flux ($\dot{m}''_F$) could be approximated as

$$\dot{m}''_F = \frac{\dot{m}''_{ox}}{v} = \frac{\rho_{ox} u}{v} = \rho_F S_{sm} \tag{5.1}$$

where $\dot{m}''_{ox}$ is the rate of oxygen supply, v is the stoichiometric coefficient, ρ_{ox} is the density of oxygen, u is the airflow rate, ρ_F is the density of fuel and S_{sm} is the smouldering propagation rate. Therefore, the smouldering burning flux increases as the airflow velocity increases, successfully explaining the increasing trend in Figure 5.6d.

Also, among these three organic wastes, Eq. (5.1) could also explain the maximum burning flux of wood waste, as it has a maximum smouldering propagation rate (see Figure 5.5b) and moderate fuel density (Table 3.1).

5.3.4 Emissions characteristics

The mass flux of gas emissions ($\dot{m}_i''$, $\mathrm{g/m^2 \cdot s}$) is defined as the average mass flow rate per area (Hu et al., 2019). In this work, the transient mass fluxes of three gases: CO_2, CO, VOCs (mainly hydrocarbons), were calculated as

$$\dot{m}_i''(t) = \frac{\rho_i \Delta X_i(t) \dot{V} \times 10^{-3}}{A} \tag{5.2}$$

where ρ_i is the density of species *i,* which is calculated based on the assumptions of the ideal gas law ($\mathrm{kg/m^3}$), $\Delta X_i(t)$ is the real-time concentration of the species *i* (ppm), which is calculated as $X_{i-plume} - X_{i-ambient}$, $\dot{V}$ is the volume flow rate in the duct ($\mathrm{m^3/s}$), and A is the cross-sectional area of the smouldering burner ($\mathrm{m^2}$).

Figure 5.7(a-c) show the maximum mass fluxes of CO_2, CO, and VOCs from the smouldering of the three organic wastes at different airflow velocities, where the detailed time evolutions could be found in Figure 5.11. In general, the maximum flux of each gas shows an increasing trend with the airflow velocity, and the mass flux of CO_2 is the largest among the three measured gases. Furthermore, at a certain airflow velocity, organic soil has a maximum mass flux of CO_2, but minimum mass fluxes for CO and VOCs. On the other hand, for coffee waste, it has a minimum mass flux of CO_2, but a maximum mass flux of VOCs.

The $\Delta CO/\Delta CO_2$ ratio (also known as the modified combustion efficiency, which is expressed as MCE= $\Delta CO_2/(\Delta CO+\Delta CO_2)$) is an important index in describing combustion completeness (Hu et al., 2018), which can also indicate the type of pollutants emitted. Therefore, Figure 5.8 further compares the $\Delta CO/\Delta CO_2$ ratios and MCE with and without the purification of flame to demonstrate the efficiency of pollution mitigation. Figure 5.8a shows that the $\Delta CO/\Delta CO_2$ratio for different organic wastes without flame purification is above 0.25. However, if a flame is applied above the smouldering front, the $\Delta CO/\Delta CO_2$ ratio decreases dramatically to be below 0.05, which drops by more than 90%. Figure 5.8b shows that the MCEs of smouldering for all organic wastes are lower than 0.8, while increasing to above 0.9 after a flame is supplied. Figure 5.8c shows that in smouldering emission, $\Delta VOCs/\Delta CO_2$ ratios for all organic wastes are lower than 0.2.

The production of VOCs from smouldering organic soil is much smaller, proving that its emission is much less flammable. On the other hand, with purification of flame, almost all VOCs is consumed in the flame, and the $\Delta VOCs/\Delta CO_2$ ratios in final emission are less than 0.0005. Therefore, this newly developed method can successfully alleviate the pollutions of the smouldering-based waste removal technology with a satisfactory efficiency of pollution mitigation.

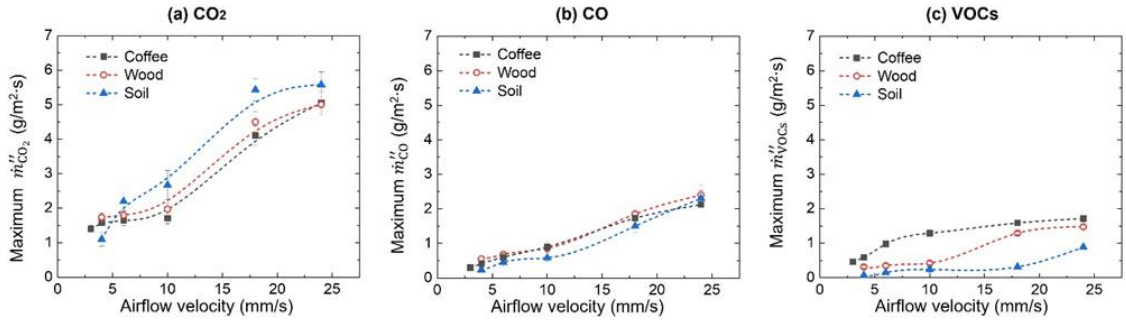

Figure 5.7. Maximum mass flux of (a) CO_2, (b) CO, and (c) VOCs from the smouldering of different organic wastes at airflow velocities from 3-24 mm/s where the error bars ($SE = \sigma/\sqrt{n}$, where n=2) represent the standard deviations.

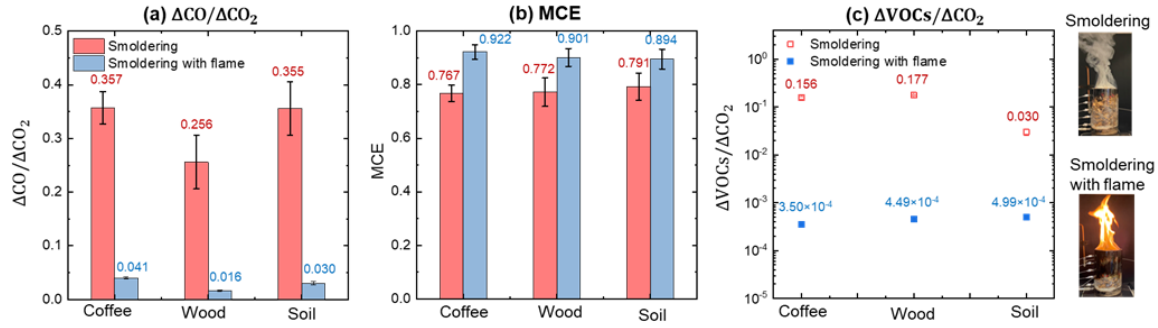

Figure 5.8. Comparison of (a) $\Delta CO/\Delta CO_2$, (b) MCE, and (c) $\Delta VOCs/\Delta CO_2$ with and without flame purification at u=18 mm/s where the error bars ($SE = \sigma/\sqrt{n}$, where n=2) represent the standard deviations.

5.3.5 Criteria for sustaining a flame on the smouldering emissions

The first column of Figure 5.9 shows the time evolution of the burning flux for coffee waste, wood waste, and organic soil under different airflow velocities. For all the organic wastes, the peak burning flux appears at the 1st stage under all airflow conditions. The second column of Figure 5.9 further summarizes the maximum smouldering burning fluxes at different airflow velocities, as well as the minimum burning flux for maintaining a flame. Herein, the solid symbols represent the conditions where the flame can be piloted and co-exists with smouldering, while the hollow symbols signify the conditions where

only smouldering can exist.

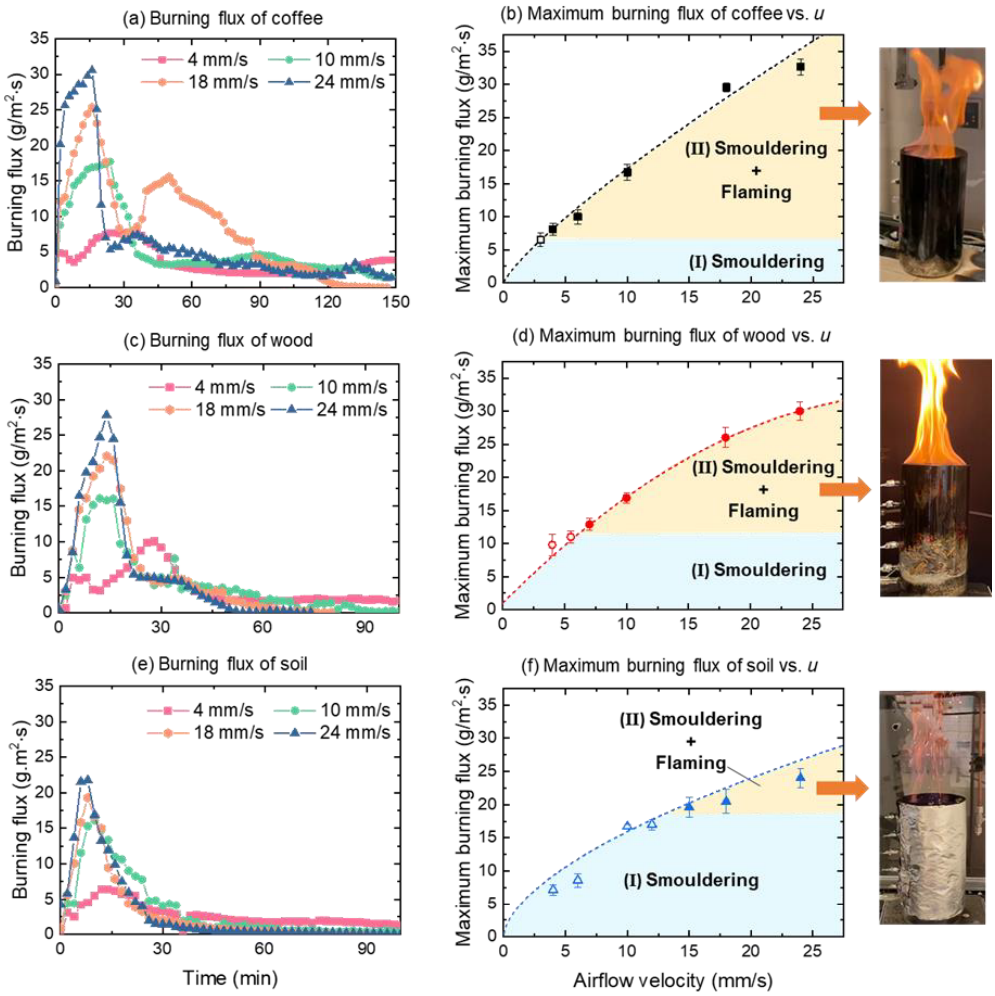

Figure 5.9. Evolution of the burning flux for (a) coffee waste, (c) wood waste, and (e) organic soil under various airflow velocities. The maximum smouldering burning flux versus the airflow velocity of (b) coffee waste, (d) wood waste, and (f) organic soil, where the error bars (SE $= \sigma/\sqrt{n}$, where n=2) show test uncertainty.

The minimum burning flux of coffee waste (Figure 5.9b), wood waste (Figure 5.9d), and organic soil (Figure 5.9e) that is necessary to maintain a stable flame of their smouldering emissions are 7±1 g/m^2·s, 11±1 g/m^2·s, 17±2 g/m^2·s, where the minimum airflow velocities required to reach such a minimum burning flux are 3.5±0.5 mm/s, 6±0.5 mm/s, and 13.5±1.5 mm/s, respectively. Thus, with the smallest required burning flux and airflow velocity to sustain a flame, the smouldering emissions of coffee waste may be easier to be purified by this newly developed method.

Moreover, as shown in Figure 5.9, the flame of the coffee waste emissions is dark orange, while the flame of the wood waste emissions is bright orange. However, the flame

of the organic soil emissions is quite different from the other two fuels, which appears to be blue accompanied by red sparks. The red sparks are caused by the flaming of organic soil particles which are blown out by the airflow. The difference in the flame colour may be owing to the different flammable components that existed in their smouldering emissions.

To ignite and maintain a flame, a minimum mass flux of fuel gas is required. In this study, the fuel gas in the smouldering emissions is simplified to a mixture of VOCs (mainly hydrocarbons) and carbon monoxide (CO), which have been proved to be the main flammable gas species in the smouldering emissions (Hu et al., 2020, 2019). Thus, the equivalent mass flux of flammable gas emissions ($\dot{m}_f''$) becomes:

$$\dot{m}_f'' = \frac{\Delta H_{HC} \cdot \dot{m}_{Hc}'' + \Delta H_{CO} \cdot \dot{m}_{CO}''}{\Delta H_{HC}} \tag{5.3}$$

where ΔH_{HC} is the heat of combustion of hydrocarbons, ΔH_{CO} is the heat of combustion of CO, $\dot{m}_{\mathrm{HC}}''$ and $\dot{m}_{\mathrm{CO}}''$ are the mass fluxes of hydrocarbons and CO, respectively.

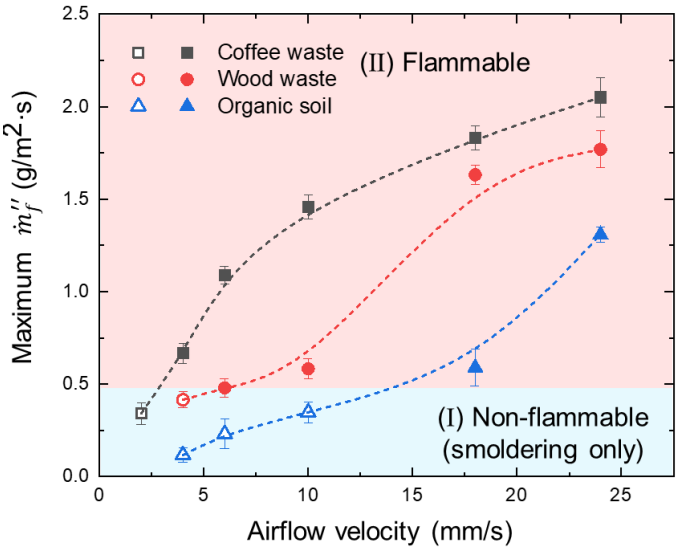

Figure 5.10. The maximum mass flux of flammable components in smouldering emissions versus the airflow velocity, where the error bars (SE $= \sigma/\sqrt{n}$, where n=2) show the experimental uncertainty of repeated tests.

Figure 5.10(a) summarizes the maximum mass flux of flammable gas emissions from three different organic wastes at different airflow velocities. For each organic waste, the maximum $\dot{m}_f''$ increases with airflow velocity (u). The $\dot{m}_f''$ of coffee waste is the largest, while the $\dot{m}_f''$ of organic soil is the smallest. For example, as the airflow velocity increases from 4 to 24 mm/s, the maximum $\dot{m}_f''$ of coffee waste increases from 0.68 to

2.2 g/m^2·s, while the maximum $\dot{m}_f''$ of organic soil increases from 0.11 to 1.27 g/m^2·s. More importantly, the minimum mass flux of flammable gas emissions ($\dot{m}_{f,crt}''$) of about 5 g/m^2·s could be found to sustain a flame of the emissions. To reach such a critical mass flux, a much larger airflow velocity smouldering (about 14 mm/s) is required for organic soil compared with another two organic wastes. These consistent with the critical airflow velocity we observed in Figure 5.9.

5.4 Concluding remarks

In this work, we successfully apply a newly developed method to purify the toxic and pollutant emissions from the smouldering-based removal of coffee waste, wood waste and simulated sludge (organic soil) via igniting a flame above the smouldering front. Once the smouldering front is ignited from the top fuel surface, it first propagates downwards to the fuel-bed bottom and then propagates upwards. The flame could only be piloted and self-sustained at the 1st stage owing to an intense pyrolysis process. The efficiency of pollution mitigation is demonstrated by significantly lower CO and VOCs emission (with $\Delta CO/\Delta CO_2<0.05$ and $\Delta VOCs/\Delta CO_2<0.0005$) after purification by self-sustained flame. The equivalent critical mass flux of flammable gases required for igniting the smouldering emissions is 0.5 g/m^2·s, regardless of the biomass fuel types.

The smouldering temperature, propagation rate and burning flux are all increased with the airflow velocity but are also slightly sensitive to the fuel type. This work demonstrates the applicability of this newly developed waste removal technology and demonstrates its efficiency of pollution mitigation, thus further enriching strategies for the clean treatment of smouldering emissions and promoting an energy-efficient and environmentally friendly method for biowaste removal. Future work will determine the effect of fuel moisture content and operational conditions on the critical conditions of flame purification.

5.5 Appendix

Figure 5.11 shows the evolution of the transient mass flux of CO_2, CO, and unburnt HC from the smouldering of different organic wastes at a representative airflow velocity of 18 mm/s. The mass fluxes of gas species peak at the 1st smouldering stage where 60% fuel mass is consumed, as shown in Figure 5.6.

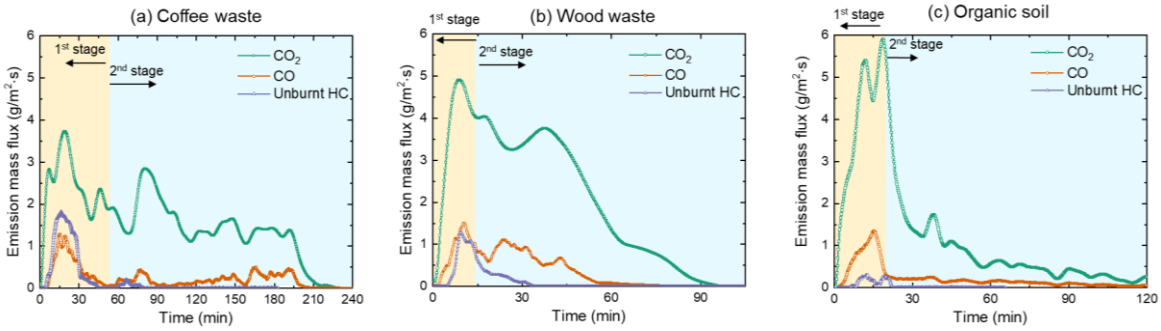

Figure 5.11. Evolution of mass flux of gas species from smouldering of (a) coffee waste, (b) wood waste, and (c) organic soil at u=18 mm/s.

The transient emission factor (EF_i, g/kg) for gas species is calculated through Eq. (5.4)

$$EF_i(t) = \frac{\dot{m}_i''(t)}{\dot{m}''(t)} \times 10^3 \tag{5.4}$$

where $\dot{m}''(t)$ is the fuel burning flux, and $\dot{m}_i''(t)$ is the mass flux of smouldering gas emissions.

Figure 5.12 shows the time evolutions of emission factors of CO_2, CO, and unburnt HC under two representative airflow velocities of 4 mm/s and 18 mm/s. Generally, the EFs of all gas species increase dramatically with the airflow velocity. Taking organic soil as an example, the maximum EF of CO_2 increases from 1300 to 3000 g/kg as the airflow velocity increases from 4 to 18 mm/s. EFs of CO_2 and CO show a similar increasing trend with time, both of which are small during the 1st stage and increase at the 2nd stage. For example, as shown in Figure 5.12(c), the average EF of organic soil during the 1st stage is about 50 g/kg and increases to about 200 g/kg at the 2nd stage. Moreover, both EFs of CO_2 and CO increase dramatically in the burnout stage, which is mainly due to the rapid decrease of the $\dot{m}''(t)$. The evolution of the EF of unburnt HC is quite different from that of CO_2 and CO. Figure 5.12(e, f) show that EF of unburnt HC usually peaks at the 1st stage which is dominated by fuel pyrolysis. Comparatively, the wood waste and organic soil have larger EFs of CO_2 and CO than coffee waste, while coffee waste has a much larger EF-unburnt HC. For example, the EF-unburnt HC of coffee waste can reach about 250 g/kg at u=18 mm/s, which is 10 times that of organic soil.

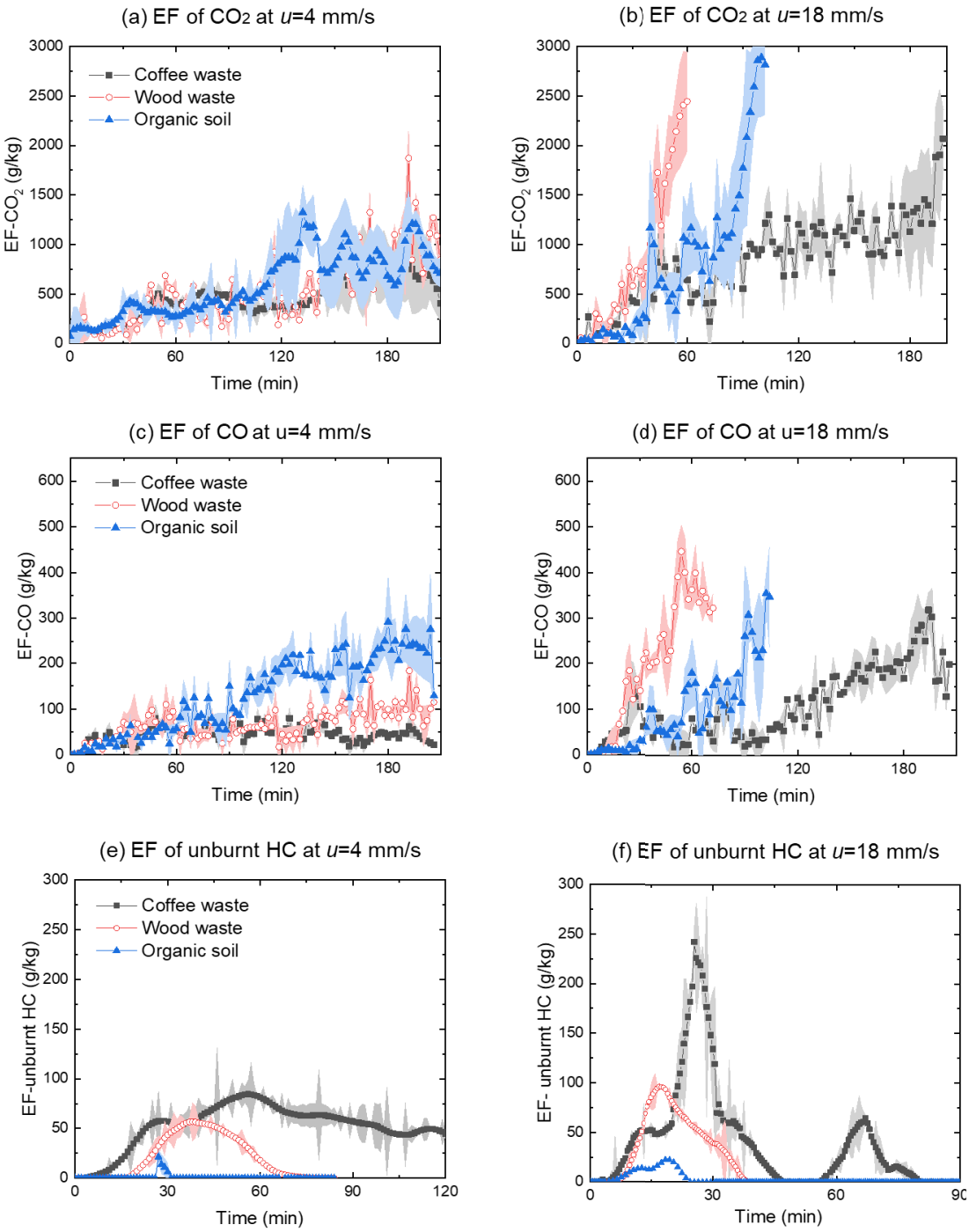

Figure 5.12. Transient emission factors of CO_2, CO, and unburnt HC from the smouldering of different fuels at a low airflow velocity of 4 mm/s and a high airflow velocity of 18 mm/s. Mean of mass flux (line with symbol) and values of range (cloud) from the repeated experiments are shown.

CHAPTER 6

Clean Smouldering Biowaste Process: Effect of Burning Direction on Smoke Purification by Self-Sustained Flame

6.1 Introduction

Smouldering is low-temperature, flameless, and persistent burning of porous fuels, which is different from flaming in terms of transport processes and time scales (Ohlemiller, 1985; Rein, 2014; Torero et al., 2020). Fundamentally, smouldering is a heterogeneous oxidative process sustained when oxygen molecules directly attack a hot charring surface, so it is the driving combustion phenomenon of reactive porous media like wood (Chen et al., 2023; Lin et al., 2022), coal (Wu et al., 2015), incense (Lin et al., 2021a; Yamazaki et al., 2020), cotton (Xie et al., 2020), and peat (Chen et al., 2022b; Hu et al., 2019; Huang and Rein, 2017, 2016b). Once ignited, smouldering can sustain in extreme conditions such as poor oxygen supply and large fuel moisture content (MC). Generally, the characteristic temperature (500-800 ℃), propagation rate (~1 cm/h), and heat of combustion (~10 MJ/kg) of smouldering are lower than those of flaming (Rein, 2014; Torero et al., 2020).

In recent years, smouldering combustion has been adopted as one of the most applicable alternatives for traditional organic waste removal technologies (e.g., incineration (He et al., 2022; Zhou et al., 2021)), exhibiting excellent application prospects (Rashwan et al., 2021; Torero et al., 2020; Wyn et al., 2020a). Currently, such a technique has been successfully applied to remove organic wastes with high moisture contents like bioliquid (Kinsman et al., 2017; Zanoni et al., 2019b), feces (Fabris et al., 2017; Yermán et al., 2015), agricultural wastes (Cheng et al., 2019), wastewater sludges (Feng et al., 2021), food wastes (Song et al., 2022), and oil shales (Marcio F Martins et al., 2010), as reviewed in (Torero et al., 2020). Compared with the traditional methods, the smouldering-based waste removal method has been proved to have many advantages. Firstly, the combustion temperature of the smouldering reactor is relatively low, improving the safety of operation and removal process. Secondly, only minimum pre-treatment processes (e.g., drying and grinding) are required (Tarek L. Rashwan et al., 2016; Yermán et al., 2015), lowering the cost of treatment. Thirdly, this technology has a great potential for improving process efficiency by controlling the oxygen supply (Yermán et al., 2016b).

On the other hand, as smouldering combustion is an incomplete burning phenomenon, many harmful emissions will be released during the process of biowaste treatment (Amaral et al., 2014; Chen et al., 2023, 2022b; Hu et al., 2018), and public

concerns about environmental pollution and potential health risks have limited its further application and promotion. Emissions released from smouldering comprise carbon dioxide (CO_2), carbon monoxide (CO), methane (CH_4), hydrogen cyanide (HCN), volatile organic compounds (VOCs) and particulate matter (PM) (Amaral et al., 2014; Wagner et al., 1991; Wyn and Perkins, 2021; Yokelson et al., 1997; Zhou et al., 2021). Specifically, emission factors (EFs) of incomplete combustion products, like CO, CH_4, and VOCs are higher than flaming combustion (Hu et al., 2019). Among all the smouldering emissions, a high level of CO is the most toxic and lethal, CO_2 and CH_4 are the most significant greenhouse gases, while NO_x and VOCs are the major precursors of O_3 and secondary organic aerosol after complex photochemical processes (Urbanski et al., 2008). Therefore, it is of vital importance for us to explore new methods to mitigate the pollution from the smouldering-based removal technology and promote its application.

A typical smouldering front includes both pyrolysis and char-oxidation reactions, so it generates substantial flammable unburnt hydrocarbons and CO (Hu et al., 2019). With a rich oxygen supply, these flammable emissions will be ignited, contributing to a smouldering-to-flaming (StF) transition process (Santoso et al., 2019). Moreover, smouldering can also co-exist with the flame (Huang and Gao, 2021; Lin et al., 2022), so there is a great potential for using a self-sustained flame without additional fuels and heat to remove these flammable and toxic smouldering emissions. In our previous work, we successfully verified the applicability of using a self-sustained flame to clean the emissions from the smouldering wood wastes, coffee wastes, and organic soil (simulated sludge) under upward airflows (see Figure 6.1) (Chen et al., 2023, 2022b). The purification effect of flame has been demonstrated, where the post-flaming emission has significantly lower CO and VOCs than the original smouldering emissions.

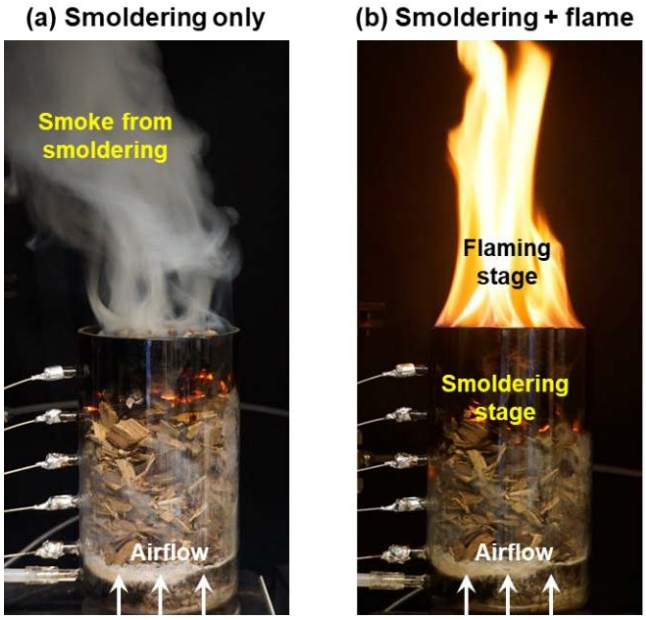

Figure 6.1. Smouldering biowaste removal (a) without and (b) with a self-sustained flame to purify the smoke.

Fundamentally, smouldering combustion is controlled by the competition between oxygen supply and heat transfer to and from the reaction zone (Huang and Gao, 2021). Depending on the relative direction between the propagation of the smouldering front and the oxidizer flow, smouldering processes are classified into two categories: forward and opposed smouldering (Rein, 2014). Generally, the opposed spread is much faster than the forward spread, but its temperature is lower (Huang and Rein, 2019). So far, most of the smouldering waste processes adopt the forward smouldering mode (Chen et al., 2022b; Feng et al., 2021; L. Yermán et al., 2017), while the opposed smouldering mode is rarely explored or compared. Therefore, whether different smouldering directions will affect the critical conditions of sustaining a flame above the smouldering front and the efficiencies of smoke purification are still poorly understood.

To fill this knowledge gap, this study aims to explore the impacts of smouldering directions on the critical conditions for maintaining a flame to purify the smouldering emissions. The experiments were conducted with wood wastes under various upward airflow velocities (5-24 mm/s) and two smouldering propagation directions (forward and opposed). The combustion phenomena, smouldering temperature and spread rate, smouldering burning flux, burnt mass fraction, and flaming ignition thresholds of different smouldering spread modes are quantified and analyzed.

6.2 Experimental method

6.2.1 Wood waste sample

Wood (or yard) waste is a common biowaste all over the world. For example, in Hong Kong, about 40,000 t of yard wastes (mostly tree wastes resulted from typhoons) are produced and directly sent to landfills annually, bringing great pressure to the limited land resources (Liu et al., 2021). Thus, wood-chip waste was chosen in this experiment, the same as our previous work (Figure 6.2) (Chen et al., 2023). The wood chips were provided by a local supplier (ECO-Greentech Ltd.), and their particle sizes range from 20 mm to 30 mm with an average of 25 mm. The dry bulk density, solid density, and porosity were measured to be 210 ± 10 kg/m^3, 600 ± 20 kg/m^3, and 0.65, respectively. The element analysis of the wood sample shows 36.6 %, 3.73 %, 59.47 %, 0.44 %, and 0.06 % mass fractions for C, H, O, N, and S, respectively. Before the test, the raw wood chips were thoroughly dried in an oven at 90 ℃ for 48 h, and their moisture contents were measured to be <8% when reaching a new equilibrium with ambient moisture. The thermal analysis for the wood samples was conducted with a PerkinElmer STA 6000 Simultaneous Thermal Analyzer in both air and N_2 atmospheres, and the representative data are shown in Figure 3.2 (a).

6.2.2 Experimental setup

Figure 6.2a shows the schematic diagram of the experimental setup, which included a cylindrical smouldering reactor, an electrical balance, an ignition system, and an air supply system. The open-top reactor was made of 3-mm thick aluminum alloys, and it had a depth of 20 cm and an internal diameter of 14 cm. A 1-cm thick ceramic insulation layer was attached to the outer surface of the reactor to reduce the lateral heat losses.

At the bottom of the burner, there is a 5-cm deep air mixer to straighten and homogenize the upward airflow. The burning area of the reactor and the air mixer are separated by a steel mesh and a 4-cm gravel layer. Before the experiment, a wood waste sample with a controlled mass of 420 ± 10 g was placed on the gravel layer with a constant height of 15 cm. To monitor the temperature and trace the position of the smouldering front, an array of eight K-type thermocouples (1.5 mm bead diameter) was inserted into the fuel along the axis from 0 cm (bottom) to 14 cm (top) with an interval of 2 cm. A top-view GoPro camera was used to record the test.

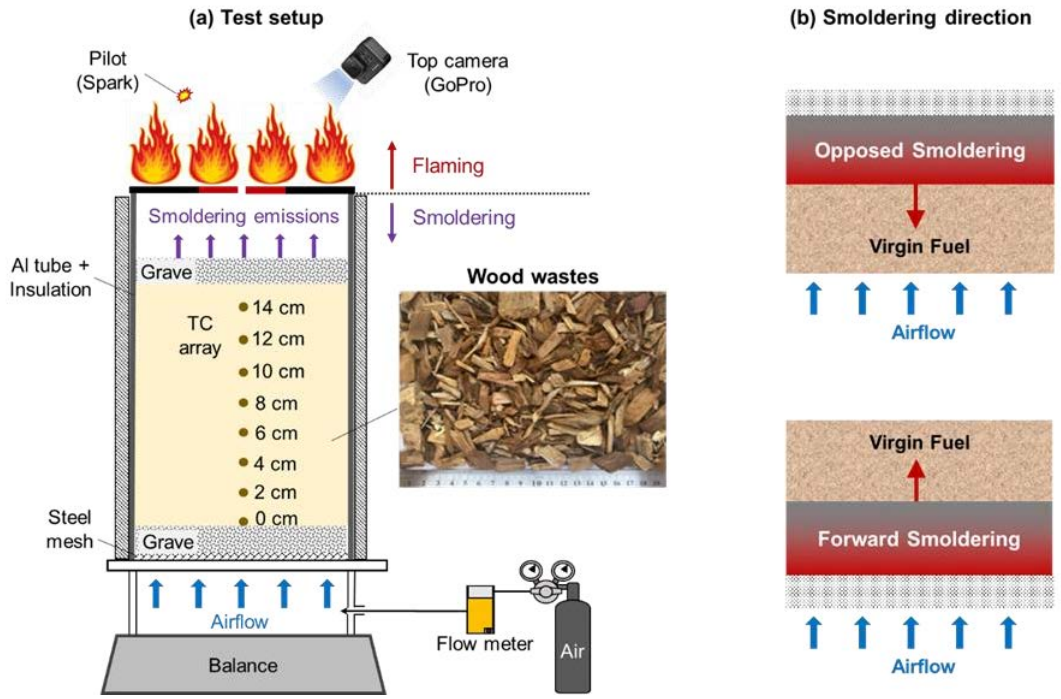

Figure 6.2. Schematic diagrams of (a) the test setup, and (b) smouldering direction.

6.2.3 Experimental procedure

Initially, 70-g pre-ignited wood chips were used to initiate smouldering for all experiments at a constant upward airflow velocity of 10 mm/s. The ignition was applied at the top surface of the wood chips to initiate an opposed smouldering, while the ignition was applied at the bottom surface of the fuel bed to initiate a forward smouldering (see Figure 6.2b). After successful ignition (a uniform and thin layer of smoke occurred on the top of the burner), a layer of fine and clean gravel with a height of 3 cm was placed on the top fuel surface. Then, the supply rate of upward forced airflow was adjusted by controlling the flow meter. For both ignition positions, the experiments were performed at various upward airflow velocities (u) ranging from 5 mm/s to 24 mm/s. Note that the airflow velocity was an overall value of the cross-section, and considering the porosity of 0.65, the average velocity through the pores was from 7.7 mm/s to 37 mm/s.

Afterward, a lighter or a spark was applied near the top outlet of the reactor, aiming to ignite the emissions emitted from smouldering. The test was initially started with the largest airflow velocity. If the smouldering emissions were successfully ignited and the flame became self-sustained, the flow velocity was gradually decreased to find the limiting conditions. The experiments were stopped when all thermocouples were below 100 °C. For each scenario, at least two repeating tests were conducted, and for the tests

near the limits, three or four repeating tests were conducted to ensure repeatability. During the experiments, the ambient temperature was 22±2 ℃, the relative humidity was 50±10%, and the ambient pressure was 101 kPa.

6.3 Results and discussion

6.3.1 Combustion phenomena

Figure 6.3 compares the combustion phenomena of the forward and opposed smouldering at a consistent internal upward airflow velocity of 24 mm/s. In both smouldering modes, a flame could be piloted and sustained at the outlet of the burner, co-existing with the smouldering combustion underneath. Therefore, we successfully demonstrated that a stable flame could be sustained above the opposed and forward smouldering fronts to remove emissions from smouldering wood wastes.

For the forward smouldering (Figure 6.3a), there was a short and unstable flash flame that lasted for a very short period (about 20 s) when a spark was applied, because of the continuous pyrolysis of the 70-g pre-ignited fuels. Such a flash was an ignition effect and was not considered as a self-sustained flame. During this transition stage (< 8 min), the smoke plume was heavy but was not flammable enough because of the insufficient flammable components and large amounts of CO_2, H_2O, and large-molecule VOCs in the smoke. Later, even if the flame became continuous, some unburnt smoke still leaked out from the flame. In contrast, for the opposed smouldering (Figure 6.3b), once piloted, the flame above the opposed smouldering front became stable with almost all visible smoke removed, similar to the observations in our previous works (Chen et al., 2023, 2022b).

More importantly, the self-sustained flame ignited on the emissions from opposed smouldering appeared earlier and burned more stably and intensively. Figure 6.4 further summarizes the flaming durations for both smouldering directions under different airflow velocities, where the flame duration above opposed smouldering is longer than that of forward smouldering and shows inverse trends with airflow velocity.

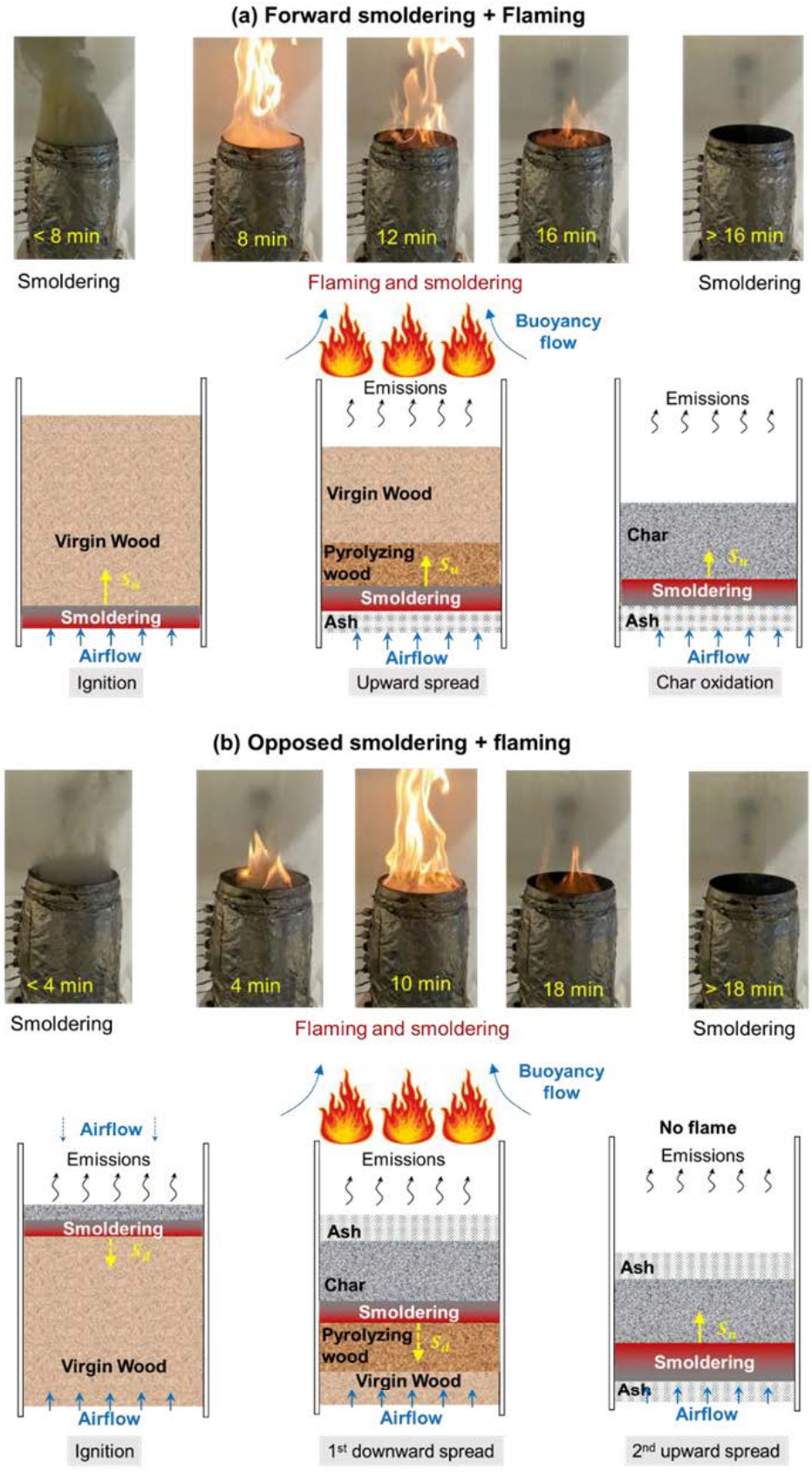

Figure 6.3. Flaming phenomena and diagrams of (a) forward smouldering and (b) opposed smouldering under the upward airflow of 24 mm/s.

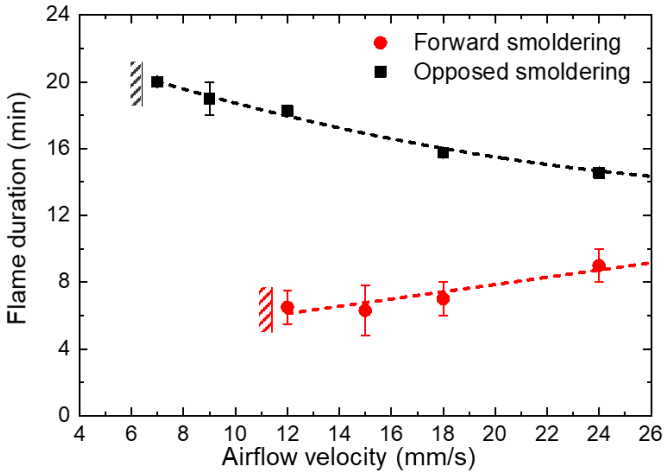

Figure 6.4. The flaming duration above forward and opposed smouldering vs. airflow velocity.

Such different flame phenomena above the smouldering fronts were related to the smouldering propagation processes and reaction sub-fronts. A complete smouldering front includes a drying sub-front, a fuel pyrolysis sub-front, and a char oxidation sub-front, among which the pyrolysis sub-front produces the most flammable emissions that contribute to sustaining a flame. For the forward smouldering, the pyrolysis is driven by an intense char-oxidation sub-front that has a higher temperature (>700 °C in Figure 6.5), and the pyrolysis front moves together with the smouldering front without fast expansion to generate more pyrolysis gases (a single-stage smouldering process). Such smouldering propagation phenomenon has also been observed in previous experiments (Huang and Rein, 2017; Lin and Huang, 2021). Thus, the pyrolysis co-exists with an extensive char oxidation process where a large number of incombustible gases (e.g., H_2O and CO_2) may lower the flammability of the emissions.

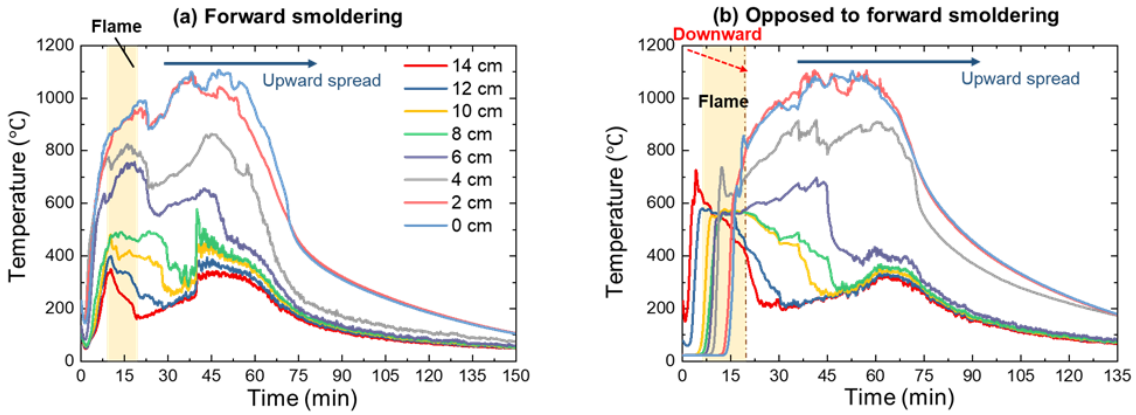

Figure 6.5. Smouldering temperature profiles of (a) forward smouldering and (b) opposed smouldering and the transition to 2nd-forward smouldering under the airflow

velocity of 18 mm/s.

For the opposed smouldering, the pyrolysis sub-front is driven by a low-temperature oxidation sub-front towards the direction of oxygen supply (<600 ℃ up to 16 min in Figure 6.5b). During this process, the pyrolysis front expanded and spread downwards rapidly, which has been demonstrated in previous experiments (Huang and Rein, 2019; Lin and Huang, 2021), leaving behind a thick char layer (1^{st}-stage opposed smouldering process). Such a process is a continuous smouldering ignition process that is controlled by heat transfer (Huang and Gao, 2021; Ohlemiller and Lucca, 1983). Therefore, the smoke from opposed smouldering primarily contains pyrolyzates from wood pyrolysis (e.g., CH_4, C_2H_4, C_2H_6, and CO), which are highly flammable, making it much easier to be ignited than that from forward smouldering. Afterward, most of the char produced from pyrolysis remains that are further oxidized in the 2^{nd}-stage upward smouldering with a higher temperature, while this process cannot sustain a flame above. Another possible reason for the difference in the flame above is that the hot opposed smouldering front is near the top surface of the fuel bed which can better support the flame above, whereas the top of the fuel bed will be cooler as the forward smouldering front is further below the surface.

6.3.2 Smouldering temperature and spread rate

Figure 6.6a shows the peak temperatures of the single-stage forward smouldering and the two-stage opposed-to-forward smouldering under varying airflow velocities. Figure 6.6b shows the average smouldering burning rates (both spread rate of the pyrolysis front and burning speed) estimated from the temperature profiles. Specifically, the average spread rate of the pyrolysis front is estimated by tracking the moments when TC (0 cm) and TC (14 cm) reach 300 °C, which is shown as the hollow symbols in Figure 6.6b. And burning speed is defined as the surface regression speed of the fuel bed, which is estimated by dividing the fuel height by the time when the bottom TC (0 cm) starts to decrease, which is shown as the solid symbols in Figure 6.6b. As expected, both the peak temperatures and the smouldering spread rates increase with the airflow velocity because of stronger char oxidation under a better oxygen supply.

Moreover, Figure 6.6a shows the peak temperature of the single-stage forward smouldering is slightly larger than that of the 2^{nd}-stage forward smouldering, and both are significantly larger than the 1^{st}-stage opposed smouldering. This is because the 1^{st}-

stage opposed smouldering is a fast-expanding process of pyrolysis front where the char oxidation is weak, resulting in a lower peak temperature (Huang and Rein, 2019; Lin and Huang, 2021). Figure 6.6b shows that the spread rate of the single-stage forward pyrolysis front is larger than that of the 1st-stage opposed pyrolysis front, while the average burning speeds for both single-stage forward smouldering and 2nd stage forward smouldering are similar. Noted that the burning speed may be slightly overestimated as the fuel bed at this moment may slightly regress, but the overall trend is not affected.

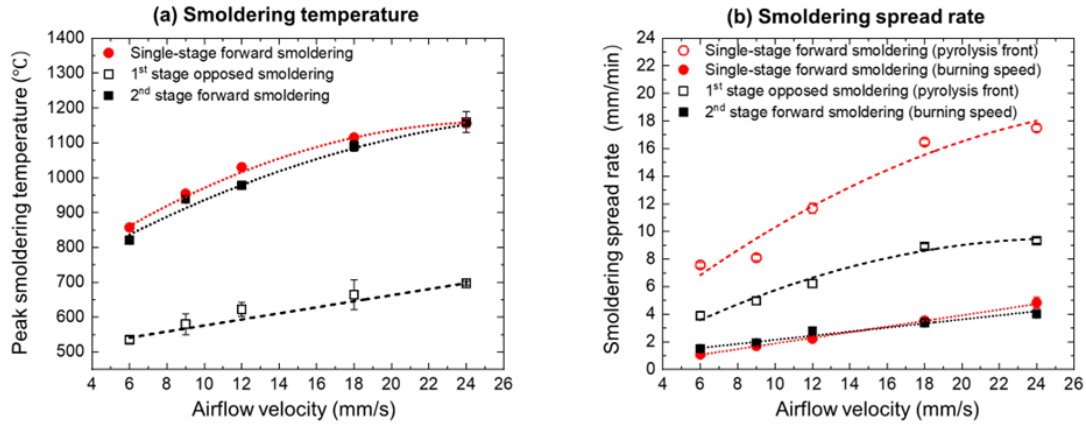

Figure 6.6. (a) Peak smouldering temperatures and (b) average smouldering spread rates of forward smouldering and the opposed-to-forward smouldering vs. airflow velocities.

6.3.3 Smouldering burning flux

The burning flux ($\dot{m}''$) is the mass loss rate per unit area of the fuel, which is an important parameter to quantify the combustion limits. Figure 6.7a-b compares the time evolution of the remaining mass fraction and the burning flux of wood under the forward smouldering and opposed smouldering under the airflow velocity of 18 mm/s. The profiles of the burning flux for both spread modes are similar: during the initial stage, the burning flux increases rapidly, reaching a peak value in a short time. Afterward, it dramatically decreases and remains at a low value of about 2-4 g/m^2·s for a longer period until burnout occurs.

The red triangle symbols in Figure 6.7a-b represent the critical smouldering burning flux for flame ignition ($\dot{m}''_{ig}$), which is determined as the value of the burning flux at the moment when a self-sustained flame is piloted on the smouldering emissions, and the blue triangle symbols signify the critical burning flux for flame extinction (or the self-sustained flame disappears) ($\dot{m}''_{ex}$). For forward smouldering (Figure 6.7a), the flame ignition occurs during the decrease period of the smouldering burning flux, at which the

critical burning flux reaches about 27 g/m^2·s, and then disappears as the burning flux decreases to about 10 g/m^2·s.

However, for the opposed smouldering (Figure 6.7b), the flame is ignited when the burning flux rises to about 11 g/m^2·s, and then extinguishes as the burning flux decreases to about 9 g/m^2·s. During the flame period, 60 % mass of the wood is burnt by opposed smouldering, while only 33 % mass fraction is burnt by the forward smouldering. Figure 6.7c further summarizes the burnt mass fraction in the flaming period under various airflow velocities. Clearly, the burnt mass fraction in both modes of smouldering propagation increases as the airflow velocity increases. More importantly, it is observed that the burnt mass fraction in the period of co-existed flame above opposed smouldering (40 %-67 %) is significantly larger than that above forward smouldering (20 %-35 %), indicating the opposed smouldering is more efficient for our proposed waste removal method.

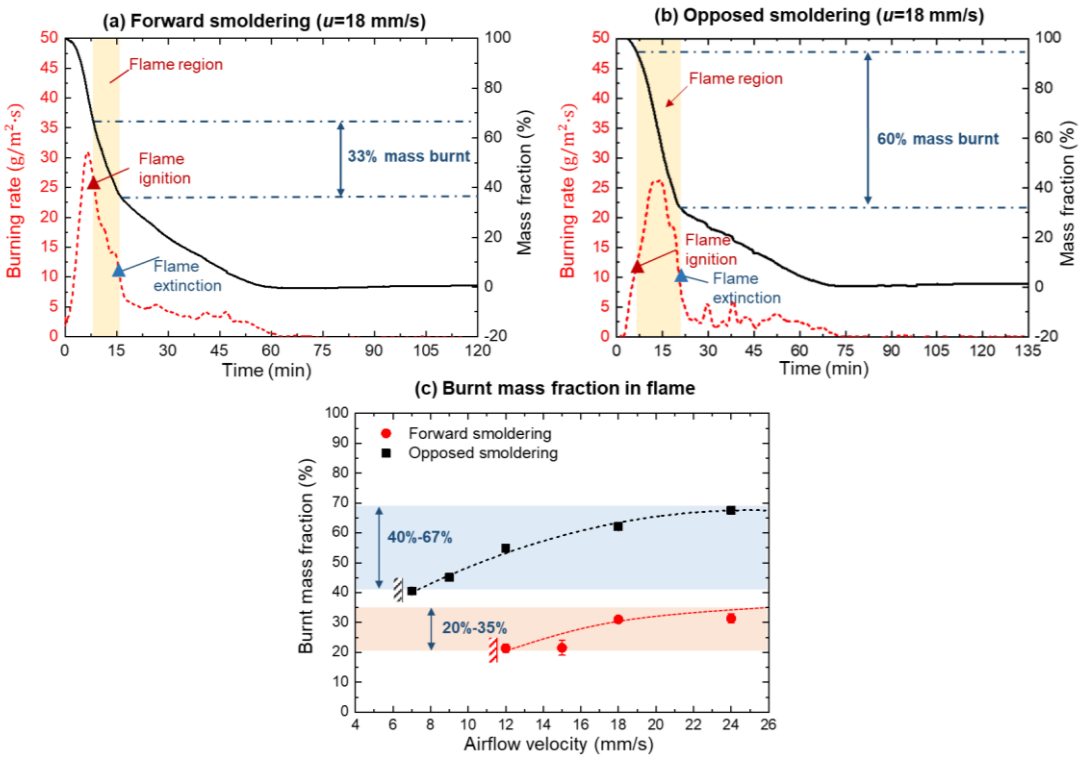

Figure 6.7. Evolution of smouldering burning flux of (a) forward smouldering and (b) opposed smouldering at the airflow velocity of 18 mm/s, and (c) the burnt mass fraction during the co-existence of flame in different smouldering propagation modes under various airflow velocities.

6.3.4 Flaming limits for smouldering emissions

Figure 6.8 summarizes the critical smouldering burning flux for flame ignition ($\dot{m}''_{ig}$) and flame extinction ($\dot{m}''_{ex}$), as well as the maximum smouldering flux ($\dot{m}''_{max}$) under various airflow velocities of different spread modes. Firstly, it is observed in Figure 6.8a that a larger airflow velocity (~11 mm/s) is required for the emissions from forward smouldering to be ignited as a stable flame compared with that of opposed smouldering (~6 mm/s). Secondly, Figure 6.8a shows the critical burning flux for flame ignition above the opposed smouldering front is almost constant at about 10 g/m^2·s, while the critical burning flux for flame ignition above the forward smouldering shows an increasing trend with the airflow velocity (increases from 16 g/m^2·s to 29 g/m^2·s as the airflow velocity increases from to 12 mm/s to 24 mm/s). Thirdly, the critical burning flux for flame extinction (Figure 6.8b) in both smouldering modes is similar at about 9±1 g/m^2·s (hollow markers), which is slightly lower than that for flame ignition above opposed smouldering (solid markers). It should be emphasized that the critical airflows required to reach such critical smouldering burning fluxes may vary at different experimental scales.

Moreover, Figure 6.8c shows that the maximum burning flux of forward smouldering is slightly larger than opposed smouldering, and both of them increase as the airflow velocity increases. Although the opposed smouldering burns wood wastes slightly slower, the emissions are much easier to be cleaned by a co-existed flame above it. Moreover, the flame duration above opposed smouldering is longer, which covers a larger burning fraction of wood, and the required airflow velocity for opposed smouldering is smaller.

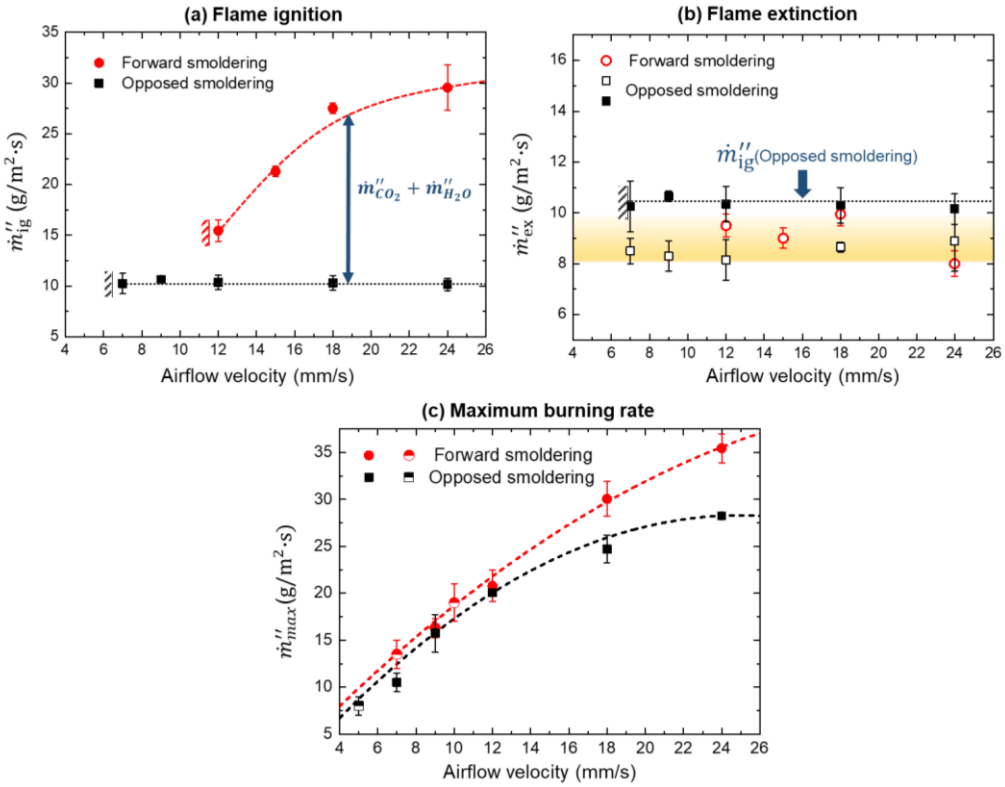

Figure 6.8. Critical smouldering burning flux for (a) flame ignition, (b) flame extinction, where flammability limits above opposed smouldering front (solid markers) are presented for comparison, and (c) maximum smouldering burning flux, where the solid makers represent flaming cases, and hemi-solid markers represent no-flame cases.

To ignite and maintain a flame, a minimum mass flux of fuel gas is required. In this experiment, the fuel gas to sustain a flame in smouldering emissions is mainly the hydrocarbons and CO released from the wood pyrolysis. Here, a simplified heat transfer analysis is introduced for the flame above the smouldering front. The flame heat release rate ($\dot{q}''_f$) by burning the pyrolysis gases should at least overcome the heat loss to the environment ($\dot{q}''_\infty$) and burner wall ($\dot{q}''_w$) as

$$\dot{q}''_f = \dot{m}''_{py,crt}\Delta H_f = \dot{q}''_\infty + \dot{q}''_w \tag{6.1}$$

where $\dot{m}''_{py,crt}$ is the minimum mass flux of pyrolysis gases, and ΔH_f is the heat of flaming combustion.

For the opposed smouldering, the dominant reaction within the smouldering front is the wood pyrolysis, which has been studied and proven in previous studies (Huang and Rein, 2019; Lin and Huang, 2021). In this way, the small amount of emissions from char oxidation (e.g. CO_2 and H_2O) can be ignored and the total smouldering emissions ($\dot{m}''_{sm}$) can be approximately regarded as all pyrolysis gas (Chen et al., 2022b), that is,

$\dot{m}''_{py} \approx \dot{m}''_{sm}$. Therefore, the required critical smouldering burning flux for a flame to be ignited above the opposed smouldering is a constant value as

$$\dot{m}''_{ig,opp} = \dot{m}''_{sm,crt} = \dot{m}''_{py,crt} = \frac{\dot{q}''_{\infty} + \dot{q}''_{w}}{\Delta H_f} \tag{6.2}$$

In this work, this constant value is found to be about 11 g/m^2·s, as shown in Figure 6.8a.

However, for the forward smouldering, because the pyrolysis sub-front only moves with the char-oxidation sub-front gradually, apart from wood pyrolysis, char oxidation also plays an important role within the smouldering front (Bartlett et al., 2019; Huang and Gao, 2021). Thus, the non-flammable H_2O and CO_2 released from oxidation cannot be ignored, which may inhibit the flame. At this moment, the total smouldering emissions ($\dot{m}''_{sm}$) include significant amounts of H_2O and CO_2 ($\dot{m}''_{sm} = \dot{m}''_{py} + \dot{m}''_{CO_2} + \dot{m}''_{H_2O}$). Then, Eq. (6.1) is re-arranged as

$$(\dot{m}''_{sm,crt} - \dot{m}''_{CO_2} - \dot{m}''_{H_2O})\Delta H_f = \dot{q}''_{\infty} + \dot{q}''_{w} \tag{6.3}$$

Therefore, the critical smouldering burning flux for a flame to be ignited above the forward smouldering is expressed as

$$\dot{m}''_{ig,for} = \dot{m}''_{sm,crt} = \frac{\dot{q}''_{\infty} + \dot{q}''_{w}}{\Delta H_f} + \dot{m}''_{CO_2} + \dot{m}''_{H_2O} \tag{6.4}$$

Eq. (6.4) and Eq. (6.2) explain why the critical burning flux in for flame ignition above the forward smouldering ($\dot{m}''_{ig,for}$) is larger than the opposed smouldering ($\dot{m}''_{ig,opp}$). Moreover, as the oxidation intensity increases with the airflow velocity, which results in an increase in $\dot{m}''_{CO_2}$ and $\dot{m}''_{H_2O}$. This also explains why $\dot{m}''_{ig,for}$ shows a significant increase with airflow velocity in Figure 6.8a. In our future work, the comparison of smouldering emissions from forward and opposed smouldering will be comprehensively compared, and tests at different scales will be conducted to demonstrate the scalability.

6.4 Concluding remarks

In this work, we successfully applied a self-sustained flame above both the forward and opposed smouldering fronts to purify the toxic smouldering emissions. It is found that the emission gases from opposed smouldering are much easier to be ignited, and the flame duration and burnt mass fraction are much larger than that of the forward smouldering. The flame sustained above the smouldering is influenced by the competition

reactions between wood pyrolysis and char oxidation within the smouldering front. For opposed smouldering, due to a fast-expanding pyrolysis zone, significant amounts of flammable pyrolyzates are released, making its emissions highly flammable. However, the forward smouldering front includes both slow wood pyrolysis and intense char oxidation, making the emissions less flammable because of fewer pyrolyzates and excessive CO_2 and H_2O from char oxidation.

To sustain a stable flame above opposed smouldering, the minimum airflow velocity required is about 6 mm/s, and the minimum smouldering burning flux is 10 ± 1 g/m^2·s. Comparatively, sustaining a flame above forward smouldering front requires a larger airflow velocity (~11 mm/s), and the minimum smouldering burning flux is not constant but increases with the airflow velocity. Moreover, the critical smouldering burning flux at flame extinction is constant at 9 ± 1 g/m^2·s, regardless of the smouldering direction and airflow velocity. A theoretical analysis based on the simplified heat transfer process successfully explains the trends between the critical burning flux for flame ignition and the smouldering propagation modes.

This work deepens the understanding of the co-existence of smouldering and flaming, enriches the theory for the clean treatment of smouldering emissions via its re-combustion, and promotes an energy-efficient and environmentally friendly method for biowaste removal. Future works will quantify and compare the emission gases and the efficiency of smoke purification in different smouldering propagation modes and conduct experiments at different scales.

CHAPTER 7

Carbon Distribution and Multi-criteria Decision Analysis of Flexible Waste Biomass Smouldering Processing Technologies

7.1 Introduction

With the growth of population and economy, the quantity of municipal solid waste (MSW) generated has increased significantly over the last decades, which endangers the environment and contributes to climate change. Waste biomass is a significant component of MSW, which typically includes kitchen waste, wood waste, grass clippings, paper waste, etc. At present, landfilling, biological conversion (composting, anaerobic digestion, fermentation), and thermochemical treatment (pyrolysis, liquefaction, gasification, combustion) are the main ways of biowaste disposal (Basu, 2010; Lohri et al., 2017). Often, landfilling and incineration are still very common in many countries as they are the easiest and cheapest ways (Assamoi and Lawryshyn, 2012). For example, Australia deposited nearly 50% of the core organic solid waste in landfill in 2020 (Department of Agriculture, 2020). Landfilling releases large amount of greenhouse gases (GHG) (IPCC, 2006), of which CH_4 (a more potent GHG than CO_2) can reach almost 60 % and accounts for 10-15 % of the global anthropogenic CH_4 emissions (Gómez-Sanabria et al., 2022). Combustion (or burning/incineration) is most effective in the volume reduction of waste and can produce substantial heat for energy recovery (Lu et al., 2017). However, it releases large quantities of CO_2, particulate matters (PM), and air pollutants (especially the dioxins) (Lin et al., 2018; Ravindra et al., 2019). According to EEA report (European Environment Agency, 2015), 150 Tg/yr of CO_2 eq were emitted from MSW incineration in 2015 Therefore, nowadays, effective and environmentally friendly treatment facilities to cope with the large quantities of biowaste are still in absence, posing a globally big challenge to mankind.

Smouldering is an emerging method for organic solid waste removal, especially for those with high moisture content, like the biowaste. Smouldering is slow, low-temperature and flameless burning of porous fuels (Ohlemiller, 1991; Rein, 2014) which often occurs on the burning of charring materials, such as wood (Tissari et al., 2008), coal (Wu et al., 2015), and peat (Huang and Rein, 2016a). Different from flaming combustion, smouldering occurs when oxygen directly attack the hot surface of reactive porous media (Ohlemiller, 1991; Rein, 2014). Generally, the characteristic temperature (500-800°C) and heat of combustion (~10 MJ/kg) of smouldering are smaller than those of a flame (Rein, 2014), and it can be easily initiated by a relatively small amount of energy and sustain the process in extreme conditions such as poor oxygen supply (~12 % O_2) and

large fuel moisture content (MC) (>100%) (Huang and Rein, 2016a). The overall smouldering combustion process can be approximated as two lumped chemical pathways, namely pyrolysis and char oxidation, as described in Eq. (7.1-7.2) (Rein, 2014). Pyrolysis generates flammable pyrolyzates and char,

$$\text{Fuel (s)} + \text{Heat} \rightarrow \text{Pyrolyzates (g)} + \text{Char (s)} \quad \text{[pyrolysis]} \quad (7.1)$$

where both can be further oxidized. The heterogeneous char oxidation leads to smouldering as

$$\text{Char (s)} + O_2 \rightarrow \text{Heat} + CO_2 + H_2O + \text{other gases} + \text{Ash} \quad \text{[smouldering]} \quad (7.2a)$$

The homogeneous gas-phase oxidation of pyrolyzates results in a flame as

$$\text{Pyrolyzates (g)} + O_2 \xrightarrow{\text{flame}} \text{Heat} + CO_2 + H_2O + \text{other gases} \quad \text{[flaming]} \quad (7.2b)$$

Over the past few decades, many existing investigations and practices have revealed the ability of smouldering to remove organic wastes like bioliquid, faeces (Fabris et al., 2017; Yermán et al., 2015), wastewater sludges (Feng et al., 2021), and food wastes (Song et al., 2022). Such a method demonstrates many attractive advantages, like a safer operation process, minimising pre-treatments (e.g., drying and grinding) (Tarek L. Rashwan et al., 2016; Yermán et al., 2015), the applicability for wastes with high moisture contents (MC), and minimum extra energy input.

In addition, smouldering also shows strong potential as a green waste-to-energy technology, which has been applied to produce biochar (Rashwan et al., 2021; Rein, 2009a) and bio-oil (Feng et al., 2022; L Yermán et al., 2017a). This is because a smouldering front contains pyrolysis reaction (Eq. (1)), and pyrolysis is an endothermic process that has been widely used to convert biomass feedstock into biochar (solid), bio-oil (liquid), and bio-gas (Babu, 2008; Demirbas and Arin, 2002; Wang et al., 2010). Biochar has potential usage in a wide field and is suitable for carbon sequestration due to its resistance to chemical and biological decomposition. Converting biomass to biochar avoids the complete return of greenhouse gases (GHG) to the atmosphere, compared to natural decay or burning processes (Lee et al., 2020; Woolf et al., 2010). However, the traditional pyrolysis technology usually requires additional energy to keep the high temperature (typically >300°C). In comparison, pyrolysis in smouldering process can be sustained by the heat generated from the weak oxidation of original fuel, thus requires no external energy or fuel gas. This feature makes smouldering a more energy-efficient way to transform waste to energy than pyrolysis and suitable for on-site applications.

However, as an incomplete burning process, smouldering tends to release many toxic

emissions, like CO, CH_4, NO_x, volatile organic compounds (VOCs) and particulate matters (PM) (Hu et al., 2018), posing severe threats to human health and the environment. This limits its further promotion and application in waste management. Considering there are still substantial flammable hydrocarbons and CO in smouldering emissions, we intend to use a flame to clean the smouldering emissions by converting most of the flammable and pollutant species into H_2O and CO_2. A flame (or flare) is a common method of disposal of unwanted waste gases in oil and gas industries (Akeredolu and Sonibare, 1998). Generally, it is often used to burn off the C1-C6 hydrocarbons and hydrogen sulfide from the upstream and downstream of oil industry (Gai et al., 2020). Besides, it has also been utilized to remove the landfill gases and biogases (mainly CH_4) in landfill management (Environmental Protection Agency, 1997). Sometimes, auxiliary fuel must be introduced to support the flame if the waste gas does not meet the minimum heating value (Environmental Protection Agency, 1995). More importantly, it has been reported that if operated properly, the combustion efficiency of the flare could reach 99%, eliminating most of the flammable waste gas (Gai et al., 2020; Pohl et al., 1986).

In the former chapters, a novel combustion method for biowaste disposal by using a self-sustained flame (without additional fuels or heat) to purify the emissions from biowaste smouldering under an appropriate air supply (Chen et al., 2023, 2022b, 2022a) has been established. After being ignited from the top surface of the fuel bed, a two-stage smouldering process was observed under an upward airflow, as illustrated in Figure. 7.1. The 1st stage is opposed smouldering (the front spreads downward), leaving abundant biochar. The 2nd stage is forward smouldering (the front spreads upwards), which burns all the char and leaves little ash. More importantly, it was found that the flame could only be piloted and sustained in the 1st stage because of the intensive pyrolysis in this stage.

Therefore, based on the two-stage smouldering process, this paper further develops a flexible suite of smouldering waste biomass processing technologies and proposes four different processing strategies. Each strategy is conducted with the wood waste under various airflow rates (6-18 mm/s). The carbon balance of each process is analysed after quantifying their gaseous, liquid, and solid products. A multi-criteria decision analysis based on PROMETHEE-GAIA algorithm is made in terms of their environmental impact, carbon sequestration, waste removal efficiency, and product value.

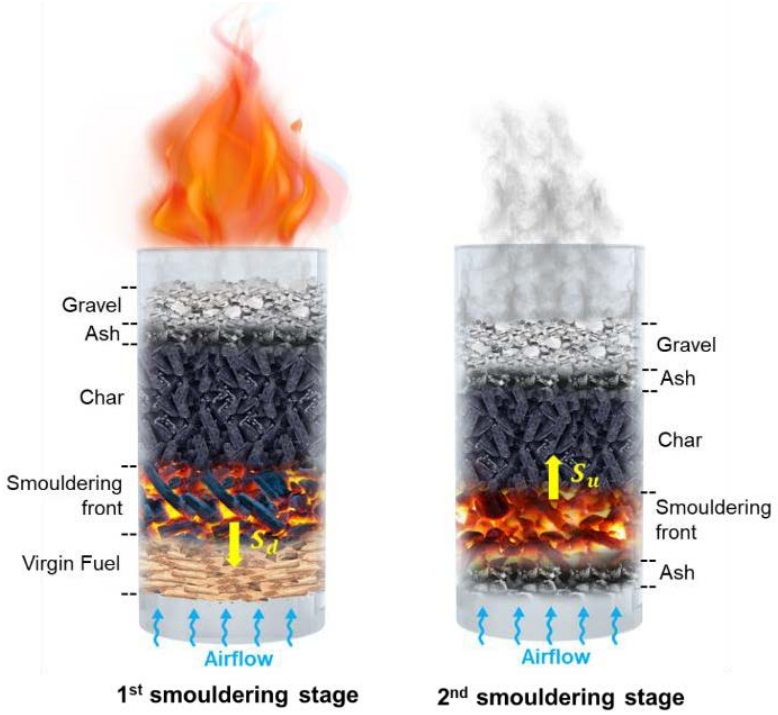

Figure 7.1. The two-stage smouldering process with a flame sustained by the emissions from the 1st stage opposed smouldering.

7.2 Materials and Methods

7.2.1 Wood waste sample

Wood (or yard) waste is a common waste biomass all over the world. For example, Hong Kong annually produces about 40,000 tonnes of wood wastes that are directly sent to landfills, bringing a huge burden to the limited land resources, and generating large amounts of GHG. Same as our previous work (Chen et al., 2023, 2022a), the wood waste was chosen in this experiment (Figure 7.2), provided by a local company (ECO-Greentech Ltd.). The particle size of the wood chips ranges from 20 mm to 30 mm, with an average of 25 mm. The dry bulk density, solid density, and porosity were measured to be 210 ± 10 kg/m^3, 600 ± 20 kg/m^3, and 0.65, respectively. The element analysis of wood waste sample shows 47.7, 6.3, 45.4, and 0.5 % mass fractions for C, H, O, and N, respectively. And the proximate analysis shows 78.4, 17.0, and 4.6 % mass fraction for volatile, fixed carbon, and ash, respectively.

Before the test, the raw wood chips were thoroughly dried in an oven at 90 °C for 48 h, and their moisture contents were measured to be <8% on a dry basis when reaching a new equilibrium with ambient moisture. Thermal analysis for the wood samples was

conducted with a PerkinElmer STA 6000, and the results are same as our previous work (Chen et al., 2023).

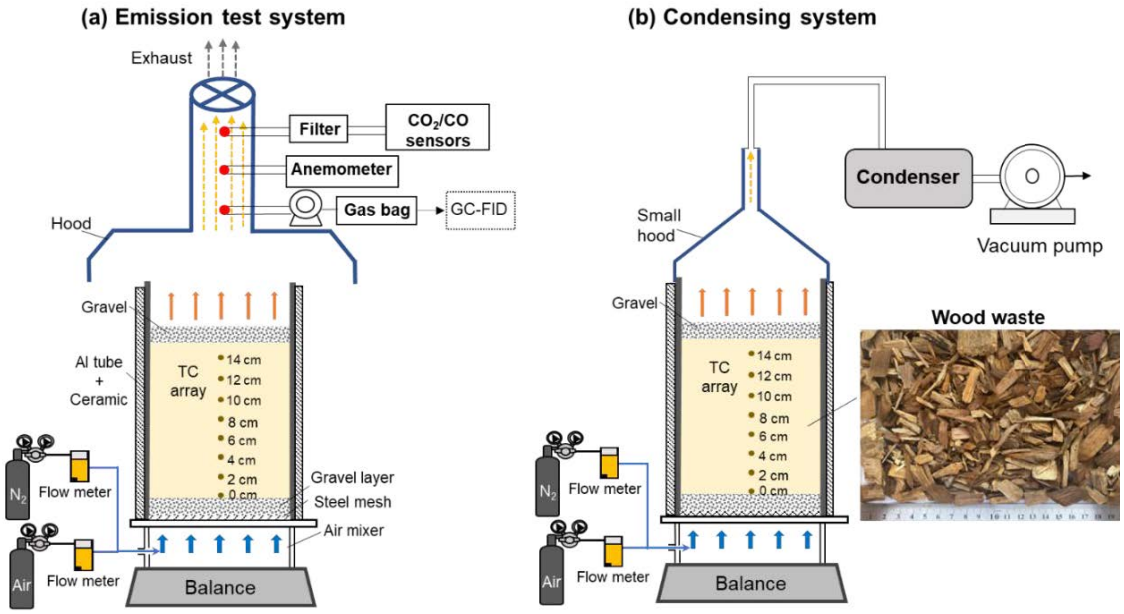

Figure 7.2. Experimental setup for (a) emission test and (b) direct condensing.

7.2.2 Experimental setup

The wood waste was burnt in an open-top cylindrical reactor with a depth of 20 cm and an internal diameter of 14 cm (Figure 7.2). More detailed information about the burner could be found in our previous work (Chen et al., 2022b). For each test, a wood waste sample with a controlled mass of 410 ± 5 g was fed into the reactor at a constant height of 15 cm. An array of eight K-type thermocouples were inserted into the fuel along the axis from 0 cm (bottom) to 14 cm (top) with an interval of 2 cm to monitor the temperature and trace the position of the smouldering front. A lighter was used to initiate the smouldering of the wood waste and ignite the smouldering emissions after the smouldering ignition. A forced airflow was supplied from the bottom end of the reactor and the airflow rate was controlled by a flow meter. A fume hood was located directly above the reactor to collect and transport all the emissions.

7.2.3 Processing strategies and experimental procedure

As shown in Figure 7.3, four processing strategies are proposed and can be achieved by ceasing the smouldering process at different stages.

(a) Full smouldering (F-SM) includes the 1st-stage opposed propagation (strong pyrolysis and weak char oxidation) and the 2nd-stage forward propagation (strong

char oxidation).

(b) Partial smouldering (P-SM) includes the 1st-stage opposed propagation (strong pyrolysis and weak char oxidation) only, after which smouldering is quenched with biochar left.

(c) Full smouldering plus flaming (F-SM+FL) upgrades the F-SM by applying a self-sustained flame to purity the smouldering emissions during the 1st stage. No bio-oil is generated from the F-SM+FL.

(d) Partial smouldering plus flaming (P-SM+FL) also upgrades the P-SM by applying a self-sustained flame to purity the smouldering emissions. No bio-oil is generated, but biochar is left.

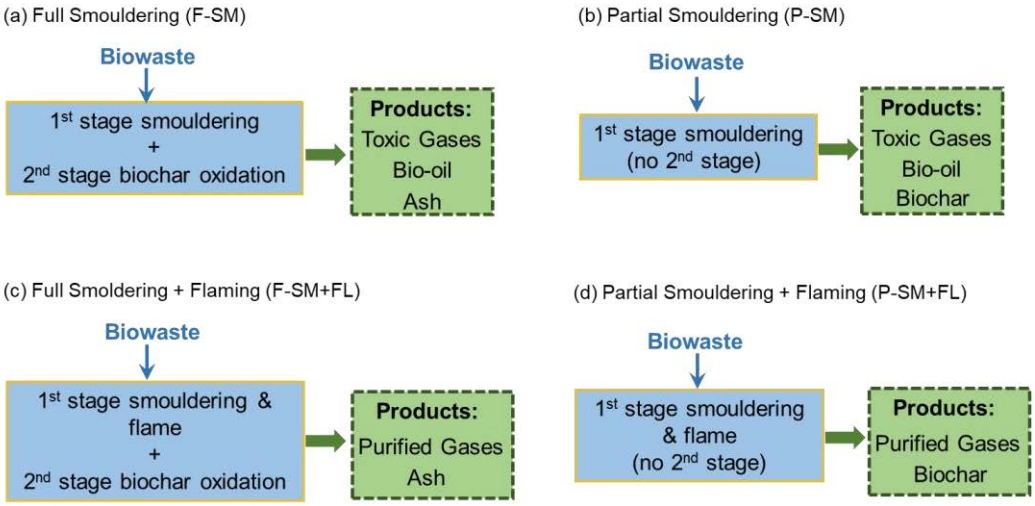

Figure 7.3. Different strategies for the waste biomass smouldering process

Initially, a lighter was used to initiate the smouldering combustion from the top surface of the fuel bed, and the ignition time was fixed for three minutes for each experiment. After successful smouldering ignition, a forced airflow was supplied from the bottom of the reactor, and the airflow rate was controlled by a flow meter. To control the airflow rate to smouldering front, we used airflow velocities (u) from 6 mm/s to 18 mm/s, where the emissions from wood waste smouldering could be ignited as a self-sustained flame, as verified in our previous experiments (Chen et al., 2022b).

To achieve different processing strategies, experimental procedure differs from each other. For the full-smouldering (F-SM), smouldering was sustained until the wood waste was completely converted into a small amount of ash after two stages. For the partial-smouldering (P-SM), smouldering was ceased after the 1st stage (when the last TC (0 cm)

reached its first peak, or when the flame disappeared, and the smoke became clearly less) by supplying sufficient N_2 from the bottom. The whole process lasted until all TCs dropped to the room temperature, leaving abundant biochar in the reactor. Furthermore, for the processes with a flame (F-SM+FL and P-SM+FL), the smouldering emissions were ignited using the lighter in the 1st stage. For the processes without a flame (F-SM and P-SM), the smouldering emissions from 1st stage were condensed via the condenser shown in Figure 7.2b.

All products (gas emissions, condensed liquid, and solid residual) from each experiment were further analyzed. And for each case, at least two repeating tests were carried out to ensure the repeatability of the experiments.

7.2.4 Product analysis

7.2.4.1 Gas products

To quantify the emissions from different smouldering-driven processing strategies, a gas collection and measurement system was built, as shown in Figure 7.2a. The emissions were entirely collected using a fume extraction hood located above the reactor. Three measuring points were designed in the centreline of the hood duct. The flow rate in the test point was measured by an anemometer (Testo 405i), which was constant at 0.038 ± 0.002 m^3/s during the tests. Two major carbon-containing gas species were measured using portable gas analysers after the particulate matter was removed via a quartz filter. Specifically, carbon dioxide (CO_2) was measured by SKY6000-M2 Gas Analyzer and carbon monoxide (CO) was measured by Testo 300. Meanwhile, the emissions were also collected using a 10-L gas bag every 10 minutes to quantify the hydrocarbons ($C_xH_y(g)$) using Gas Chromatography Plus Flame Ionization Detection (GC-FID).

7.2.4.2 Liquid products

As a pyrolysis-dominant process, significant liquid (called bio-oil) including the condensable organic compounds (tar) and water is generated from the 1st downward-propagation stage (Neves et al., 2011). Thus, a condensation system was built to quantify the liquid product from the 1st stage, as shown in Figure 7.2b. The pyrolysis emission from the opposed propagation was collected via a hood entirely covering the top outlet of the burner. Then, the vapour was passed through a long pipe and finally condensed in the

ice-cooled trappers. The mass of the bio-oil produced was obtained by weighing the trappers.

7.2.4.3 Solid products

After each experiment (when all TCs drop to room temperature), the total solid residue was collected, and its mass was measured via an electrical balance. To quantify the carbon content and stability of the solid residue, all solid samples were further analysed by elemental and thermal analysis. Before analysis, all samples were milled to a homogenous fine powder and dried at 90 °C for 48 h.

Elemental analysis was carried out using PerkinElmer Elemental Analyzer. Moreover, for all biochar samples, H:C and O:C molar ratios were calculated and plotted on a van Krevelen diagram to estimate their stability, where H:C is an indicator of the condensation degree and O:C reflects the oxidation degree (Santin et al., 2020).

Moreover, thermal analysis of biochar was conducted with a PerkinElmer STA 6000 Simultaneous Thermal Analyzer in an air atmosphere at a heating rate of 15 K/min. The recalcitrance index R_{50}, another important parameter to evaluate the char stability, was calculated from the TG results as (Harvey et al., 2012):

$$R_{50} = T_{50,char}/T_{50,graphite} \tag{7.3}$$

where $T_{50,char}$ is the temperature value at which 50% of the mass of the char sample is lost, and $T_{50,graphite}$ is the temperature value at which 50% of the total mass of graphite is lost, which is given as 823 °C (Harvey et al., 2012). The recalcitrance/carbon sequestration potential of the studied material can be classified as Class A: $R_{50}<0.50$; Class B: $0.50 \leq R_{50}<0.70$; Class C: $R_{50} \geq 0.70$, where higher R_{50} represents better carbon sequestration potential (Harvey et al., 2012).

7.2.5 Carbon balance calculations

The carbon balance of each strategy calculated in this study includes the total carbon in permanent gaseous emissions, solid residues, and liquid products (tar). For each smouldering-driven processing strategy, 410 g of wood waste with the carbon content ($X_{C,F}$) of 47.7 % is provided. Thus, the total carbon of the fuel ($m_{C,F}$) is:

$$m_{C,F} = m_F \cdot X_{C,F} = 410 \times 47.7\% = 195.6\ \text{g} \tag{7.4}$$

The carbon from the gaseous emissions ($m_{C,G}$) is defined as a sum of the carbon content in the major gas species as

$$m_{C,G} = \sum_j m_j \cdot X_{C,j} \tag{7.5}$$

where m_j is the mass of gas species j (g), $X_{C,j}$ is the carbon molar mass fraction in species j (%), and subscript j indicates the major carbon-containing gases, e.g., CO_2, CO, CH_4, C_2H_4, and C_2H_6. The gas mass can be calculated as

$$m_j = \int_0^t \rho_j [j](t) \dot{V} \times 10^{-3} \tag{7.6}$$

where ρ_j is the density of species j calculated based on the assumptions of the ideal gas law (kg/m^3), $[j](t)$ is the real-time concentration of the species j (ppm) (subtracting species' background concentration), $\dot{V}$ is the volume flow rate in the duct (m^3/min), and t is the total processing time (min). A representative concentration evolution of the gas species is shown in Figure 7.9 in Appendix of this chapter.

The carbon from the solid residue ($m_{C,S}$) is calculated as

$$m_{C,S} = m_S \cdot X_{C,S} \tag{7.7}$$

where m_S is the mass of the solid residue (g), which is directly measured via a balance after the smouldering process, $X_{C,S}$ is the mass fraction of carbon content of the burnt residue (%), which is determined via the elemental analysis.

The carbon inside the liquid product tar ($m_{C,T}$) is calculated as

$$m_{C,T} = m_T \cdot X_{C,T} = (m_L - m_W) \cdot X_{C,T} \tag{7.8}$$

where m_T is the mass of the tar (g), m_L is the mass of the condensed liquid (g) and m_W is the mass of the condensed water (g), $X_{C,T}$ is the carbon mass fraction of the tar (%). In this work, the average value of m_W is about 30 % m_L (Xiu and Shahbazi, 2012). $X_{C,T}$ is estimated from its relationship with $X_{C,F}$ according to previous research (Neves et al., 2011), where $X_{C,T}$=1.14$X_{C,F}$. As a result, $X_{C,T}$ is calculated as 54.4 % here.

7.2.6 PROMETHEE-GAIA algorithm

Preference Ranking Organization Method for Enrichment Evaluations and Geometrical Analysis for Interactive Aid (PROMETHEE-GAIA) is a kind of multicriteria decision analysis (MCDA) algorithm and has been proved to be a useful approach in environmental applications (Behzadian et al., 2010; Surawski et al., 2013). It helps to make a rational decision, which is achieved by virtue of a decision vector that directs the decision maker toward "preferred" solutions (Brans and Mareschal, 1994). The explanation of PROMETHEE-GAIA algorithm is based on the works performed by the developers in Brans and Vincke (Vincke and Brans, 1985), Brans et al. (Brans and

Mareschal, 1994), and Mareschal and Brans (Mareschal and Brans, 1988).

This study applies the PROMETHEE-GAIA algorithm to the proposed four processing strategies under five different airflow velocities (totally 20 conditions) to decide the most preferred condition (alternative) for achieving different goals by considering seven criteria. A full listing of the abbreviations used for alternatives and criteria, along with information on how each criterion is treated by the PROMETHEE-GAIA algorithm is provided in Table 7.3-7.6.

7.3 Results and Discussion

7.3.1 Smouldering temperature

Figure 7.4 exhibits the smouldering temperatures of the full smouldering process and the partial smouldering process at a representative airflow velocity of 14 mm/s. It should be noted that the flame and the smouldering are separated by a gravel layer, so the flame above will not affect the smouldering temperatures. As expected, there are two separate characteristic peaks in Figure 7.4a which correspond to the two-stage propagation of full smouldering process. The peak temperature of the 1st stage ($T_{max,1}$) is generally lower than that of the 2nd stage ($T_{max,2}$) because the endothermic fuel pyrolysis dominates in the 1st stage while the exothermic char oxidation dominates the 2nd stage. Comparatively, for the partial smouldering process, there is only one peak in Figure 7.4b of which the value is the same as $T_{max,1}$ in Figure 7.4a. Once the bottom thermocouple (0 cm) reached its maximum, the air supply was replaced by the pure nitrogen (N_2). Afterwards, the smouldering temperature starts to decline to room temperature under the cooling effect of the supplied N_2. The summary of T_{max1} and T_{max2} under various airflow velocities is shown in Figure. B2. In general, T_{max2} is larger than T_{max1}, and both T_{max1} and T_{max2} increase with the increased airflow velocity because of stronger char oxidation.

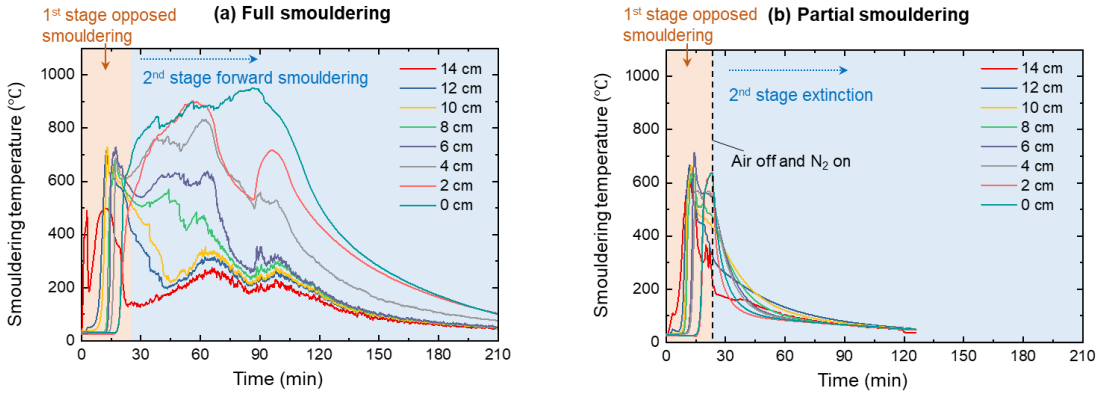

Figure 7.4. Smouldering temperature evolution of (a) full smouldering process and (b) partial smouldering process at u=14 mm/s.

7.3.2 Carbon distribution

Different processing strategies will cause a considerable distinction in the carbon distribution in different by-products (gas, liquid, and solid), thus leading to different environmental impacts. The carbon balance of each strategy is calculated according to the method presented above. As a result, the by-products yields and corresponding carbon distributions are illustrated in Table 7.1.

Figure 7.5 shows the mass fraction of carbon (Y_C, %) in the gas, liquid, and solid products from different strategies. Here, $Y_{\Delta C}$ (carbon difference) for all the tests are lower than 20%, which is acceptable for carbon balance research (Dufour et al., 2009). As exhibited in Figure 7.5a, after the full smouldering process (F-SM), about 70 % of the carbon is distributed into the gaseous product, with about 20% into the liquid product and less than 5% into the solid residue (ash). This means that most of the carbon is released into the atmosphere after F-SM, which can be a detriment in view of its effect of accelerating global warming. Further, if a flame is applied (Figure 7.5c), the carbon in gas will increase to over 90% because tar is mostly consumed by the flame, and its carbon distribution is insensitive to the airflow velocity within the tested range.

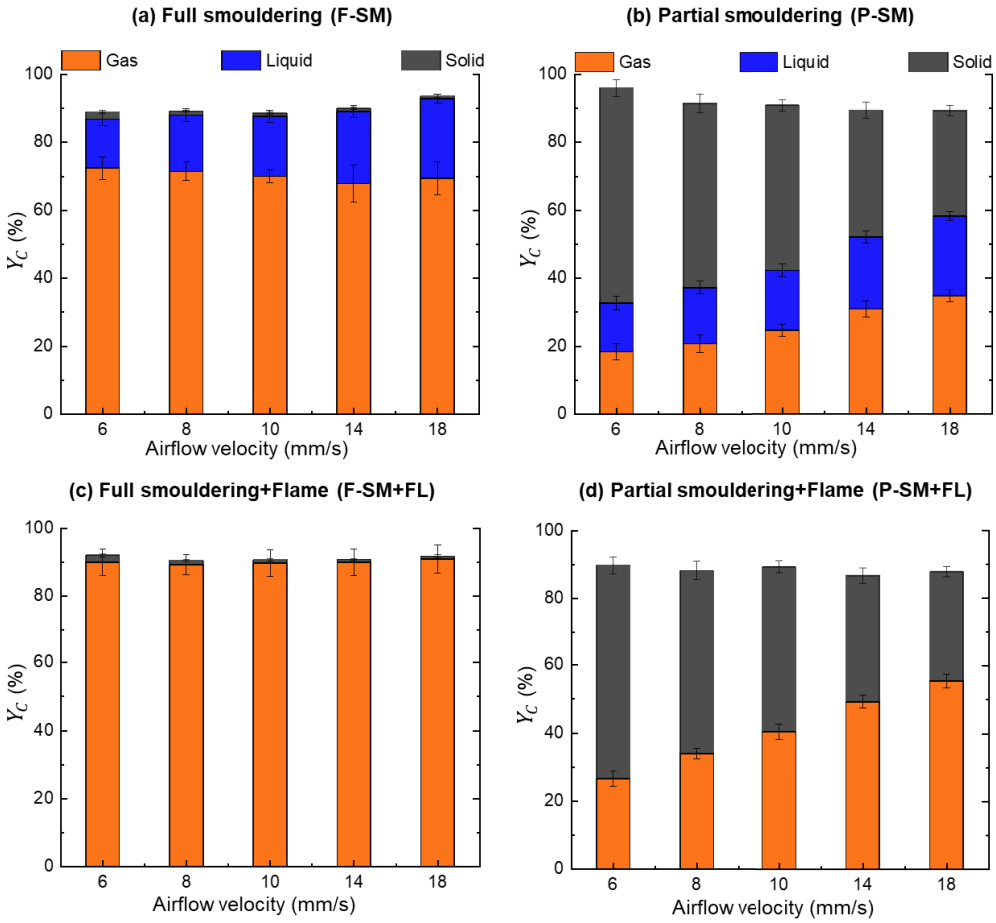

Figure 7.5. Carbon fraction in gas, liquid, and solid products under various airflow velocities for four different strategies, (a) full smouldering (F-SM), (b) partial smouldering (P-SM), (c) full smouldering plus flame (F-SM+FL), and (d) partial smouldering plus flame (P-SM+FL).

Regarding the partial smouldering, Figure 7.5(b, d) show that over 30% carbon is fixed in the solid residue (biochar), and this carbon fraction decreases with the increased airflow velocity. In contrast, the carbon in the gaseous products from partial smouldering increases with the airflow velocity. Specifically, as the airflow velocity increases from 6 mm/s to 8 mm/s, the carbon fraction in gas from P-SM and P-SM+FL increases from 16 % and 21 % to 34 % and 49 %, respectively. This is because a larger airflow velocity strengthens the oxidation process existing in the 1st stage, and more heat is released to decompose more organic material into volatile matters through pyrolysis. In addition, only processes without flame can generate liquid (mainly water and condensable organic compounds), and the carbon fraction in liquid increases with the airflow velocity.

In a short summary, such a thermochemical conversion process has significant effects on carbon partitioning in the products. Full smouldering will release much more

carbon into the atmosphere, while partial smouldering can effectively generate biochar and achieve carbon sequestration. Therefore, by regulating the processing strategies and controlling the supplied airflow, we can achieve different objectives. Besides the distribution of carbon in different forms of products, the properties of the products are also very important as their characteristics determine their environmental impacts and their potential usage (Lehmann et al., 2021). Therefore, a detailed discussion of the properties of the products from each processing strategy is given in the following sections with a focus on the gaseous and solid products.

7.3.3 Gas-phase emissions characteristics

In this work, we measure five major carbon-containing gas species, that is, carbon dioxide (CO_2), carbon monoxide (CO), methane (CH_4), ethylene (C_2H_4), and ethane (C_2H_6). Among these gases, CO_2 and CH_4 are well-known greenhouse gases (GHG), which contribute significantly to global warming (Wang et al., 2014). CO is the second main compound emitted from any combustion process of biomass, which is toxic and may cause poisoning deaths in humans (Manisalidis et al., 2020). In terms of the gaseous hydrocarbons (C_xH_y(g)), the mass of CH_4 is the largest, while the masses of C_2H_4 and C_2H_6 are much less and similar.

To characterize the environmental impacts of the emissions from different strategies and various airflow velocities, we quantify four widely used parameters in environmental research, that is, the CO/CO_2 mass ratio, CH_4/CO_2 mass ratio, C_xH_y (g)/CO_2 mass ratio, and equivalent GHG (Figure 7.6). Figure 7.6a shows that the CO/CO_2 ratio decreases with the airflow velocity for all processes. The reason is that the combustion is more complete under larger airflow (sufficient oxygen supply). In addition, it is observed that the CO/CO_2 ratios of processes with flames (F-SM+FL and P-SM+FL) are all lower than 0.1, which is significantly smaller than those without flame. This proves that the flame could effectively reduce the toxic CO in smouldering emissions, agreeing well with our previous work (Chen et al., 2022b). Figure 7.6(b, c) show CH_4/CO_2 ratio and C_xH_y (g)/CO_2 ratio respectively, which are very close as CH_4 accounts for the majority. For the gases emitted from landfilling of MSW, CH_4 accounts for a primary component with the CH_4/CO_2 mass ratio usually larger than 0.36 (0.36-0.80) (Davis et al., 2022; Hilger and Humer, 2003; Krause et al., 2016; Valencia et al., 2009). In comparison, the CH_4/CO_2 ratios of all the four smouldering processes are significantly smaller than that of the MSW landfilling (see Figure 7.6b).

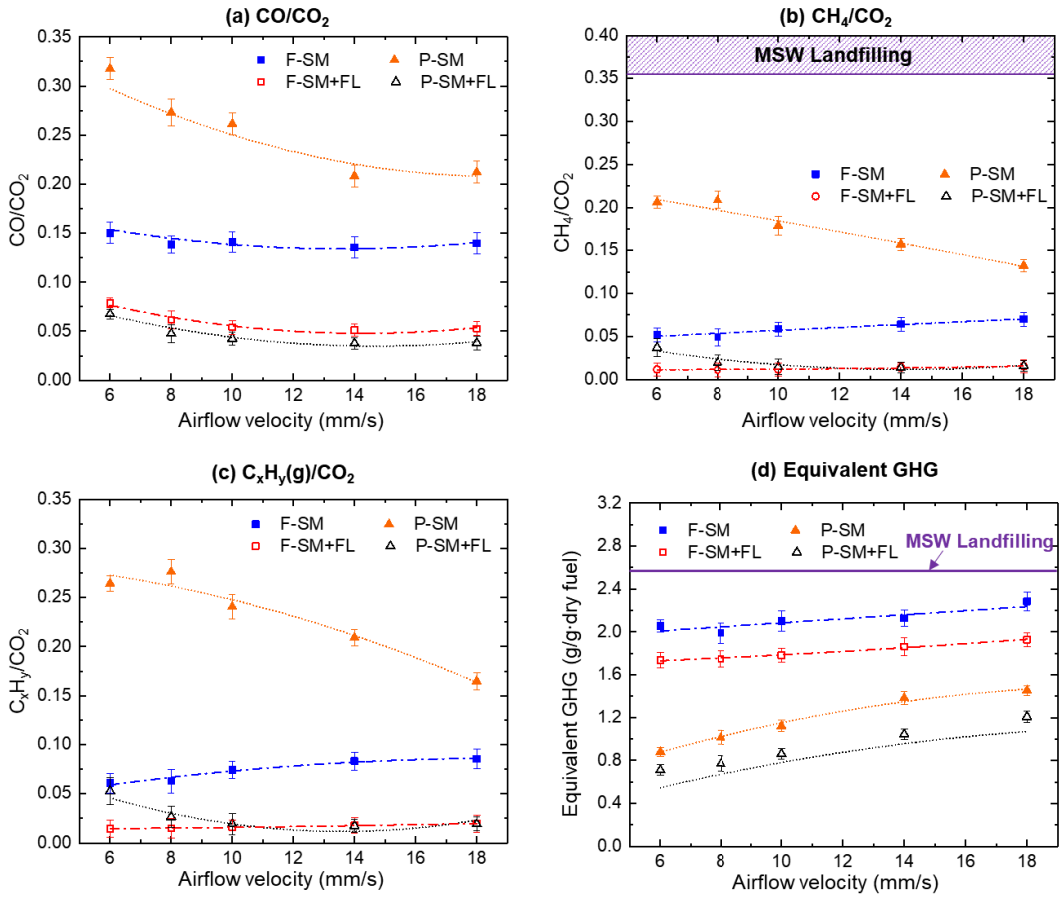

Figure 7.6. (a) CO/CO_2 ratio, (b) CH_4/CO_2 ratio, (c) $C_xH_y(g)/CO_2$ ratio, and (d) equivalent GHG of different processing strategies under various airflow velocities, where the shadow area indicates the emission parameters of treating MSW via landfill in literature.

Global warming caused by GHG emissions has attracted worldwide attention. Each GHG has a different global warming potential (GWP) and persists for different lengths of time in the atmosphere (Buss et al., 2022). Equivalent GHG is a parameter that converts all greenhouse gas emissions into CO_2 equivalents so they can be correctly compared in terms of their greenhouse impacts (Lee et al., 2020). In this work, we simplify the GHG from each process as a mixture of CO_2 and CH_4 (the amount N_2O is very small and is ignored here), and the equivalent GHG (m_{GHG}, g/g· dry fuel) is estimated as

$$m_{GHG} = \frac{GWP_{CO_2} \cdot m_{CO_2} + GWP_{CH_4} \cdot m_{CH_4}}{GWP_{CO_2} \cdot m_F} \tag{7.9}$$

where *GWP* refers the 100-year global warming potential of the species. CO_2 is taken as the reference gas and given a 100-year *GWP* of 1, and the 100-year GWP_{CH_4} is given as

25 here (IPCC, 2006). m_{CO_2} and m_{CH_4} are the total mass of CO_2 and CH_4 produced from waste treatment process, respectively. m_F = 410 g is the mass of fuel.

The calculated results of the equivalent GHG (m_{GHG}) are shown and compared with that from MSW landfilling (Lou and Nair, 2009) in Figure 7.6d. Various theoretical and experimental investigations have suggested that a large variation of GHG emitted from 1 ton of waste landfilling (Ayalon et al., 2000; Humer and Lechner, 1999; Themelis and Ulloa, 2007). For comparison, we take an average 1.28 ton $CO_{2\text{-}e}$/ ton of waste generated from landfills (Kumar and Sharma, 2014; Lou and Nair, 2009) and assume that the moisture content of the waste is 50%, then 2.56 ton $CO_{2\text{-}e}$/ ton dry waste is obtained. As shown in Figure 7.6d, the equivalent GHG (m_{GHG}) emitted from our proposed waste processing strategies is basically lower than that of waste landfilling, especially for the partial smouldering processes. Moreover, m_{GHG} increases as the airflow velocity increases for all processing strategies. For example, m_{GHG} of F-SM increases from 2 to 2.3 g/(g dry fuel) as the airflow velocity increases from 6 mm/s to 18 mm/s. Besides, m_{GHG} from partial smouldering plus flame (P-SM+FL) is the smallest, followed by that from P-SM, F-SM+FL and F-SM. Specifically, m_{GHG} from P-SM+FL is about 30 % smaller than that from P-SM, 55 % smaller than that from F-SM+FL, 60 % smaller than that from F-SM, and 67 % smaller than that from landfilling.

Therefore, on the one hand, the process of partial smouldering plus self-sustained flame can effectively reduce the global warming effect and toxicity degree of emissions. On the other hand, the supplied airflow velocity is much better to be regulated at a moderate degree (~6-10 mm/s), where not only the emissions are cleaner with lower CO/CO_2 and CH_4/CO_2 ratios, but also generating less greenhouse effect with a lower m_{GHG}.

7.3.4 Char yield and stability

The partial smouldering process can generate abundant biochar, which is a solid product of biomass pyrolysis and is a promising concept for climate change mitigation and adaptation (Woolf et al., 2010). In this section, we investigate the char yield and its stability from each process. Note that the char produced from processes P-SM and P-SM+FL are the same because their pyrolysis conditions are same under the same airflow supply.

Figure 7.7a shows the char yield as well as carbon mass fraction fixed in char of the partial smouldering process under various airflow velocities. Two smaller airflow

velocities (2 and 4 mm/s) were also measured here to show the carbon sequestration potential of the proposed partial smouldering process under smaller airflow velocities. The blue symbols in Figure 7.7a indicate the average peak smouldering temperature of the 1st smouldering stage. As suggested, both the char yield and fixed carbon fraction decrease as the airflow velocity is increased. Specifically, when the airflow velocity decreases from 18 mm/s to 2 mm/s, the char yield increases from 21 % to 45 % and the fixed carbon fraction increases from 31 % to 66 %. This is because more organic material inside the fuel will be decomposed into volatile material and released to the atmosphere under higher temperatures (T_{max1}) (Tripathi et al., 2016), leaving less char and fixing less carbon.

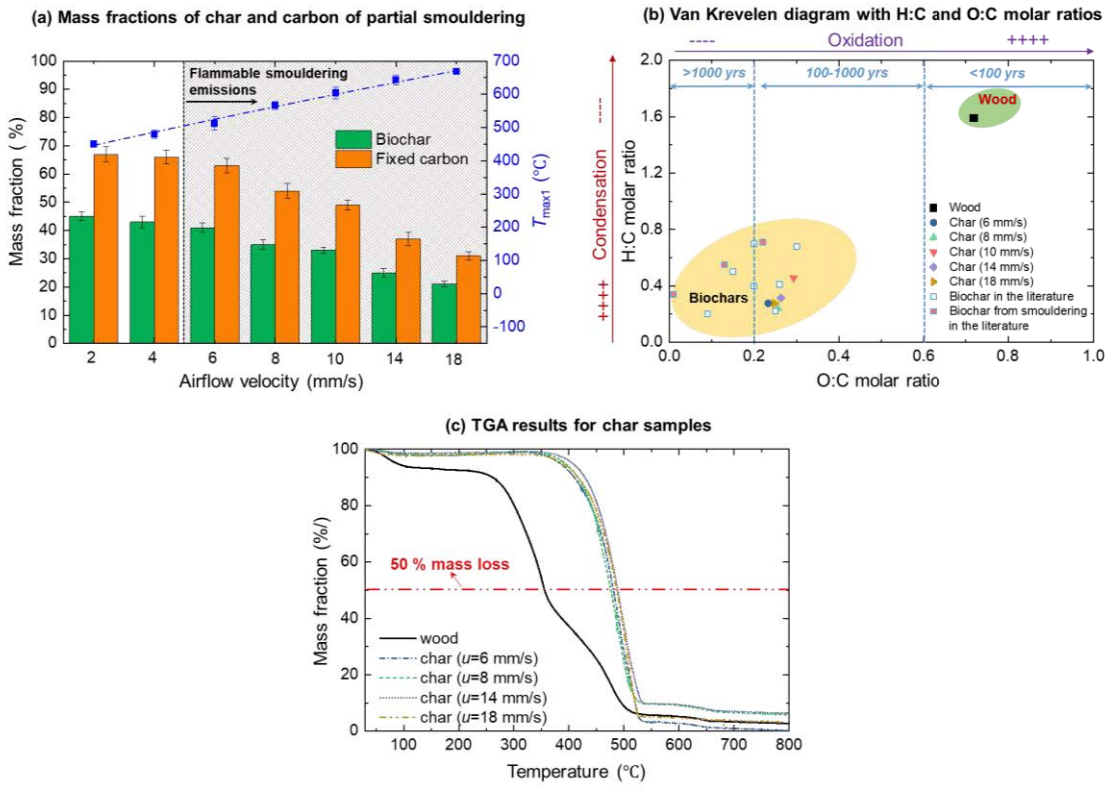

Figure 7.7. (a) Mass fractions of char and carbon from the partial smouldering process with average T_{max1} marked, where the shadow region indicates the smouldering emissions is flammable enough to sustain a flame, (b) Van Krevelen diagram with H:C and O:C molar ratios, where the half-lives range in the X-axis is defined according to Spokas (Spokas, 2010), and (c) TGA results for char samples under various airflow velocities.

Char stability is an essential property which demonstrates the longevity of stored carbon and therefore establishes an effective means for carbon abatement (Crombie et al., 2013). In this work, the stability of the produced biochar is assessed by two methods: O:C

and H:C molar ratios (Santin et al., 2020), and recalcitrance index R_{50} (Harvey et al., 2012). The O:C and H:C ratios are plotted in Figure 7.7b (elemental analysis results are shown in Table 7.2). For comparison, the H:C and O:C molar ratios of biochar in literature are also summarized in Figure 7.7b (Crombie et al., 2013; Kambo and Dutta, 2015; Santin et al., 2020). The finding is that the char samples produced from partial smouldering have similar condensation ($0.2<H:C<0.5$) and oxidation ($0.2<O:C<0.3$) degrees. The relatively low O:C ratio indicates that the biochar obtained in this work can be preserved in the environment over long timescales with half-lives of over 100 years. R_{50} of wood and biochar are calculated from their TG curves (Figure 7.7c) according to Eq. (7.3). It is found that R_{50} of the char from partial smouldering is similar under all airflow velocities, which is about 0.6, larger than that of the virgin wood (~0.4). According to the classification (Harvey et al., 2012), the char produced belongs to Class B ($0.5\leq R_{50}<0.7$), which has intermediate carbon sequestration potentials. In this way, we prove that the proposed partial smouldering is a good biowaste disposal method for long-term carbon sequestration from both char yield and char stability.

7.3.5 Multi-criteria analysis

A multi-criteria decision analysis based on PROMETHEE-GAIA algorithm is conducted, which analyses three scenarios, and each scenario considers seven criteria. Specifically, the seven criteria include emission of CO_2, CO, CH_4, C_2H_4, C_2H_6, and the amount of fixed carbon and produced tar. Three scenarios indicate maximum carbon sequestration with minimum environmental impact (Scenario (a)), maximum removal efficiency with minimum environmental impact (Scenario (b)), and maximum by-product value with minimum environmental impact (Scenario (c)).The outranking result for each scenario is thoroughly listed in Figure 7.11, which involves ranking the alternatives from most preferred to least preferred based on the value of their net outranking flow (Φ).

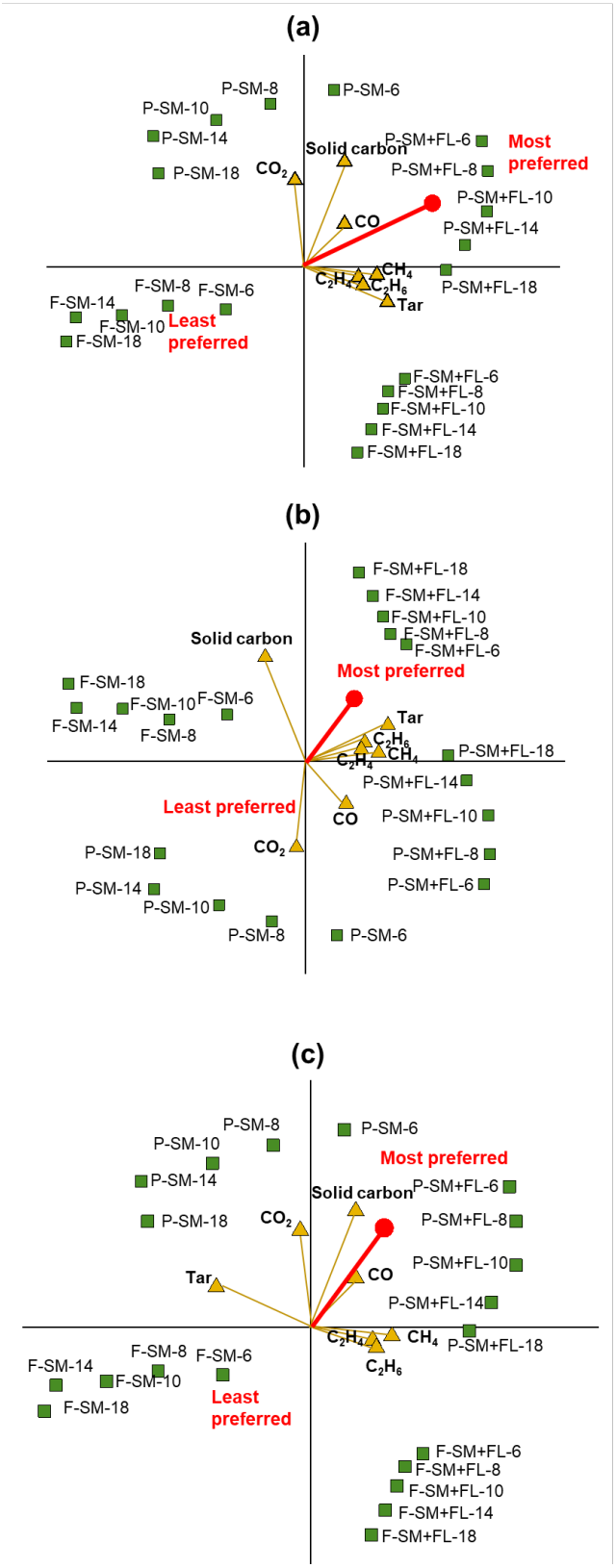

Figure 7.8. GAIA plot of alternatives and criteria with the decision vector for different scenarios: (a) maximum carbon sequestration with minimum environmental impact, (b) maximum removal efficiency with minimum environmental impact, and (c) maximum

by-product value with minimum environmental impact.

Figure 7.8 shows the two-dimensional views of alternatives (green symbols) and criteria (yellow symbols with yellow lines) for a multidimensional problem obtained by Principal Component Analysis with a decision vector (red line) marked. A longer decision vector indicates greater decision-making power. In general, the length of the decision vectors for three scenarios is nearly similar, which all imply strong decision-making power. For scenario (a) (Figure 7.8a), processes P-SM+FL-6, P-SM+FL-8, P-SM+FL-10, and P-SM+FL-14 are all located in close proximity to the decision vector, which means the strategy of partial smouldering plus a flame can achieve the maximum carbon sequestration and minimum environmental impact (emitted less carbon and toxic species). Moreover, a smaller airflow is preferred for this scenario. Figure 7.8b shows 5 alternatives, namely, F-SM+FL-18, F-SM+FL-14, F-SM+FL-10, F-SM+FL-8, and F-SM+FL-6, are close to the decision vector, indicating that the strategy of full smouldering plus a flame is more recommended to achieve a high removal efficiency (maximum mass reduction of the waste) with least environmental impact, and a larger airflow is preferred. For scenario (c), it is revealed by Figure 7.8c that both the partial smouldering processes with and without a flame under a relatively small airflow velocity (i.e., P-SM-6, P-SM+FL-6, P-SM+FL-8, and P-SM+FL-10) are able to produce valuable by-products (either biochar or bio-oil) with minimum harm to the environment. In contrast, the full smouldering process (F-SM) located at the left-bottom side of the plot are least preferred for this scenario.

7.4 Concluding remarks

In summary, our proposed flexible suite of smouldering waste biomass processing technologies can be regulated with different strategies to achieve different goals. Partial smouldering process can sequester abundant stable carbon in biochar (with $0.2<H:C<0.5$, $0.2<O:C<0.3$, and $R_{50}=0.6$) and thus reduce the carbon released to the atmosphere. And a smaller airflow rate is recommended for this strategy to fix more carbon. Full smouldering process can achieve the largest waste removal efficiency, and the larger airflow rate is preferred. With a flame applied, both partial and full smouldering processes can significantly reduce the toxic emissions with lower CO/CO_2 and C_xH_y (g)/CO_2 ratios compared with the processes without flame. The equivalent GHG and the CH_4/CO_2 ratio from our four proposed processing strategies are all smaller than those from the conventional landfilling treatment.

Finally, according to a multi-criteria analysis, the process of partial smouldering with a flame under small airflow rates is preferred to achieve the maximum carbon sequestration and by-products value with minimum environmental impact. The process of full smouldering with a flame under larger airflow rates is recommended to achieve the largest removal efficiency and the least environmental harm. Altogether, our newly developed technology shows great promise for achieving sustainable municipal solid waste management.

7.5 Appendix

Figure 7.9 shows a representative concentration evolution of the gas species from full smouldering process under the airflow velocity of 18 mm/s, where Figure 7.9(a) depicts the concentrations of CO_2 and CO recorded by a portable gas analyzer and Figure 7.9(b) shows the concentrations of CH_4, C_2H_4, and C_2H_6, which are measured every 10 minutes by GC-FID.

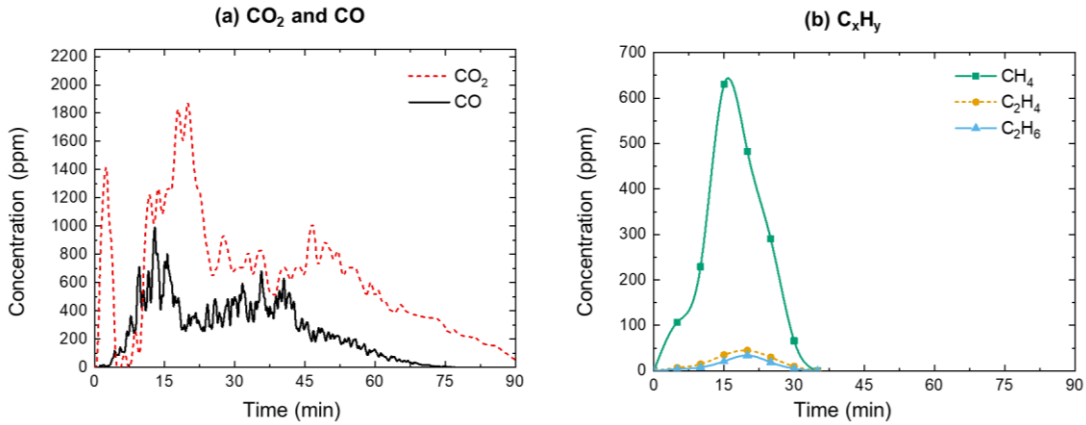

Figure 7.9. Evolution of concentration of gas species from full smouldering under u=18 mm/s.

Figure 7.10 further summarizes the average T_{max1} and T_{max2} under various airflow velocities. It should be noted that T_{max1} of all strategies is the same under the same airflow velocity which represents the peak temperature of the 1st smouldering stage. And T_{max2} is only applicable for the full smouldering process. Both T_{max1} and T_{max2} increase with the increased airflow velocity because of stronger char oxidation. T_{max1} is highly related to the char (product from 1st stage) yield and stability.

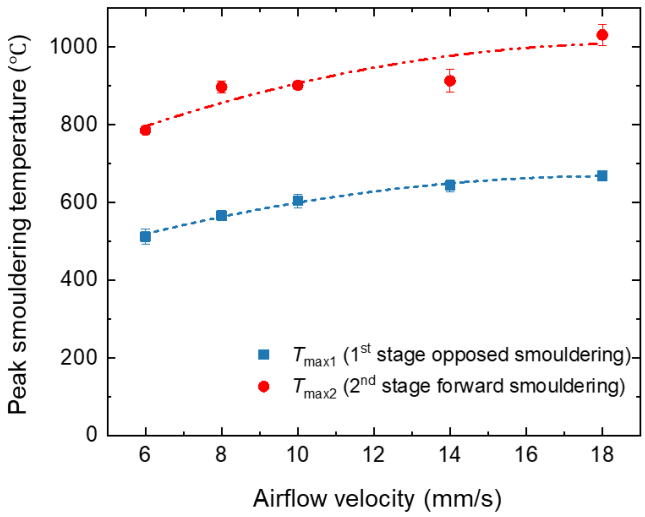

Figure 7.10. Average peak smouldering temperature of 1st opposed smouldering stage and 2nd forward smouldering stage.

Figure 7.11 shows the PROMETHEE outranking for three scenarios, which involves ranking the alternatives from most preferred to least preferred based on the value of their net outranking flow (Φ). For example, as for Scenario (a), the most preferred alternative is P-SM+FL-6 (process of partial smouldering with flaming under the airflow velocity of 6 mm/s) with the maximum Φ of 0.53, while the least preferred alternative is F-SM-18 (process of full smouldering under the airflow velocity of 18 mm/s) with the minimum Φ of -0.57.

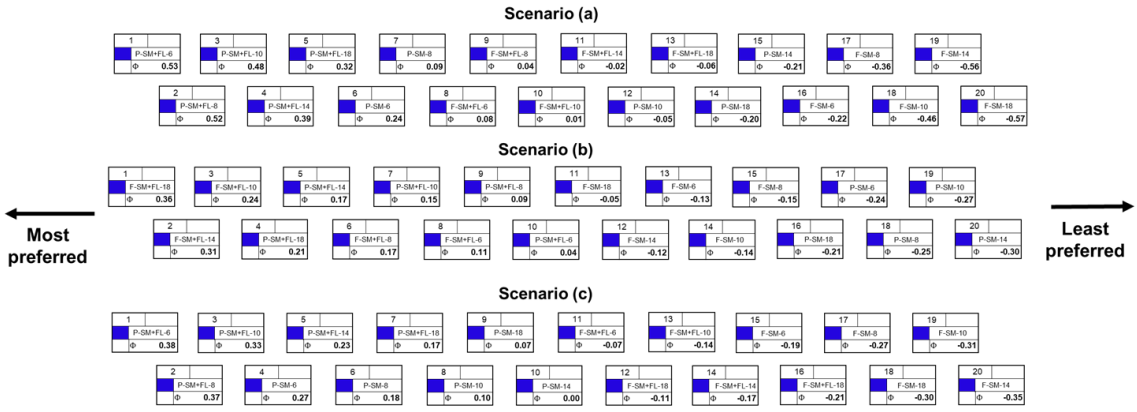

Figure 7.11. PROMETHEE outranking for three scenarios. Top panel: maximum carbon sequestration with minimum environmental impact, middle panel: maximum removal efficiency with minimum environmental impact, and bottom panel: maximum by-product value with minimum environmental impact.

Table 7.1. Product distribution and corresponding carbon content from different strategies.

Strategy	Airflow velocity (mm/s)	Gaseous emissions (G)							Solid residues (S)				Tar (T)				$Y_{\Delta C}$ (%)
		m_{CO_2} (g)	m_{CO} (g)	m_{CH_4} (g)	$m_{C_2H_4}$ (g)	$m_{C_2H_6}$ (g)	$m_{C,G}$ (g)	$Y_{C,G}$ (%)	m_S (g)	$X_{C,S}$ (%)	$m_{C,S}$ (g)	$Y_{C,S}$ (%)	m_L (g)	m_T (g)	$m_{C,T}$ (g)	$Y_{C,T}$ (%)	
F-SM: 1st stage opposed smouldering + 2nd stage forward smouldering	6	368.5	55.3	18.7	1.6	1.9	140.5	72.1	22.0	18.5	4.07	2.1	68.7	48.1	26.2	14.3	11.1
	8	366.4	46.7	18.0	2.6	2.5	139.7	71.4	20.1	11.9	2.39	1.2	84.9	59.4	32.3	16.5	10.9
	10	349.9	49.3	20.5	2.7	2.8	136.7	69.9	17.9	11.0	1.97	1.0	90.7	63.5	34.5	17.7	11.5
	14	335.2	45.5	21.6	3.3	3.1	132.5	67.8	16.5	10.8	1.78	0.9	108.9	76.2	41.5	21.2	10.1
	18	340.4	47.6	23.9	2.7	2.5	134.6	69.3	14.4	10.8	1.56	0.8	120.2	84.1	45.8	23.4	6.5
P-SM: 1st stage opposed smouldering + 2nd stage extinction	6	59.5	18.6	12.1	1.6	1.8	35.8	18.3	167.0	74.0	123.6	63.2	68.7	48.1	26.2	14.3	4.1
	8	67.1	18.3	14.0	2.3	2.2	40.4	20.6	144.1	73.5	105.9	54.2	84.9	59.4	32.3	16.5	8.7
	10	84.2	22.0	15.1	2.6	2.6	48.1	24.6	135.4	70.2	95.1	48.6	90.7	63.5	34.5	17.7	9.2
	14	115.2	24.1	18.0	3.0	3.0	60.3	30.8	102.8	70.8	72.8	37.2	108.9	76.2	41.5	21.2	10.7
	18	138.5	29.4	18.3	2.3	2.2	67.9	34.7	85.8	70.9	60.9	31.1	120.2	84.1	45.8	23.4	10.7
F-SM+FL: 1st stage opposed smouldering with flame + 2nd stage forward smouldering	6	552.5	43.5	6.4	0.8	0.9	175.3	89.9	22.0	18.5	4.07	2.1	-		-	-	8.1
	8	562.4	34.6	6.3	1.0	1.2	174.4	89.3	20.1	11.9	2.39	1.2	-		-	-	9.6
	10	568.3	30.8	6.5	1.2	1.2	175.3	89.6	17.9	11.0	1.97	1.0	-		-	-	9.4
	14	568.5	29.1	7.8	1.4	1.0	175.6	89.8	16.5	10.8	1.78	0.9	-		-	-	9.5
	18	571.9	30.1	8.8	1.5	1.0	177.7	90.9	14.4	10.8	1.56	0.8	-		-	-	8.3
P-SM+FL: 1st stage opposed smouldering with flame +2nd stage extinction	6	121.1	5.8	3.7	0.8	0.9	40.2	20.6	167.0	74.0	123.6	63.2	-		-	-	14.2
	8	181.4	5.5	3.5	0.6	0.6	55.5	28.4	144.1	73.5	105.9	54.2	-		-	-	17.5
	10	248.8	6.3	3.2	0.6	0.4	73.8	37.7	135.4	70.2	95.1	48.6	-		-	-	13.6
	14	299.0	7.1	3.7	1.2	0.3	88.6	45.3	102.8	70.8	72.8	37.2	-		-	-	17.0
	18	316.6	7.8	5.0	1.4	0.4	95.0	48.6	85.8	70.9	60.9	31.1	-		-	-	19.2

Note: $Y_{\Delta C}$ is the carbon difference in this work, which is caused by the inevitable measurement errors of gas sensors and the condensing system, and other non-tested carbon-containing components in the emissions.

Table 7.2. Elemental analysis of the char samples and corresponding O:C and H:C molar ratios under various airflow velocities.

Airflow velocity (mm/s)	C	H	O*	N	O:C molar ratio	H:C molar ratio
6	75.03±1.12	1.76±0.19	23.22±1.32	0	0.233±0.073	0.276±0.024
8	73.47±0.14	1.46±0.08	24.06±0.22	0	0.256±0.004	0.240±0.012
10	70.01±1.39	2.65±0.04	27.34±1.43	0	0.293±0.007	0.456±0.011
14	73.34±2.82	1.15±0.11	25.51±2.93	0	0.263±0.046	0.315±0.012
18	73.94±1.46	1.74±0.09	24.33±1.56	0	0.248±0.017	0.276±0.012

*: O is determined by difference.

Table 7.3. A listing of the abbreviations used for alternatives in PROMETHEE-GAIA.

Alternatives code	**Strategy**	**Airflow velocity (mm/s)**
F-SM-6	1st stage opposed smouldering + 2nd stage forward smouldering	6
F-SM-8	1st stage opposed smouldering + 2nd stage forward smouldering	8
F-SM-10	1st stage opposed smouldering + 2nd stage forward smouldering	10
F-SM-14	1st stage opposed smouldering + 2nd stage forward smouldering	14
F-SM-18	1st stage opposed smouldering + 2nd stage forward smouldering	18
P-SM-6	1st stage opposed smouldering + 2nd stage extinction	6
P-SM-8	1st stage opposed smouldering + 2nd stage extinction	8
P-SM-10	1st stage opposed smouldering + 2nd stage extinction	10
P-SM-14	1st stage opposed smouldering + 2nd stage extinction	14
P-SM-18	1st stage opposed smouldering + 2nd stage extinction	18
F-SM+FL-6	1st stage opposed smouldering with flame + 2nd stage forward smouldering	6
F-SM+FL-8	1st stage opposed smouldering with flame + 2nd stage forward smouldering	8
F-SM+FL-10	1st stage opposed smouldering with flame + 2nd stage forward smouldering	10
F-SM+FL-14	1st stage opposed smouldering with flame + 2nd stage forward smouldering	14
F-SM+FL-18	1st stage opposed smouldering with flame + 2nd stage forward	18

	smouldering	
P-SM+FL-6	1st stage opposed smouldering with flame +2nd stage extinction	6
P-SM+FL-8	1st stage opposed smouldering with flame +2nd stage extinction	8
P-SM+FL-10	1st stage opposed smouldering with flame +2nd stage extinction	10
P-SM+FL-14	1st stage opposed smouldering with flame +2nd stage extinction	14
P-SM+FL-18	1st stage opposed smouldering with flame +2nd stage extinction	18

Table 7.4. A listing of the abbreviations used for criteria, and how each criterion is treated by the PROMETHEE-GAIA analysis for Scenario (a).

Criterion code	Description and units	How the variable was treated by PROMETHEE-GAIA	Preference function#	Weighting
CO_2	Mass of carbon dioxide emitted from waste processing (g)	Minimised*	V-shape	14.3%
CO	Mass of carbon monoxide emitted from waste processing (g)	Minimised*	Linear	14.3%
CH_4	Mass of methane emitted from waste processing (g)	Minimised*	V-shape	14.3%
C_2H_4	Mass of ethylene emitted from waste processing (g)	Minimised*	Level	14.3%
C_2H_6	Mass of ethane emitted from waste processing (g)	Minimised*	Level	14.3%
$m_{C,S}$	Mass of carbon fixed in the solid residues after waste processing (g)	Maximised**	Usual	14.3%
m_T	Mass of tar generated from waste processing (g)	Minimised*	Usual	14.3%

Table 7.5. A listing of the abbreviations used for criteria in this manuscript, and how each criterion is treated by the PROMETHEE-GAIA analysis for Scenario (b).

Criterion code	Description and units	How the variable was treated by	Preference function#	Weighting

		PROMETHEE-GAIA		
CO_2	Mass of carbon dioxide emitted from waste processing (g)	Minimised*	V-shape	10.5%
CO	Mass of carbon monoxide emitted from waste processing (g)	Minimised*	Linear	10.5%
CH_4	Mass of methane emitted from waste processing (g)	Minimised*	V-shape	10.5%
C_2H_4	Mass of ethylene emitted from waste processing (g)	Minimised*	Level	10.5%
C_2H_6	Mass of ethane emitted from waste processing (g)	Minimised*	Level	10.5%
$m_{C,S}$	Mass of carbon fixed in the solid residues after waste processing (g)	Minimised*	Usual	40.0%
m_T	Mass of tar generated from waste processing (g)	Minimised*	Usual	10.5%

Table 7.6. A listing of the abbreviations used for criteria in this manuscript, and how each criterion is treated by the PROMETHEE-GAIA analysis for Scenario (c).

Criterion code	**Description and units**	**How the variable was treated by PROMETHEE-GAIA**	**Preference function#**	**Weighting**
CO_2	Mass of carbon dioxide emitted from waste processing (g)	Minimised*	V-shape	14.3%
CO	Mass of carbon monoxide emitted from waste processing (g)	Minimised*	Linear	14.3%
CH_4	Mass of methane emitted from waste processing (g)	Minimised*	V-shape	14.3%
C_2H_4	Mass of ethylene emitted from waste processing (g)	Minimised*	Level	14.3%
C_2H_6	Mass of ethane emitted from waste processing (g)	Minimised*	Level	14.3%
$m_{C,S}$	Mass of carbon fixed	Maximised**	Usual	14.3%

	in the solid residues after waste processing (g)			
m_T	Mass of tar generated from waste processing (g)	Maximised**	Usual	14.3%

* Lower variable values were preferred
** Higher variable values were preferred
# The choice of the preference function is guided by the "Help me..." function of the Visual PROMETHEE software.

CHAPTER 8

Conclusions and Recommendations

8.1 Conclusions

This thesis proposes a novel combustion method for biowaste removal which uses a self-sustained flame co-existing with smouldering to clean the toxic smouldering emissions. Laboratory-scale experiments for the smouldering of various biowastes and flaming of their smouldering emissions have been performed under different oxygen supply rates. The mechanism of the proposed combustion process has been investigated and a systematical analysis of the process has been conducted. Therefore, one of the major contributions of this work is to reveal the critical conditions for the co-existence of smouldering and flaming on biomass fuel. Secondly, the purification effects of the flame on the smouldering smoke is quantified. The third main contribution is to assess the proposed combustion process in terms of its removal efficiency, by-product value, and carbon footprint.

Chapter 4 has successfully verified that (1) the smouldering emission of woody biomass can be piloted to sustain a flame and (2) flame can co-exist with smouldering combustion. With the smouldering ignition from the top and the flow from the bottom, the smouldering front first propagates downwards (1^{st}-stage opposed smouldering) to the fuel-bed bottom and then propagates upward (2^{nd}-stage forwards smouldering). It has been observed that the flame could only be piloted and self-sustained in the 1^{st}-stage smouldering because of an intense pyrolysis process within the smouldering front. The critical smouldering burning mass flux for maintaining a stable flame remains constant at 10-12 $g/m^2 \cdot s$. The co-existence of flaming and smouldering depends on the oxygen supply to the smouldering front, which is verified by the theoretical analysis. The minimum opposed flow velocity required to maintain the stable flaming increases from 6 mm/s to 24 mm/s, as the oxygen concentration decreases from 21% to 14%. Moreover, increasing oxygen supply enhances the flame intensity and height, but the flame duration is reduced due to the accelerated burning processes.

The proposed combustion method was then further applied to other kinds of biowastes (coffee waste and simulated sludge) in *Chapter 5*. The effects of the fuel properties on the proposed combustion mode (smouldering with a flame) and the purification effects of the flame on the toxic emissions from smouldering have been investigated. The efficiency of pollution mitigation is demonstrated by a significantly lower $\Delta CO/\Delta CO_2$ ratio after purification. The equivalent critical mass flux of flammable

gases required for igniting the smouldering emissions is 0.5 g/m^2·s, regardless of the fuel types. The smouldering temperature, propagation rate and burning flux are all increased with the airflow velocity but are also slightly sensitive to the fuel type. Together with *Chapter 4*, the applicability of this newly developed waste removal method and its efficiency of pollution mitigation were demonstrated.

After the verification of the co-existence of the opposed smouldering and flaming on various biowaste fuels, *Chapter 6* further investigated the effect of the smouldering propagation directions (opposed or forward) on the proposed combustion process. Results show that a flame can be sustained above both the forward and opposed smouldering fronts under appropriate airflow. It has been found that the emission gases from opposed smouldering are much easier to be ignited, and the flame duration and burning fraction are much larger than that of the forward smouldering. The flame sustained above the smouldering is influenced by the competition reactions between wood pyrolysis and char oxidation within the smouldering front. To sustain a stable flame above opposed smouldering, the minimum airflow velocity required is about 6 mm/s, and the minimum smouldering burning rate is 10±1 g/m^2·s. Comparatively, sustaining a flame above forward smouldering front requires a larger airflow velocity (~11 mm/s) and minimum smouldering burning rate which is not constant but increases with the airflow velocity. Moreover, the critical smouldering burning rate at flame extinction is constant at 9±1 g/m^2·s, regardless of the smouldering direction and airflow velocity.

Based on the results obtained in *Chapter 4* to *6*, we further developed a flexible suite of smouldering-based biowaste processing technologies and proposed four processing strategies in *Chapter 7*. The four strategies are named (a) full smouldering, (b) partial smouldering, (c) full smouldering with a flame, and (d) partial smouldering with a flame. The gaseous, liquid, and solid products of each strategy have been quantified under various oxygen supply rates. And a multi-criteria analysis in terms of environmental impact, carbon sequestration, waste removal efficiency, and by-product value has been performed. Our results have shown that full smouldering achieves the highest removal efficiency but generates significant greenhouse and toxic gases. Partial smouldering effectively generates stable biochar, sequesters over 30% carbon, and therefore reduces the greenhouse gases to the atmosphere. By applying a self-sustained flame, the toxic gases are significantly reduced to clean smouldering emissions. Finally, the process of partial smouldering with a flame is recommended to process the biowaste that can

sequester more carbon as biochar, minimize carbon emissions and mitigate the pollution. And the process of full smouldering with a flame is preferred to maximally reduce the waste volume with minimum environmental impact.

8.2 Future works

Application of smouldering in waste disposal is an emerging technology and the research on it is still limited. Many aspects are still not well understood and deserve more in-depth research. And to be a promising, efficient, and sustainable waste removal method, there are still some limitations required to be solved. Here, some interesting ideas are suggested for future works:

1. The moisture content of biowaste is usually high (>100%), and this parameter may affect both smouldering and flaming. Therefore, it is important to investigate whether the smouldering emission from the fuel with high moisture content is still flammable and how the moisture content affects the critical conditions of the co-existence of smouldering and flaming. In the future, more experiments with fuels with various high moisture contents can be performed and the way to improve the flammability of their emissions can be explored.
2. Current experiments are limited in bench scale, and how burner scale affects the proposed combustion process is still unknown. Thus, the effects of scale deserve to be explored. To achieve this goal, a numerical model can be developed to conduct the scale analysis and predict the performances of the burners with larger scales. This numerical model can be exploited in either an academic code (Gpyro) or a commercial code (Fluent or COMSOL).
3. In Chapter 6, a theoretical analysis model was developed to explain the difference of the critical smouldering rate for flame ignition between opposed and forward smouldering. However, the experimental data of the emissions from two smouldering directions to support our analysis and assumption is still lacked. Therefore, future experiments should be conducted to compare the emissions from forward and opposed smouldering processes.
4. At present, this thesis only applied the proposed combustion process in the single type of biowaste fuel, while the performance of the co-burning of multiple types of waste and burning in matrix (like sand or coal) were not determined. Considering the composition of the waste in real world is always complex, it is essential to

evaluate the performance of the co-burning of different wastes. Besides, whether the removal efficiency or emission flammability can be improved by adding some matrix also requires further explorations.

5. Currently, this thesis only measured the yield of the bio-oil from biowaste smouldering. However, the composition of it has not been quantified. Thus, many physicochemical analyses of the bio-oil, like elementary analysis, liquid chromatography, nuclear magnetic resonance spectroscopy (NMR), and Fourier transform infrared spectroscopy (FTIR) can be conducted to determine its quality.

References

Abbas, Z., Moghaddam, A.P., Steenari, B.M., 2003. Release of salts from municipal solid waste combustion residues. Waste Management 23, 291–305.

Akeredolu, F.A., Sonibare, J.A., 1998. A review of the usefulness of gas flares in air pollution control.

Amaral, S.S., de Carvalho Junior, J.A., Costa, M.A.M., Neto, T.G.S., Dellani, R., Leite, L.H.S., 2014. Comparative study for hardwood and softwood forest biomass: Chemical characterization, combustion phases and gas and particulate matter emissions. Bioresource Technology 164, 55–63.

Anca-Couce, A., Zobel, N., Berger, A., Behrendt, F., 2012. Smouldering of pine wood: Kinetics and reaction heats. Combustion and Flame 159, 1708–1719.

Assamoi, B., Lawryshyn, Y., 2012. The environmental comparison of landfilling vs. incineration of MSW accounting for waste diversion. Waste management 32, 1019–1030.

Ayalon, O., Avnimelech, Y., Shechter, M., 2000. Alternative MSW treatment options to reduce global greenhouse gases emissions-the Israeli example. Waste Management & Research 18, 538–544.

Babu, B. V, 2008. Biomass pyrolysis: a state-of-the-art review. Biofuels, Bioproducts and Biorefining: Innovation for a sustainable economy 2, 393–414.

Barnes, D.I., 2015. Understanding pulverised coal, biomass and waste combustion - A brief overview. Applied Thermal Engineering 74, 89–95.

Bartlett, A.I., Hadden, R.M., Bisby, L.A., 2019. A Review of Factors Affecting the Burning Behaviour of Wood for Application to Tall Timber Construction. Fire Technology 55, 1–49.

Basu, P., 2010. Biomass Gasification and Pyrolysis: practical design and theory.

Behzadian, M., Kazemzadeh, R.B., Albadvi, A., Aghdasi, M., 2010. PROMETHEE: A comprehensive literature review on methodologies and applications. European journal of Operational research 200, 198–215.

Belviso, C., 2018. State-of-the-art applications of fly ash from coal and biomass: A focus on zeolite synthesis processes and issues. Progress in Energy and Combustion Science 65, 109–135.

Bilbao, R., Mastral, J.F., Aldea, M.E., Ceamanos, J., Betrán, M., Lana, J.A., 2001. Experimental and theoretical study of the ignition and smoldering of wood including convective effects. Combustion and Flame 126, 1363–1372.

Brans, J.-P., Mareschal, B., 1994. The PROMCALC & GAIA decision support system for multicriteria decision aid. Decision support systems 12, 297–310.

Buss, W., Wurzer, C., Manning, D.A.C., Rohling, E.J., Borevitz, J., Mašek, O., 2022. Mineral-enriched biochar delivers enhanced nutrient recovery and carbon dioxide removal. Communications Earth & Environment 3, 1–11.

Chen, Y., Liang, Z., Lin, S., Huang, X., 2023. Limits of sustaining a flame above smoldering woody biomass. Combustion Science and Technology 195, 2801–2819.

Chen, Y., Lin, S., Liang, Z., Huang, X., 2022a. Clean Smoldering Biowaste Process : Effect of Burning Direction on Smoke Purification by Self-Sustained Flame. Fuel Processing Technology.

Chen, Y., Lin, S., Liang, Z., Huang, X., 2023. Combustion and Flame Limits of Sustaining a Flame above Smoldering Biomass. Combustion Science and Technology.

Chen, Y., Lin, S., Liang, Z., Surawski, N.C., Huang, X., 2022b. Smouldering organic waste removal technology with smoke emissions cleaned by self-sustained flame. Journal of Cleaner Production 362, 132363.

Cheng, X., Huang, Z., Wang, Z., Ma, C., Chen, S., 2019. A novel on-site wheat straw pretreatment method: Enclosed torrefaction. Bioresource Technology 281, 48–55.

Combustion, S., 2016. Smoldering Combustion 581–603.

Crombie, K., Mašek, O., Sohi, S.P., Brownsort, P., Cross, A., 2013. The effect of pyrolysis conditions on biochar stability as determined by three methods. GCB Bioenergy 5, 122–131.

Daouk, E., Van de Steene, L., Paviet, F., Martin, E., Valette, J., Salvador, S., 2017. Oxidative pyrolysis of wood chips and of wood pellets in a downdraft continuous fixed bed reactor. Fuel 196, 408–418.

Davis, A., Whitehead, C., Lengke, M., 2022. Subtle early-warning indicators of landfill subsurface thermal events. Environmental Forensics 23, 179–197.

Demirbas, A., Arin, G., 2002. An overview of biomass pyrolysis. Energy sources 24, 471–482.

Department of Agriculture, W. and the E., 2020. National Waste Report 2020.

Dmitrienko, M.A., Legros, J.C., Strizhak, P.A., 2018. Experimental evaluation of main emissions during coal processing waste combustion. Environmental Pollution 233, 299–305.

Donghoon, S., Sangmin, C., 2000. The combustion of simulated waste particles in a fixed bed. Combustion and Flame 121, 167--180.

Drysdale, D., 2011. An Introduction to Fire Dynamics, 3rd ed. John Wiley & Sons, Ltd, Chichester, UK.

Dufour, A., Celzard, A., Fierro, V., Martin, E., Broust, F., Zoulalian, A., 2008. Catalytic decomposition of methane over a wood char concurrently activated by a pyrolysis gas. Applied Catalysis A: General 346, 164–173.

Dufour, A., Girods, P., Masson, E., Rogaume, Y., Zoulalian, A., 2009. Synthesis gas production by biomass pyrolysis : Effect of reactor temperature on product distribution. International Journal of Hydrogen Energy 34, 1726–1734.

Emberley, R., Inghelbrecht, A., Yu, Z., Torero, J.L., 2017. Self-extinction of timber. Proceedings of the Combustion Institute 36, 3055–3062.

Environmental Protection Agency, 1997. Sources and Air Emission Control Technologies at Waste Management Facilities. Washington, DC.

Environmental Protection Agency, 1995. Survey of Control Technologies for Low Concentration Organic Vapour Gas Streams.

Environmental Protection Department of Hong Kong, 2019. Monitoring of Solid Waste in Hong Kong-Waste Statistics for 2018. Hong Kong Environment Bureau, Environmental Protection Department 1, 4–10.

EPA, 2020. Advancing Sustainable Materials Management. United States Environmental Protection Agency. Office of Resource Conservation and Recovery 184.

European Environment Agency, 2015. Annual European Union Greenhouse Gas Inventory 1990-2013 and Inventory Report 1015.

Fabris, I., Cormier, D., Gerhard, J.I., Bartczak, T., Kortschot, M., Torero, J.L., Cheng, Y.-L., 2017. Continuous, self-sustaining smouldering destruction of simulated faeces. Fuel 190, 58–66.

Feng, C., Huang, J., Yang, C., Li, C., Luo, X., Gao, X., Qiao, Y., 2021. Smouldering combustion of sewage sludge: Volumetric scale-up, product characterization, and economic analysis. Fuel 305, 121485.

Feng, C., Xie, W., Zhang, D., Gao, X., 2022. Pyrolysis of sewage sludge under conditions relevant to applied smouldering combustion. Proceedings of the Combustion Institute 000, 1–10.

Gai, H., Wang, A., Fang, J., Lou, H.H., Chen, D., Li, X., Martin, C., 2020. ScienceDirect

Clean combustion and flare minimization to reduce emissions from process industry. Current Opinion in Green and Sustainable Chemistry 23, 38–45.

Gao, J., Qi, X., Zhang, D., Matsuoka, T., Nakamura, Y., 2021. Propagation of glowing combustion front in a packed bed of activated carbon particles and the role of CO oxidation. Proceedings of the Combustion Institute 38, 5023–5032.

Gómez-Sanabria, A., Kiesewetter, G., Klimont, Z., Schoepp, W., Haberl, H., 2022. Potential for future reductions of global GHG and air pollutants from circular waste management systems. Nature Communications 13, 1–12.

Hadden, R.M., Rein, G., Belcher, C.M., 2013. Study of the competing chemical reactions in the initiation and spread of smouldering combustion in peat. Proceedings of the Combustion Institute 34, 2547–2553.

Haixiang Chen, W.Z., 2014. Influence of particle size on the spreading rate of peat smoldering: An experimental study. Fire Safety Science.

Harvey, O.R., Kuo, L.-J., Zimmerman, A.R., Louchouarn, P., Amonette, J.E., Herbert, B.E., 2012. An index-based approach to assessing recalcitrance and soil carbon sequestration potential of engineered black carbons (biochars). Environmental science & technology 46, 1415–1421.

Hasselriis, F., Licata, A., 1996. Analysis of heavy metal emission data from municipal waste combustion. Journal of Hazardous Materials 47, 77–102.

HE F, TANG Q X, L.Y.J., 2012. Effects of moisture content on smoldering of corn stalk powder. Journal of Combustion Science & Technology 18, 415–420.

He, F., Behrendt, F., 2011. Experimental investigation of natural smoldering of char granules in a packed bed. Fire Safety Journal 46, 406–413.

He, F., Yi, W., Li, Y., Zha, J., Luo, B., 2014. Effects of fuel properties on the natural downward smoldering of piled biomass powder: Experimental investigation. Biomass and Bioenergy 67, 288–296.

He, J., Li, L., Feng, H., Jiang, M., Li, J., Guo, L., Zhang, J., Zhang, P., Gong, J., Huang, Q., 2022. Morphology and nanostructure of flame-formed soot particles from combustion of typical municipal solid waste. Fuel Processing Technology 232, 107269.

Hernandez-Soriano, M.C., Kerré, B., Kopittke, P.M., Horemans, B., Smolders, E., 2016. Biochar affects carbon composition and stability in soil: A combined spectroscopy-microscopy study. Scientific Reports 6, 1–13.

Hilger, H., Humer, M., 2003. Biotic landfill cover treatments for mitigating methane emissions. Environmental Monitoring and Assessment 84, 71–84.

Hu, Y., Christensen, E., Restuccia, F., Rein, G., 2019. Transient gas and particle emissions from smouldering combustion of peat. Proceedings of the Combustion Institute 37, 4035–4042.

Hu, Y., Cui, W., Rein, G., 2020. Haze emissions from smouldering peat: The roles of inorganic content and bulk density. Fire Safety Journal 113, 102940.

Hu, Y., Fernandez-Anez, N., Smith, T.E.L., Rein, G., 2018. Review of emissions from smouldering peat fires and their contribution to regional haze episodes. International Journal of Wildland Fire 27(5), 293.

Huang, X., Gao, J., 2021. A review of near-limit opposed fire spread. Fire Safety Journal 120, 103141.

Huang, X., Rein, G., 2019. Upward-and-downward spread of smoldering peat fire. Proceedings of the Combustion Institute 37, 4025–4033.

Huang, X., Rein, G., 2017. Downward spread of smouldering peat fire: The role of moisture, density and oxygen supply. International Journal of Wildland Fire 26, 907–918.

Huang, X., Rein, G., 2016a. Interactions of Earth's atmospheric oxygen and fuel moisture in smouldering wildfires. Science of the Total Environment 572, 1440–1446.

Huang, X., Rein, G., 2016b. Thermochemical conversion of biomass in smouldering combustion across scales: The roles of heterogeneous kinetics, oxygen and transport phenomena. Bioresource Technology 207, 409–421.

Huang, X., Restuccia, F., Gramola, M., Rein, G., 2016. Experimental study of the formation and collapse of an overhang in the lateral spread of smouldering peat fires 168, 393–402.

Humer, M., Lechner, P.P., 1999. Alternative approach to the elimination of greenhouse gases from old landfills. Waste Management and research 17, 443–452.

Iinuma, Y., Brüggemann, E., Gnauk, T., Müller, K., Andreae, M.O., Helas, G., Parmar, R., Herrmann, H., 2007. Source characterization of biomass burning particles: The combustion of selected European conifers, African hardwood, savanna grass, and German and Indonesian peat. Journal of Geophysical Research Atmospheres 112.

Incropera, F.P., 2007. Principles of heat and mass transfer, Fundamentals of Heat and Mass Transfer. John Wiley.

IPCC, 2006. IPCC Guidelines for National Greenhouse Gas Inventories.

Kambo, H.S., Dutta, A., 2015. A comparative review of biochar and hydrochar in terms of production, physico-chemical properties and applications. Renewable and Sustainable Energy Reviews 45, 359–378.

Kinsman, L., Torero, J.L., Gerhard, J.I., 2017. Organic liquid mobility induced by smoldering remediation. Journal of Hazardous Materials 325, 101–112.

Krause, M.J., Chickering, G.W., Townsend, T.G., Debra, R., Krause, M.J., Chickering, G.W., Townsend, T.G., Debra, R., 2016. Technology Critical review of the methane generation potential of municipal solid waste. Critical Reviews in Environmental Science and Technology 46, 1117–1182.

Kumar, A., Sharma, M.P., 2014. Estimation of GHG emission and energy recovery potential from MSW landfill sites. Sustainable Energy Technologies and Assessments 5, 50–61.

Łach, M., Mikuła, J., Hebda, M., 2016. Thermal analysis of the by-products of waste combustion. Journal of Thermal Analysis and Calorimetry 125, 1035–1045.

Law, C.K., 2010. Combustion Physics. Cambridge university press.

Lee, M., Lin, Y.L., Chiueh, P. Te, Den, W., 2020. Environmental and energy assessment of biomass residues to biochar as fuel: A brief review with recommendations for future bioenergy systems. Journal of Cleaner Production 251, 119714.

Lehmann, J., Cowie, A., Masiello, C.A., Kammann, C., Woolf, D., Amonette, J.E., Cayuela, M.L., Camps-Arbestain, M., Whitman, T., 2021. Biochar in climate change mitigation. Nature Geoscience 14, 883–892.

Lin, C., Huang, R.-J., Ceburnis, D., Buckley, P., Preissler, J., Wenger, J., Rinaldi, M., Facchini, M.C., O'Dowd, C., Ovadnevaite, J., 2018. Extreme air pollution from residential solid fuel burning. Nature Sustainability 1, 512–517.

Lin, S., Cheung, Y.K., Xiao, Y., Huang, X., 2020. Can rain suppress smoldering peat fire? Science of the Total Environment 727, 138468.

Lin, S., Chow, T.H., Huang, X., 2021a. Smoldering propagation and blow-off on consolidated fuel under external airflow. Combustion and Flame 234, 111685.

Lin, S., Huang, X., 2021. Quenching of smoldering: Effect of wall cooling on extinction. Proceedings of the Combustion Institute 38, 5015–5022.

Lin, S., Huang, X., Gao, J., Ji, J., 2022. Extinction of wood fire: A near-limit blue flame above smoldering surface. Fire Technology 58, 415–434.

Lin, S., Huang, X., Gao, J., Ji, J., 2021b. Extinction of wood fire: A near-limit blue flame above smoldering surface. Fire Technology,1-20.

Lin, S., Sun, P., Huang, X., 2019a. Can peat soil support a flaming wildfire? International Journal of Wildland Fire 28, 601–613.

Lin, S., Sun, P., Huang, X., 2019b. Can peat soil support a flaming wildfire? International Journal of Wildland Fire 28, 601–613.

Liu, Y., Wu, S., Zhang, H., Xiao, R., 2021. Fast pyrolysis of holocellulose for the preparation of long-chain ether fuel precursors: Effect of holocellulose types. Bioresource Technology 338, 125519.

Lohri, C.R., Diener, S., Zabaleta, I., Mertenat, A., Zurbrügg, C., 2017. Treatment technologies for urban solid biowaste to create value products: a review with focus on low- and middle-income settings. Reviews in Environmental Science and Biotechnology 16, 81–130.

Lou, X.F., Nair, J., 2009. Bioresource Technology The impact of landfilling and composting on greenhouse gas emissions – A review. Bioresource Technology 100, 3792–3798.

Lu, J.-W., Zhang, S., Hai, J., Lei, M., 2017. Status and perspectives of municipal solid waste incineration in China: A comparison with developed regions. Waste Management 69, 170–186.

Malow M, K.U., 2018. Smoldering Combustion of Solid Bulk Materials at Different Volume Fractions of Oxygen in the Surrounding Gas. Fire Safety Science 9, 303–314.

Manisalidis, I., Stavropoulou, E., Stavropoulos, A., Bezirtzoglou, E., 2020. Environmental and health impacts of air pollution: a review. Frontiers in public health 14.

Mareschal, B., Brans, J.-P., 1988. Geometrical representations for MCDA. European journal of operational research 34, 69–77.

Martins, M.F., Salvador, S., Thovert, J.-F., Debenest, G., 2010. Co-current combustion of oil shale – Part 1: Characterization of the solid and gaseous products. Fuel 89, 144–151.

Martins, Marcio F, Salvador, S., Thovert, J.-F., Debenest, G., 2010. Co-current combustion of oil shale–Part 1: Characterization of the solid and gaseous products. Fuel 89, 144–151.

Melody, S.M., Johnston, F.H., 2015. Coal mine fires and human health: What do we know? International Journal of Coal Geology 152, 1–14.

Michel, C., Liousse, C., Grégoire, J., Tansey, K., Carmichael, G.R., Woo, J., 2005. Biomass burning emission inventory from burnt area data given by the SPOT-VEGETATION system in the frame of TRACE-P and ACE-Asia campaigns. Journal of Geophysical Research: Atmospheres 110.

Neves, D., Thunman, H., Matos, A., Tarelho, L., Gómez-Barea, A., 2011. Characterization and prediction of biomass pyrolysis products. Progress in Energy and Combustion Science 37, 611–630.

Ohlemiller, T.J., 1991. Smoldering Combustion Propagation On Solid Wood. Fire Safety Science 3, 565–574.

Ohlemiller, T.J., 1990. Smoldering combustion propagation through a permeable horizontal fuel layer. Combustion and Flame 81, 341–353.

Ohlemiller, T.J., 1985. Modeling of smoldering combustion propagation. Progress in Energy and Combustion Science 11, 277–310.

Ohlemiller, T.J., Lucca, D.A., 1983. An experimental comparison of forward and reverse smolder propagation in permeable fuel beds. Combustion and flame 54, 131–147.

Page, S.E., Siegert, F., Rieley, J.O., Boehm, H.-D. V, Jaya, A., Limin, S., 2002. The amount of carbon released from peat and forest fires in Indonesia during 1997. Nature 420, 61–65.

Palmer, K.N., 1957. Smouldering combustion in dusts and fibrous materials. Combustion and Flame 1, 129–154.

Pironi, P., Switzer, C., Gerhard, J.I., Rein, G., Torero, J.L., 2011. Self-Sustaining Smoldering Combustion for NAPL Remediation : Laboratory Evaluation of Process Sensitivity to Key Parameters 2980–2986.

Pironi, P., Switzer, C., Rein, G., Fuentes, A., Gerhard, J.I., Torero, J.L., 2009. Small-scale forward smouldering experiments for remediation of coal tar in inert media. PROCEEDINGS OF THE COMBUSTION INSTITUTE 32, 1957–1964.

Pohl, J.H., Tichenor, B.A., Lee, J., Payne, R., 1986. Combustion efficiency of flares. Combustion science and technology 50, 217–231.

Porteiro, J., Patiño, D., Collazo, J., Granada, E., Moran, J., Miguez, J.L., 2010. Experimental analysis of the ignition front propagation of several biomass fuels in a fixed-bed combustor. Fuel 89, 26–35.

Prat-Guitart, N., Rein B, G., Hadden, R.M., Belcher, C.M., Yearsley, J.M., n.d. Propagation probability and spread rates of self-sustained smouldering fires under controlled moisture content and bulk density conditions. CSIRO.

Prat-Guitart, N., Rein, G., Hadden, R.M., Belcher, C.M., Yearsley, J.M., 2016a. Effects of spatial heterogeneity in moisture content on the horizontal spread of peat fires. Science of The Total Environment 572, 1422–1430.

Prat-Guitart, N., Rein, G., Hadden, R.M., Belcher, C.M., Yearsley, J.M., 2016b. Effects of spatial heterogeneity in moisture content on the horizontal spread of peat fires. Science of the Total Environment 572, 1422–1430.

Prat, N., Belcher, C.M., Hadden, R.M., Rein, G., Yearsley, J.M., 2015. A laboratory study of the effect of moisture content on the spread of smouldering in peat fires. Flamma 6, 35–38.

Putzeys, O., Bar-Ilan, A., Rein, G., Fernandez-Pello, A.C., Urban, D.L., 2007. The role of secondary char oxidation in the transition from smoldering to flaming. Proceedings of the Combustion Institute 31, 2669–2676.

Putzeys, O.M., Fernandez-Pello, A.C., Rein, G., Urban, D.L., 2008. The piloted transition to flaming in smoldering fire retarded and non-fire retarded polyurethane foam. FIRE AND MATERIALS 32, 485–499.

Putzeys Olivier, Carlos Fernandez-Pello, D.L.U., 2006. Ignition of Combustion Modified Polyurethane Foam. Journal of ASTM International 3, 13558.

Quintiere, J.G., 2006a. Fundamental of Fire Phenomena, Fundamentals of Fire Phenomena. John Wiley, New York.

Quintiere, J.G., 2006b. Fundamentals of fire phenomena, Fundamentals of Fire Phenomena. John Wiley.

Rashwan, T.L., Fournie, T., Green, M., Duchesne, A.L., Brown, K., Grant, G.P., Torero, L., Gerhard, J.I., 2023. Applied smouldering for co-waste management : Benefits and trade-offs 240.

Rashwan, T.L., Fournie, T., Torero, L., Grant, G.P., Gerhard, J.I., 2021. Scaling up self-sustained smouldering of sewage sludge for waste-to-energy. Waste Management 135, 298–308.

Rashwan, Tarek L., Gerhard, J.I., Grant, G.P., 2016. Application of self-sustaining smouldering combustion for the destruction of wastewater biosolids. Waste Management 50, 201–212.

Rashwan, Tarek L, Gerhard, J.I., Grant, G.P., 2016. Application of self-sustaining smouldering combustion for the destruction of wastewater biosolids. Waste Management 50, 201–212.

Ravindra, K., Singh, T., Mor, S., 2019. Emissions of air pollutants from primary crop residue burning in India and their mitigation strategies for cleaner emissions. Journal of Cleaner Production 208, 261–273.

Rein, G., 2016. Smoldering combustion, in: SFPE Handbook of Fire Protection Engineering. Springer, pp. 581–603.

Rein, G., 2014. Smoldering Combustion. SFPE Handbook of Fire Protection Engineering 2014, 581–603.

Rein, G., 2013. Smouldering Fires and Natural Fuels, in: Claire M. Belcher (Ed.), Fire Phenomena in the Earth System. John Wiley & Sons, Ltd., New York, pp. 15–34.

Rein, G., 2009a. Gains and Threats from Smouldering Combustion to Biochar Production and Storage 74, 2009.

Rein, G., 2009b. Smouldering Combustion Phenomena in Science and Technology. International Review of Chemical Engineering 1, 3–18.

Rein, G., Cohen, S., Simeoni, A., 2009. Carbon emissions from smouldering peat in shallow and strong fronts. Proceedings of the Combustion Institute 32, 2489–2496.

Rein, G., Huang, X., Restuccia, F., McArdle, T., 2017. Detection of landmines in peat soils by controlled smouldering combustion: Experimental proof of concept of O-Revealer. Experimental Thermal and Fluid Science 88, 632–638.

Rich, D., Lautenberger, C., Torero, J.L., Quintiere, J.G., Fernandez-Pello, C., 2007. Mass flux of combustible solids at piloted ignition. Proceedings of the Combustion Institute 31 II, 2653–2660.

Richter, F., Jervis, F.X., Huang, X., Rein, G., 2021. Effect of Oxygen on the Charring Rate of wood. Combustion and Flame 234, 111591.

Rizkiana, J., Guan, G., Widayatno, W.B., Hao, X., Li, X., Huang, W., Abudula, A., 2014. Promoting effect of various biomass ashes on the steam gasification of low-rank coal. Applied Energy 133, 282–288.

Ronda, A., Della Zassa, M., Biasin, A., Martin-Lara, M.A., Canu, P., 2017. Experimental investigation on the smouldering of pine bark. Fuel 193, 81–94.

Ryu, C., Yang, Y. Bin, Khor, A., Yates, N.E., Sharifi, V.N., Swithenbank, J., 2006. Effect of fuel properties on biomass combustion: Part I. Experiments—fuel type,

equivalence ratio and particle size. Fuel 85, 1039–1046.

Saastamoinen, J.J., Taipale, R., Horttanainen, M., Sarkomaa, P., 2000. Propagation of the ignition front in beds of wood particles. Combustion and Flame 123, 214–226.

Santin, C., Doerr, S.H., Jones, M.H., Merino, A., Roberts, J.M., 2020. The relevance of pyrogenic carbon for carbon budgets from fires : insights from the FIREX experiment. Global biogeochemical cycles 0–3.

Santoso, M.A., Christensen, E.G., Yang, J., Rein, G., 2019. Review of the Transition From Smouldering to Flaming Combustion in Wildfires. Frontiers in Mechanical Engineering 5.

Schmidt, M., Lohrer, C., Krause, U., 2003. Self-ignition of dust at reduced volume fractions of ambient oxygen. Journal of Loss Prevention in the Process Industries 16, 141–147.

Song, Z., He, T., Li, M., Wu, D., You, F., 2022. Self-sustaining smoldering as a novel disposal approach for food waste with high moisture content. Fuel Processing Technology 228, 107144.

Spokas, K.A., 2010. Review of the stability of biochar in soils: Predictability of O:C molar ratios. Carbon Management 1, 289–303.

Surawski, N.C., Miljevic, B., Bodisco, T.A., Brown, R.J., Ristovski, Z.D., Ayoko, G.A., 2013. Application of multicriteria decision making methods to compression ignition engine efficiency and gaseous, particulate, and greenhouse gas emissions. Environmental Science and Technology 47, 1904–1912.

Switzer, C., Pironi, P., Gerhard, J.I., Rein, G., Torero, J.L., 2014. Volumetric scale-up of smouldering remediation of contaminated materials. Journal of Hazardous materials 268, 51–60.

Tarelho, L.A.C., Neves, D.S.F., Matos, M.A.A., 2011. Forest biomass waste combustion in a pilot-scale bubbling fluidised bed combustor. Biomass and Bioenergy 35, 1511–1523.

Themelis, N.J., Ulloa, P.A., 2007. Methane generation in landfills. Renewable energy 32, 1243–1257.

Tillman, D.A., 2000. Biomass cofiring: The technology, the experience, the combustion consequences. Biomass and Bioenergy 19, 365–384.

Tissari, J, Lyyränen, J., Hytönen, K., Sippula, O., Tapper, U., Frey, A., Saarnio, K., Pennanen, A.S., Hillamo, R., Salonen, R.O., Hirvonen, M.-R., Jokiniemi, J., 2008.

Fine particle and gaseous emissions from normal and smouldering wood combustion in a conventional masonry heater. Atmospheric Environment 42, 7862–7873.

Torero, J.L., Gerhard, J.I., Martins, M.F., Zanoni, M.A.B., Rashwan, T.L., Brown, J.K., 2020. Processes defining smouldering combustion: Integrated review and synthesis. Progress in Energy and Combustion Science 81.

Tripathi, M., Sahu, J.N., Ganesan, P., 2016. Effect of process parameters on production of biochar from biomass waste through pyrolysis: A review. Renewable and Sustainable Energy Reviews 55, 467–481.

Turetsky, M.R., Benscoter, B., Page, S., Rein, G., Van Der Werf, G.R., Watts, A., 2015. Global vulnerability of peatlands to fire and carbon loss. Nature Geoscience 8, 11–14.

Urbanski, S.P., Hao, W.M., Baker, S., 2008. Chapter 4 Chemical Composition of Wildland Fire Emissions. Developments in Environmental Science 8, 79–107.

Vainikka, P., Tsupari, E., Sipilä, K., Hupa, M., 2012. Comparing the greenhouse gas emissions from three alternative waste combustion concepts. Waste Management 32, 426–437.

Valencia, R., Zon, W. Van Der, Woelders, H., Lubberding, H.J., Gijzen, H.J., 2009. Achieving ‘‘ Final Storage Quality ” of municipal solid waste in pilot scale bioreactor landfills. Waste Management 29, 78–85.

Van Der Werf, G.R., Randerson, J.T., Giglio, L., Collatz, G.J., Kasibhatla, P.S., Arellano Jr, A.F., 2006. Interannual variability of global biomass burning emissions from 1997 to 2004.

Vantelon, J.-P., Lodeho, B., Pignoux, S., Ellzey, J.L., Torero, J.L., 2005. Experimental observations on the thermal degradation of a porous bed of tires. Proceedings of the Combustion Institute 30, 2239–2246.

Vincke, J.P., Brans, P., 1985. A preference ranking organization method. The PROMETHEE method for MCDM. Management Science 31, 647–656.

Wagner, J.P., Soderman, K.L., Konzen, R., 1991. Particle size distributions and heavy metals emissions from guayule fireplace logs. Bioresource technology 35, 209–216.

Wang, F., Jiao, L., Lian, P., Zeng, J., 2019. Apparent gas permeability, intrinsic permeability and liquid permeability of fractal porous media: Carbonate rock study with experiments and mathematical modelling. JOURNAL OF PETROLEUM SCIENCE AND ENGINEERING 173, 1304–1315.

Wang, H., Tian, Z.F., Eyk, P.J. Van, Medwell, P.R., Possell, M., Huang, X., Birzer, C.H., 2021. Smouldering fire and emission characteristics of Eucalyptus litter fuel 1–11.

Wang, H., van Eyk, P.J., Medwell, P.R., Birzer, C.H., Tian, Z.F., Possell, M., 2017. Effects of Oxygen Concentration on Radiation-Aided and Self-sustained Smoldering Combustion of Radiata Pine. ENERGY & FUELS 31, 8619–8630.

Wang, H., van Eyk, P.J., Medwell, P.R., Birzer, C.H., Tian, Z.F., Possell, M., 2016. Identification and Quantitative Analysis of Smoldering and Flaming Combustion of Radiata Pine. ENERGY & FUELS 30, 7666–7677.

Wang, J., Huang, L., Yang, R., Zhang, Z., Wu, J., Gao, Y., Wang, Q., O'Hare, D., Zhong, Z., 2014. Recent advances in solid sorbents for CO 2 capture and new development trends. Energy & Environmental Science 7, 3478–3518.

Wang, S., Ding, P., Lin, S., Huang, X., Usmani, A., 2021. Deformation of wood slice in fire: Interactions between heterogeneous chemistry and thermomechanical stress. Proceedings of the Combustion Institute 38, 5081–5090.

Wang, Z., Liu, W., Ni, Z., Wang, L., Gao, B., 2018. An Experimental Investigation on the Effect of Wind Speed on Cotton Combustion. Procedia Engineering 211, 788–793.

Wang, Z., Wang, F., Cao, J., Wang, J., 2010. Pyrolysis of pine wood in a slowly heating fixed-bed reactor: Potassium carbonate versus calcium hydroxide as a catalyst. Fuel Processing Technology 91, 942–950.

Watts, A.C., Kobziar, L.N., 2012. Smoldering combustion in organic soils: Peat and muck fires in the southeastern US. Southern Fire Exchange.

Werther, J., 2007. Gaseous emissions from waste combustion. Journal of Hazardous Materials 144, 604–613.

Wiedinmyer, C., Quayle, B., Geron, C., Belote, A., McKenzie, D., Zhang, X., O'Neill, S., Wynne, K.K., 2006. Estimating emissions from fires in North America for air quality modeling. Atmospheric Environment 40, 3419–3432.

Woolf, D., Amonette, J.E., Street-Perrott, F.A., Lehmann, J., Joseph, S., 2010. Sustainable biochar to mitigate global climate change. Nature Communications 1.

Wu, D., Huang, X., Norman, F., Verplaetsen, F., Berghmans, J., Van den Bulck, E., 2015. Experimental investigation on the self-ignition behaviour of coal dust accumulations in oxy-fuel combustion system. Fuel 160, 245–254.

Wu, D., Schmidt, M., Huang, X., Verplaetsen, F., 2017. Self-ignition and smoldering

characteristics of coal dust accumulations in O2/N2 and O2/CO2 atmospheres. Proceedings of the Combustion Institute 36, 3195–3202.

Wyn, H.K., Konarova, M., Beltramini, J., Perkins, G., Yermán, L., 2020a. Self-sustaining smouldering combustion of waste: A review on applications, key parameters and potential resource recovery. Fuel Processing Technology 205, 106425.

Wyn, H.K., Perkins, G., 2021. Fuel Gas Production From Self-Sustaining Smouldering Combustion of Lignocellulosic Waste. Research Square.

Wyn, H.K., Zarate, S., Carrascal, J., Yerman, L., 2020b. A Novel Approach to the Production of Biochar with Improved Fuel Characteristics from Biomass Waste. WASTE AND BIOMASS VALORIZATION 6467–6481.

Xiang ZHE, Weitao ZHAO, H.C., 2016. Influence of moisture content on spreading rate of peat smoldering. Journal of Combustion Science & Technology.

Xie, Q., Zhang, Z., Lin, S., Qu, Y., Huang, X., 2020. Smoldering Fire of High-Density Cotton Bale Under Concurrent Wind. Fire Technology 56, 2241–2256.

Xin, X., Dell, K., Udugama, I.A., Young, B.R., Baroutian, S., 2021. Transforming biomass pyrolysis technologies to produce liquid smoke food flavouring. Journal of Cleaner Production 294, 125368.

Xiu, S., Shahbazi, A., 2012. Bio-oil production and upgrading research: A review. Renewable and Sustainable Energy Reviews 16, 4406–4414.

Yamazaki, T., Matsuoka, T., Li, Y., Nakamura, Y., 2020. Applicability of a Low-Pressure Environment to Investigate Smoldering Behavior Under Microgravity. Fire Technology.

Yang, Y. Bin, Ryu, C., Khor, A., Yates, N.E., Sharifi, V.N., Swithenbank, J., 2005. Effect of fuel properties on biomass combustion. Part II. Modelling approach - Identification of the controlling factors. Fuel 84, 2116–2130.

Yang, J., Chen, H., Liu, N., 2016. Modeling of Two-Dimensional Natural Downward Smoldering of Peat. Energy and Fuels 30, 8765–8775.

Yang, J., Liu, N., Chen, H., Gao, W., Tu, R., 2019. Effects of atmospheric oxygen on horizontal peat smoldering fires: Experimental and numerical study. Proceedings of the Combustion Institute 37, 4063–4071.

Yermán, L, Cormier, D., Fabris, I., Carrascal, J., Torero, J.L., Gerhard, J.I., Cheng, Y.-L., 2017a. Potential bio-oil production from smouldering combustion of faeces. Waste and biomass valorization 8, 329–338.

Yermán, L., Hadden, R.M., Carrascal, J., Fabris, I., Cormier, D., Torero, J.L., Gerhard, J.I., Krajcovic, M., Pironi, P., Cheng, Y.-L., 2015. Smouldering combustion as a treatment technology for faeces: exploring the parameter space. Fuel 147, 108–116.

Yermán, L., Wall, H., Torero, J., Gerhard, J.I., Cheng, Y.L., 2016a. Smoldering Combustion as a Treatment Technology for Feces: Sensitivity to Key Parameters. Combustion Science and Technology 188, 968–981.

Yermán, L., Wall, H., Torero, J., Gerhard, J.I., Cheng, Y.L., 2016b. Smoldering Combustion as a Treatment Technology for Feces: Sensitivity to Key Parameters. Combustion Science and Technology 188, 968–981.

Yermán, L, Wall, H., Torero, J.L., 2017b. Experimental investigation on the destruction rates of organic waste with high moisture content by means of self-sustained smoldering combustion. Proceedings of the Combustion Institute 36, 4419–4426.

Yermán, L., Wall, H., Torero, J.L., 2017. Experimental investigation on the destruction rates of organic waste with high moisture content by means of self-sustained smoldering combustion. Proceedings of the Combustion Institute 36, 4419–4426.

Yokelson, R.J., Susott, R., Ward, D.E., Reardon, J., Griffith, D.W.T., 1997. Emissions from smoldering combustion of biomass measured by open-path Fourier transform infrared spectroscopy. Journal of Geophysical Research: Atmospheres 102, 18865–18877.

Zanoni, M.A.B., Torero, J.L., Gerhard, J.I., 2019a. Determining the conditions that lead to self-sustained smouldering combustion by means of numerical modelling. Proceedings of the Combustion Institute 37, 4043–4051.

Zanoni, M.A.B., Torero, J.L., Gerhard, J.I., 2019b. The role of local thermal non-equilibrium in modelling smouldering combustion of organic liquids. Proceedings of the Combustion Institute 37, 3109–3117.

Zanoni, M.A.B., Torero, J.L., Gerhard, J.I., 2018. The role of local thermal non-equilibrium in modelling smouldering combustion of organic liquids. Proceedings of the Combustion Institute 000, 1–9.

Zhou, Z., Qiu, X., Wang, Y., Duan, Y., Li, L., Lin, H., Luo, Y., Sun, Z., Duan, L., 2021. Particulate matter formation during shoe manufacturing waste combustion in a full-scale CFB boiler. Fuel Processing Technology 221, 106914.